STABILIZATION OF ATOMIC HYDROGEN AND DEUTERIUM

ACADEMISCH PROEFSCHRIFT

ter verkrijging van de graad van doctor in de Wiskunde en Natuurwetenschappen aan de Universiteit van Amsterdam, op gezag van de Rector Magnificus, Dr. D. W. Bresters, hoogleraar in de Faculteit der Wiskunde en Natuurwetenschappen, in het openbaar te verdedigen in de Aula der Universiteit (tijdelijk in de Lutherse kerk, ingang Singel 411, hoek Spui) op woensdag 1 september 1982 te 15.00 uur precies

door

JOANNES THEODORUS MARIA WALRAVEN

geboren te AMSTERDAM

krips repro meppel

Promotor : Prof. Dr. I.F. Silvera

Co-referent : Prof. Dr. N.J. Trappeniers

The work described in this thesis was carried out at the 'Natuurkundig Laboratorium' of the University of Amsterdam and supported financially by the 'Stichting voor Fundamenteel Onderzoek der Materie' (FOM).

STELLINGEN

1. De grote belangstelling voor experimentele resultaten in het stabiliseren van atomaire waterstof, de hevige concurrentie en de nieuwheid van de resultaten hebben niet geleid tot de door Jochemsen verwachte onzorgvuldigheden bij de eerste publicaties op dit gebied.

   R. Jochemsen, proefschrift, stelling 4, Universiteit van Amsterdam (1978).

2. Bij de berekening van de invloed van nulpuntsfluctuaties van een heliumoppervlak op de kernspinrelaxatietijd (T_1) van geadsorbeerde atomaire waterstof hebben Yapple en Guyer de invloed van hoogfrequente modes sterk overschat.

   J.Y. Yapple en R.A. Guyer, preprint.

3. De mobiliteit van triplet excitonen in vast stikstof kan goed bestudeerd worden door excitatie met een atomaire stikstof bundel en detectie met behulp van het luminescentie spectrum van geïsoleerde stikstof atomen binnen de moleculaire matrix.

   J.T.M. Walraven, E.R. Eliel en I.F. Silvera, Phys.Lett.73A, 119 (1979).

4. Gebruik makend van een supergeleidende afscherming van NbTi moet het mogelijk zijn om zeer kleine en laagfrequente magnetisatieveranderingen {van de orde van 5×10^{10} Bohrmagnetonen /(cm^3sec)} nog waar te nemen in externe velden van 10 Tesla.

   J.T.M. Walraven en I.F. Silvera, Physica 107B, 517 (1981).

5. Bij hun studie van tijdelijke poreusheid van fosfolipide vesicles, geïnduceerd door electrische velden, nemen Teissie en Tsong ten onrechte aan dat deze deeltjes bolvormig zijn.

   J. Teissie en T.Y. Tsong, Biochemistry 20, 1548 (1981).

6. Bij de interpretatie van de vacature concentratie metingen aan CoGa en NiGa werd door Neumann en Chang, ten onrechte, de entropieverstoring bij defect formatie buiten beschouwing gelaten.

   J.P. Neumann en Y. Chang, Z.Metallkunde 70, 118 (1979).

7. Bij de methode om de anisotrope potentiaal tussen twee waterstof moleculen te ontwikkelen in bolfuncties en de coëfficienten te bepalen uitgaande van een beperkt aantal geometrische configuraties zoals berekend door Ree en Bender, is het essentieel om alle significante termen mee te nemen, daar anders ook voor de wel beschouwde termen geheel onjuiste resultaten kunnen worden verkregen.

   F.H. Ree en C.F. Bender, J.Chem. Phys. 71, 5362 (1979).

   J. van Kranendonk, preprint.

8. Recente metingen van Hsiang et.al. aan de soortgelijke warmte van Pd, hebben het spinfluctuatie onderzoek aan sterk paramagnetische metalen onnodig in discrediet gebracht.

   T.Y. Hsiang, J.W. Reister, H. Weinstock, G. Crabtree, J.J. Vuillemin Phys.Rev.Lett. 47, 523 (1981).

   M.T. Béal Monod, Physica 1982, preprint.

9. Om de experimenteel interessante N=1 → N=5 rotationele Raman overgang in moleculaire zuurstof waar te nemen, verdient het aanbeveling gebruik te maken van een supersone expansie.

   K. Altman, G. Strey, J.G. Hochenbleicher en J. Brandmüller, Z.Naturforsch, 27a, 56 (1972).

10. Toegang tot ongepubliceerde wetenschappelijke informatie is essentieel voor goed onderzoek. Dit geldt met name voor zich snel ontwikkelende vakgebieden.

Amsterdam, 1 september 1982 J.T.M. Walraven

Aan mijn ouders

Aan Marian

INTRODUCTION

The gaseous state of atomic hydrogen (H) is one of the simplest and most interesting systems provided by nature. The simplicity arises from the simple structure of the hydrogen atom: one proton and one electron. Since the early days of quantum mechanics this aspect has stimulated physicists to use the hydrogen atom as a test probe to verify physical hypotheses. Its electronic spectrum has played a central role in the development of quantum mechanics itself. The experiments of Lamb and Retherford were decisive for our present understanding of the quantum electrodynamics. The hydrogen maser provided a breakthrough in the development of lasers and time and frequency measurement.

As a result of this intensive and continual study and the relative simplicity of the problem, the hydrogen atom is by far the best understood atomic system. Not only the atomic properties of hydrogen are studied intensively, but also the interactions between two, three and four hydrogen atoms. In particular the hydrogen molecule (H_2) may be described with an unequaled accuracy for molecular systems on the basis of "first principles".

The detailed knowledge of the atomic and molecular states of hydrogen provides a firm basis to also enhance our knowledge of many-body atomic systems. The reason why H has not yet served this interesting purpose is very simple. With a textbook notion atomic hydrogen is said to recombine explosively to form a "stable" molecular state (H_2, H_2O, CH_4 etc.).

This thesis deals with atomic hydrogen in the gaseous state. It is meant to demonstrate rigorously that atomic hydrogen may be subjected to experimental investigation under (quasi-) equilibrium conditions as any "normal" gas. The use of low temperature technology enables an enhancement of the "lifetime" of a sample by orders of magnitude, so that recombination no longer appears explosive to the human observer, but rather slow (in the course of hours). This is experimentally realized by polarizing the electronic spins in a high

($\sim$ 10 Tesla) magnetic field and by minimizing surface interactions by covering all low temperature ($T \lesssim 0.6$ Kelvin) surfaces with a film of superfluid helium-4. Hydrogen in this (meta-) stable state is commonly referred to as Spin Polarized Atomic Hydrogen (H$\downarrow$) and is predicted to exhibit fascinating properties as a quantum fluid below its degeneracy temperature. The recombination, although detremental from many points of view, may be put to advantage as it enables an elegant determination of the adsorption energy of hydrogen on various surfaces. This is demonstrated for the isotope atomic deuterium and the surface of ^{4}He. These points represent the main physical yield of my thesis work and are subject of four letters to the Physical Review, reproduced here as chapter 3, 4, 5 and 6. For the experiments, the development of a reliable source of low temperature hydrogen atoms was of crucial importance. This source is described in detail in a paper accepted for publication by the Review of Scientific Instruments and presented in chapter 2 along with a description of the low temperature apparatus. Chapter 1 provides the theoretical frame work that places the work into an appropriate perspective.

CHAPTER 1

THEORETICAL SURVEY

1.1. FUNDAMENTALS

1.1.1. *Spin Polarized Atomic Hydrogen*

The interaction between a pair of hydrogen atoms depends strongly on the electronic state of the constituent atoms and, limiting ourselves to the electronic ground state, in particular on the electronic spin state of the pair.

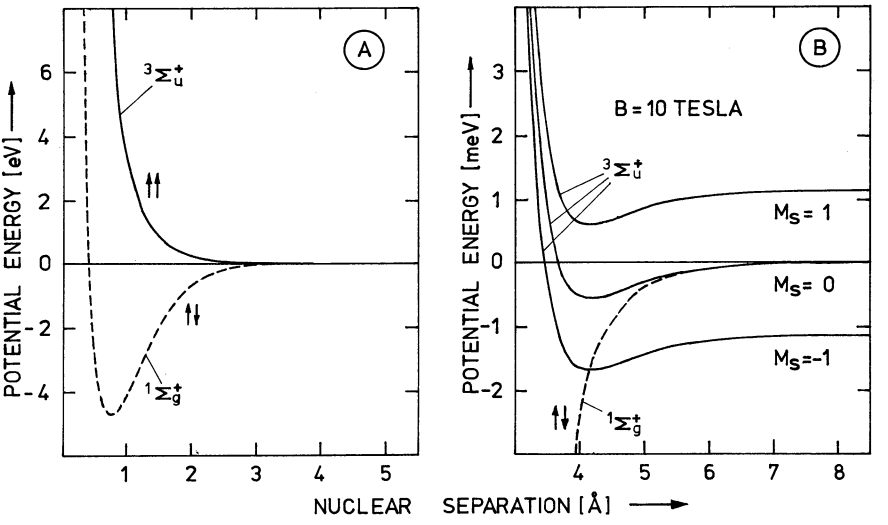

Fig. 1A-Interatomic potentials for a pair of hydrogen atoms in the singlet (dashed line) and triplet (solid line) states. Fig. B shows, on an expanded scale, the shallow minimum of the triplet potential. In a magnetic field the degeneracy of the triplet is lifted and one of the triplet potentials is shifted below the singlet.

Phenomenologically the presence of spin leads to two potentials, the $^1\Sigma_g^+$ -potential in case of an anti-symmetric electronic spin state and the $^3\Sigma_u^+$ -potential in case of a symmetric electronic spin state. Accurate calculations of these potentials were made by Kolos and Wolniewicz.[1,2,3] Both potentials are shown in Fig. 1.

The $^1\Sigma_g^+$ potential has a deep attractive well with a minimum of 4.75 eV at a nuclear separation of 0.74 Å. This potential gives rise to the strong covalent bond in the hydrogen molecule. In contrast the $^3\Sigma_u^+$ potential has a very shallow non-bonding minimum of 0.56 meV at an internuclear distance of 4.15 Å. By polarization of the electronic spin states, the atoms are forced to interact pairwise via the non-bonding triplet potential which results, in the absence of depolarizing forces, to a complete suppression of hydrogen molecule formation. A many-body system of hydrogen atoms, interacting pairwise via this $^3\Sigma_g^+$ potential will be referred to as spin polarized atomic hydrogen. The polarized gas is characterized by the symbol H↓ or H↑ where the arrow denotes the direction of polarization of the electronic spins with respect to the magnetic field. At low temperature H↓ is the energetically favored state. A positive scattering length[4] $a \approx 0.72$ Å may be associated with the triplet potential, indicating that the energy of the gas increases with growing density. The gas remains stable against liquid formation at higher densities. This was established on the basis of numerical calculations by Hecht[5], Etters and coworkers[6,7,8] and Nosanow and coworkers.[9] We note that historically the symbol H↑ was used for both H↑ and H↓ but this habit was left to avoid confusion between the two states of polarization.

1.1.2. *The method of spin polarization*

The hamiltonian describing the spin states of the H-atom is given by

$$\hat{\mathcal{H}} = g_\beta \mu_\beta B \hat{S}_z - g_n \mu_n B \hat{I}_z + a \hat{\vec{I}} . \hat{\vec{S}} \qquad (1.1.)$$

The first two terms are the electronic and nuclear Zeeman contributions respectively, and the third term represents the hyperfine interaction with coupling constant a. $\hat{\vec{S}}$ and $\hat{\vec{I}}$ are the electronic and nuclear spin operators with components S_z and I_z along the magnetic field B. The electronic and nuclear g-factors are written as g_β and g_n ; μ_β is the Bohr magneton, μ_n the nuclear magneton. Applying (1.1.) to the S = 1/2, I = 1/2 case of atomic hydrogen one easily obtains the well known hyperfine level diagram named after Breit and Rabi[10] and shown in Fig. 2.

The eigenstates corresponding to hamiltonian (1.1.) are commonly labeled a, b, c and d with growing energy:

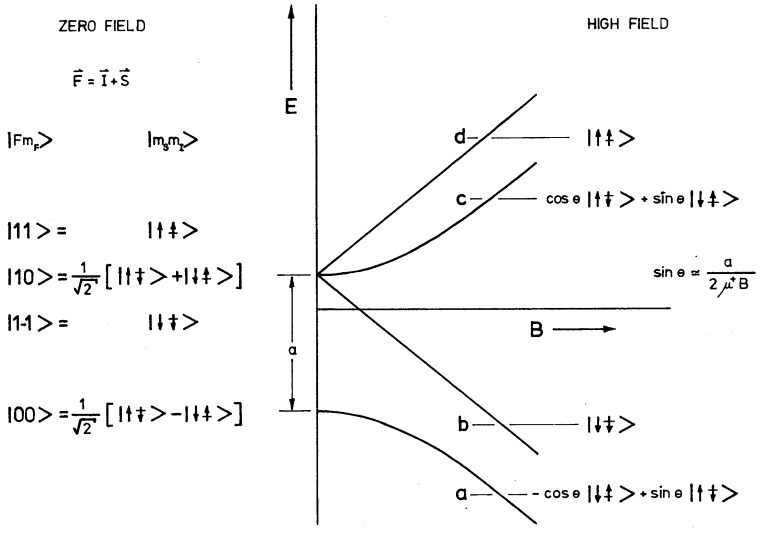

Fig. 2-The hyperfine level diagram of an isolated hydrogen atom in a magnetic field B. Expressions for the spin states are given for both the zero field and the high field limits. In zero field F and M_F are good quantum numbers.

$$\begin{aligned} |\,d\,\rangle &= |\uparrow\ddagger\rangle \\ |\,c\,\rangle &= \cos\theta\,|\uparrow\ddagger\rangle + \sin\theta\,|\downarrow\ddagger\rangle \\ |\,b\,\rangle &= |\downarrow\ddagger\rangle \\ |\,a\,\rangle &= -\cos\theta\,|\downarrow\ddagger\rangle + \sin\theta\,|\uparrow\ddagger\rangle \end{aligned} \qquad (1.2.)$$

where the simple arrows refer to the electronic spin states ($\uparrow \sim m_S = +\frac{1}{2}$) and the arrows with a bar to the nuclear spin states ($\ddagger \sim m_I = +\frac{1}{2}$).

$$\varepsilon \equiv \sin\theta = \left\{ 1 + \left[\frac{\mu^+ B}{a} + \sqrt{1 + \left(\frac{\mu^+ B}{a}\right)^2}\right]^2 \right\}^{-1/2} \qquad (1.3.)$$

where $\mu^{\pm} \equiv g_\beta\,\mu_\beta \pm g_n\,\mu_n$. In high fields ($B >> a/\mu^+ \simeq 506.2$ Gauss) the mixing parameter ε approaches zero asymptotically ($\theta \to 0$) according to

$$\varepsilon \approx \frac{a}{2\mu^+ B} \qquad (1.3a.)$$

In zero field $\theta = \pi/4$ or $\varepsilon = \frac{1}{2}\sqrt{2}$

The energy levels are given by (see Fig. 2):

$$
\begin{aligned}
E^d &= \quad 1/4\ a\ [1 + 2\ \frac{\bar{\mu}B}{a}] \\
E^c &= -\ 1/4\ a\ [1 - 2\sqrt{1 + (\frac{\bar{\mu}B}{a})^2}\ ] \\
E^b &= \quad 1/4\ a\ [1 - 2\ \frac{\bar{\mu}B}{a}] \\
E^a &= -\ 1/4\ a\ [1 + 2\sqrt{1 + (\frac{\bar{\mu}B}{a})^2}\ ]
\end{aligned}
\qquad (1.4.)
$$

Spin polarization can be achieved in various ways. First[11] we concentrated our efforts on preparing a pure electronic spin state with an atomic beam technique and Stern and Gerlach's principle to obtain a spatial separation between spin "up" and spin "down". The spin selected atoms were subsequently condensed on a surface to study their properties. In a second stage it became clear that the original goal of our research could best be realized with another approach. A flux of hydrogen atoms is guided into a high ($B \approx 10$ T) magnetic field through a tube which also serves to cool the gas down to $T \lesssim 400$ mK. At $B = 10$ T the splitting between the lowest and highest pair of hyperfine levels equals $\Delta E/k_B \approx 13$ K (k_B is Boltzmann's constant) so that at $T = 400$ mK the thermal occupation of the upper two ($|c\rangle$ and $|d\rangle$) levels is suppressed by a factor $e^{-32} \approx 10^{-14}$. Physically this means that atoms in the $|c\rangle$ or $|d\rangle$ spin states cannot enter the magnetic field. The atoms experience a force proportional to their effective magnetic moment and the gradient of the magnetic field.

$$\vec{F}^i = \mu^i_{eff}\ \vec{\nabla}B \qquad (1.5.)$$

where

$$\mu^i_{eff} = -\frac{\partial E^i}{\partial B} \qquad i \in (a, b, c, d) \qquad (1.6.)$$

As a result $|a\rangle$ and $|b\rangle$ state atoms are pulled into the magnetic field whereas atoms in the $|c\rangle$ and $|d\rangle$ states are repelled. This last group will recombine in low field or relax their electron spin and then enter the the field in a second stage. Note that this process is not the same as "Brute Force Polarization" where one fully relies on relaxation to obtain thermal equilibrium. Such a process is likely to be inefficient in atomic hydrogen as a major fraction of the gas could have recombined before the spins achieve thermal equilibrium.

Unfortunately the enormous suppression of the occupation of the $|c\rangle$ and $|d\rangle$ state does not mean that the electron spin "up" component is also suppressed by this amount, because the lowest hyperfine state (state $|a\rangle$

in Fig.2) has an admixture of spin "up" due to the hyperfine coupling between the nuclear and electronic spins. As the level of this admixture depends only weakly on the magnetic field, as shown by equation (1.3a.) it may not be rendered negligible with currently accessible fields. The probability of finding a spin "up" is ε^2.For a field of 10 T, $\varepsilon^2 = 6.4 \times 10^{-6}$ which is a rather small but by no means negligible amount. In Section 1.4. the consequences of this admixture in relation to recombination processes wil be discussed.

1.1.3. *The Bose-nature of* $H\downarrow$

On the basis that quasi-equilibrium conditions may be achieved for a gas of spin-polarized atomic hydrogen, one of the first questions that comes to mind concerns its statistical nature in relation to the internal structure of the atoms. For properties where this internal structure need not be considered the situation is unambiguous; $H\downarrow$ should obey Bose statistics as any other "composite" system with an even number of (tightly bound) elementary fermions per particle. In general the effects of quantum statistics will not show unless the particles come close enough. The only way to identify two identical particles is by specifying their position and momentum sufficiently accurately. As shown by Heisenberg this becomes fundamentaly impossible at short distances. Then quantum mechanical interference effects originating from the indistinguishability have to be taken into account by symmetrizing (or anti-symmetrizing) the wave functions according to the nature of the particles. These points may be illustrated by the following elementary example.[12]

Consider a system of two *non-interacting* identical particles with spin, represented by wavefuctions (wave packets) $\Psi_\mu(\vec{r}_1\sigma_1)$ and $\varphi_\nu(\vec{r}_2\sigma_2)$, where $\vec{r}_i$ and σ_i represent the dynamical variables for position and spin of particle i; μ and ν define the (in general not orthogonal) spin states of the particles. We assume the wave functions to be separable of the form

$$\Psi_\mu(\vec{r}\sigma) = \Psi(\vec{r})\,\chi_\mu(\sigma) \qquad (1.7a.)$$

where Ψ and χ_μ represent the orbital and spin states respectively, both normalized to unity

$$\sum_\sigma |\chi_\mu(\sigma)|^2 = 1 \qquad (1.7b.)$$

$$\int |\Psi(\vec{r})|^2 = 1 \qquad (1.7c.)$$

Analogous expressions are assumed for $\varphi_\nu(\vec{r}\sigma)$.

We now raise the question how does particle indistinguishability affect the distribution of particles over space? The hamiltonian is invariant under permutation of the particles, implying that the symmetry of the pair wave function under permutation is a constant of the motion. The symmetrization postulate then teaches that the dynamical states of the system are either all symmetric or anti-symmetric, depending on the nature of the particles, thus the total wave function is written as

$$\frac{1}{2}\left(\frac{2}{1\pm S^2}\right)^{\frac{1}{2}}\left[\Psi_\mu(\vec{r}_1\sigma_1)\,\varphi_\nu(\vec{r}_2\sigma_2) \pm \Psi_\mu(\vec{r}_2\sigma_2)\,\varphi_\nu(\vec{r}_1\sigma_1)\right] \qquad (1.8.)$$

where the + sign refers to the boson-case and the - sign to the fermion-case, S represents an overlap integral required to conserve normalization. The probability density of finding one of the particles at $\vec{r}_1$ and the other at $\vec{r}_2$ is

$$P_s^{\pm}(\vec{r}_1, \vec{r}_2) =$$
$$= (1 \pm S^2)^{-1} \sum_{\sigma_1\sigma_2} \frac{1}{2}\left|\Psi_\mu(\vec{r}_1\sigma_1)\,\varphi_\nu(\vec{r}_2\sigma_2) \pm \Psi_\mu(\vec{r}_2\sigma_2)\,\varphi_\nu(\vec{r}_1\sigma_1)\right|^2 \qquad (1.9a.)$$

which is rewritten, using (1.7a.) and (1.7b.) to obtain

$$P_s^{\pm}(\vec{r}_1, \vec{r}_2) = (1 \pm S^2)^{-1}\{P_u(\vec{r}_1, \vec{r}_2) \pm$$
$$\pm \frac{1}{2}\sum_{\sigma_1\sigma_2}\left[\Psi_\mu^*(\vec{r}_1\sigma_1)\,\varphi_\nu^*(\vec{r}_2\sigma_2)\,\Psi_\mu(\vec{r}_2\sigma_2)\,\varphi_\nu(\vec{r}_1\sigma_1) + (1 \leftrightarrow 2)\right]\} \qquad (1.9b.)$$

here (1↔2) indicates an exchange of the indices 1 and 2 and

$$P_u(\vec{r}_1, \vec{r}_2) \equiv \frac{1}{2}\{\,|\Psi(\vec{r}_1)|^2 \cdot |\varphi(\vec{r}_2)|^2 + |\Psi(\vec{r}_2)|^2 \cdot |\varphi(\vec{r}_1)|^2\} \qquad (1.9c.)$$

Note that $P_u(\vec{r}_1, \vec{r}_2)$ expresses the probability density of finding one out of two *distinguishable* particles at $\vec{r}_1$ and the other at $\vec{r}_2$. If $P_s^{\pm}(\vec{r}_1, \vec{r}_2) \equiv P_u(\vec{r}_1, \vec{r}_2)$ symmetrization is not required to calculate the spatial distribution of the pair. From equation (1.9b.) it can be seen that this is the case if

- the particles occupy disjunct regions of space:

$$\Psi(\vec{r}) \neq 0 \rightarrow \varphi(\vec{r}) = 0 \qquad (1.10.)$$
and vice versa

or

- the particles are in orthogonal spin states

$$\sum_\sigma \chi_\mu^*(\sigma)\,\chi_\nu(\sigma) = 0 \qquad (1.11.)$$

More generally it can be shown that symmetrization is not required for the evaluation of the expectation value of any operator $\hat{O}$ if

$$\sum_{\sigma_1\sigma_2} \iint \psi_\mu^*(\vec{r}_1\sigma_1)\,\varphi_\nu^*(\vec{r}_2\sigma_2)\,\hat{O}\,\psi_\mu(\vec{r}_2\sigma_2)\,\varphi_\nu(\vec{r}_1\sigma_1)\,d\vec{r}_1 d\vec{r}_2 = 0 \quad (1.12.)$$

which is satisfied in particular for any spin-independent operator if condition (1.11.) applies. However, if symmetrization is required, interference effects between $\psi_\mu(\vec{r}_1\sigma_1)\varphi_\nu(\vec{r}_2\sigma_2)$ and $\psi_\mu(\vec{r}_2\sigma_2)\varphi_\nu(\vec{r}_1\sigma_1)$ may dominate the physics: note that in general $P_s^+(r\sigma;r\sigma) \neq 0$, whereas $P_s^-(r\sigma;r\sigma) \equiv 0$.

There are two aspects in our present introductory survey of the H↓ system, where the foregoing considerations may be applied. First, we can establish at what densities quantum statistics will become important and, secondly, when the composite particle approximation must break down. The translational states of the H↓ atoms may be described by wave packets of typical size w. Exchange effects become important when the wave functions overlap, thus for densities

$$n \gtrsim (1/w)^3 \quad (1.13a.)$$

The uncertainty $\Delta x \equiv [\langle x^2\rangle - \langle x\rangle^2]^{1/2}$ in the position x of the atoms ($\Delta x \equiv w/2$) is estimated using Heisenberg's uncertainty relation $\Delta x \cdot \Delta p \approx \hbar$. The uncertainty $\Delta p \equiv [\langle p^2\rangle - \langle p\rangle^2]^{1/2}$ in momentum p of the particles depends on the temperature and is estimated for a Maxwellian gas using results of simple kinetic theory: $\langle p^2\rangle = 3mk_BT$ and $\langle p\rangle^2 = 8mk_BT/\pi$. We find

$$w \approx \left[\frac{2\pi\hbar^2}{mk_BT}\right]^{\frac{1}{2}} \equiv \lambda_{th} \quad (1.13b.)$$

λ_{th} is the "thermal" de Broglie wave length of the particles. For H↓ at T = 100 mK this means that deviations from classical statistics are to be expected for densities $n \gtrsim n_d = 6 \times 10^{18}$ H↓/cm^3, $n_d \equiv \lambda_{th}^{-3}$ is the degeneracy density of the gas.

Again, along the same line of reasoning, one predicts the composite particle approximation to break down if the electronic wave functions of separate atoms overlap and thus quantum interference of the electronic wave functions is no longer negligible.[13] For two H↓ atoms this happens at an internuclear separation of $\sim$ 4Å as demonstrated dramatically by the difference between the singlet and triplet potentials (see Fig. 1). This difference originates from the dependence of the electrostatic interaction on the distance between the electronic charges, which depends in turn strongly on

the absence ($^1\Sigma_g^+$) or presence ($^3\Sigma_u^+$) of the exchange effects. Hence for a (non-interacting) gas of H↓ these effects only become important for densities $n \gtrsim (\frac{1}{4})^3$ Å^{-3} = 1.6 × 10^{22} H↓/cm^3, orders of magnitude higher than the Bose degeneracy density of the H↓ and thus of no practical consequence for observing effects associated with the Bose statistics.

We consider this second point in more detail, this time accounting explicitly for the internal structure of the atom. In view of the relevance for high field, low temperature experiments we limit the discussion to the lowest hyperfine states (|a> and |b>).

Within the Born-Oppenheimer approximation the unsymmetrized "a-b" pair wave function is written as

$$\Psi_{ab}(R_1R_2r_1r_2) = \Phi(R_1R_2)\ \phi(R_1r_1;R_2r_2)|ab) \qquad (1.14.)$$

$$\phi(R_1r_1;R_2r_2) \equiv \varphi(R_1r_1)\varphi(R_2r_2) \qquad (1.14a.)$$

where R_1 and r_1 represent the proton and electron coordinates respectively, $\varphi(R_i r_i)$ are s-state electronic wave functions around the position R_i, $\Phi(R_1R_2)$ the orbital wave function of the pair and |ab) is the unsymmetrized spin state.

$$|ab) \equiv |a\rangle_1|b\rangle_2 = -\cos\theta\ |\downarrow\downarrow\rangle_e|\pm\mp)_n + \sin\theta\ |\uparrow\downarrow)_e|\mp\mp)_n \qquad (1.15.)$$

where sin θ is defined in equation (1.3.).

To symmetrize Ψ_{ab} with respect to protons and electrons we first decompose |ab) in terms of symmetric and anti-symmetric (electronic and nuclear) spin parts. This is most easily done by a transformation to the coupled spin representation using the appropriate Clebsch Gordon coefficients.[14] Defining $\vec{S} = \vec{S}_1 + \vec{S}_2$ and $\vec{I} = \vec{I}_1 + \vec{I}_2$ the coupled representation is spanned by the state vectors $|S, M_S\rangle_e|I, M_I\rangle_n$:

$$\begin{aligned} |ab) = &-\frac{1}{\sqrt{2}}\cos\theta\ |1,-1\rangle_e|1,0\rangle_n \\ &-\frac{1}{\sqrt{2}}\cos\theta\ |1,-1\rangle_e|0,0\rangle_n \\ &+\frac{1}{\sqrt{2}}\sin\theta\ |1,0\rangle_e|1,-1\rangle_n \\ &+\frac{1}{\sqrt{2}}\sin\theta\ |0,0\rangle_e|1,-1\rangle_n \end{aligned} \qquad (1.16.)$$

The symmetrization is now completed by multiplying the various terms of (1.16.) with appropriately symmetrized electronic and orbital wave functions. The electronic wave functions are Heitler-London like

$$\phi^{(\pm)}(R_1R_2r_1r_2) = \phi(R_1r_1;R_2r_2) \pm \phi(R_1r_2;R_2r_1) \qquad (1.17.)$$

where + is used for the "bonding"-case and - for the "anti-bonding"-case. The orbital wave functions are also either symmetric (S) or anti-symmetric (AS) under exchange of R_1 and R_2

$$\Phi^{S,AS}(R_1R_2) = (\pm)\,\Phi^{S,AS}(R_2R_1) \tag{1.18.}$$

Thus the totally symmetrized pair wave function becomes

$$\begin{aligned}\Psi_{ab}(R_1R_2r_1r_2) = &-\frac{1}{\sqrt{2}}\cos\theta\,|1\text{-}1\rangle_e|1\ 0\rangle_n\,\phi^{(-)}(R_1R_2r_1r_2)\Phi^{S}(R_1R_2)\\ &-\frac{1}{\sqrt{2}}\cos\theta\,|1\text{-}1\rangle_e|0\ 0\rangle_n\,\phi^{(-)}(R_1R_2r_1r_2)\Phi^{AS}(R_1R_2)\\ &+\frac{1}{\sqrt{2}}\sin\theta\,|1\ 0\rangle_e|1\text{-}1\rangle_n\,\phi^{(-)}(R_1R_2r_1r_2)\Phi^{S}(R_1R_2)\\ &+\frac{1}{\sqrt{2}}\sin\theta\,|0\ 0\rangle_e|1\text{-}1\rangle_n\,\phi^{(+)}(R_1R_2r_1r_2)\Phi^{AS}(R_1R_2)\end{aligned} \tag{1.19a.}$$

Analogously one may write totally symmetrized wave functions for the "a" and "b-" case

$$\begin{aligned}\Psi_{aa}(R_1R_2r_1r_2) = &\cos^2\theta\,|1,\text{-}1\rangle_e|1,\ 1\rangle_n\,\phi^{(-)}(R_1R_2r_1r_2)\Phi^{S}(R_1R_2)\\ &-\frac{1}{2}\sin 2\theta\,|1,\ 0\rangle_e|1,\ 0\rangle_n\,\phi^{(-)}(R_1R_2r_1r_2)\Phi^{S}(R_1R_2)\\ &+\frac{1}{2}\sin 2\theta\,|0,\ 0\rangle_e|0,\ 0\rangle_n\,\phi^{(+)}(R_1R_2r_1r_2)\Phi^{S}(R_1R_2)\\ &+\sin^2\theta\,|1,\ 1\rangle_e|1,\text{-}1\rangle_n\,\phi^{(-)}(R_1r_2r_1r_2)\Phi^{S}(R_1R_2)\end{aligned} \tag{1.19b.}$$

$$\Psi_{bb}(R_1R_2r_1r_2) = |1,\text{-}1\rangle_e|1,\text{-}1\rangle_n\,\phi^{(-)}(R_1R_2r_1r_2)\Phi^{S}(R_1R_2) \tag{1.19c.}$$

As is to be expected, in the limit of high fields ($\theta\to 0$) only anti-bonding electronic wave functions appear; i.e. in a Born-Oppenheimer picture the atoms interact via the triplet potential in the presence of electrostatic interaction between the particles. We also note from (1.19a) that symmetry does not exclude anti-symmetric orbital wave functions, even in high magnetic fields. The appearance of odd orbital wave functions is no surprise for a pair of hydrogen atoms. The most abundant modification of H_2 (ortho H_2) falls in this class (in combination with the bonding electronic orbital $\phi^{(+)}$).

Again focussing our attention on states $|a\rangle$ and $|b\rangle$ we now investigate to what extent two hydrogen atoms may be considered (composite) bosons. Bose-nature means that the total wave function of the pair should be symmetric under exchange of particles constituting the pair, i.e. under the simultaneous exchange of both protons and electrons. As before we decompose $|ab)$

in symmetric and anti-symmetric spin parts, however this time with respect to the total atomic spin states (i.e. the hyperfine states)

$$|ab) = \frac{1}{2}\,[\,|ab) + |ba)] + \frac{1}{2}\,[\,|ab) - |ba)] \qquad (1.20.)$$

and to complete the symmetrized (composite particle) pair wave function we have to add the orbital wave function of the pair as well as the electronic state. Since the individual electrons are not to be exchanged in our present approach the electron wave function is given by (1.14a.). The orbital motion of the atoms is again described by Φ^S or Φ^{AS}, see (1.18.).

$$\begin{aligned}\Psi^c_{ab}(R_1R_2r_1r_2) = {} & \frac{1}{2}\,[\,|ab) + |ba)]\ \phi(R_1r_1;R_2r_2)\ \Phi^S(R_1R_2) \\ & + \frac{1}{2}\,[\,|ab) - |ba)]\ \phi(R_1r_1;R_2r_2)\ \Phi^{AS}(R_1R_2)\end{aligned} \qquad (1.21a.)$$

Analogously

$$\Psi^c_{aa}\ (R_1R_2r_1r_2) = |aa\rangle\ \phi(R_1r_1;R_2r_2)\ \Phi^S(R_1R_2) \qquad (1.21b.)$$

$$\Psi^c_{bb}\ (R_1R_2r_1r_2) = |bb\rangle\ \phi(R_1r_1;R_2r_2)\ \Phi^S(R_1R_2) \qquad (1.21c.)$$

To enable a direct comparison with (1.19a.) we express the spin part in terms of the coupled representation of the electronic and nuclear spin states. This is done in two steps. First (1.21.) is rewritten in terms of electronic and nuclear spin states and then terms are collected to yield

$$\begin{aligned}\Psi^c_{ab}(R_1R_2r_1r_2) = {} & -\frac{1}{\sqrt{2}}\cos\theta\,|1,-1\rangle_e|1,\ 0\rangle_n\ \phi(R_1r_1;R_2r_2)\ \Phi^S(R_1R_2) \\ & + \frac{1}{\sqrt{2}}\sin\theta\,|1,\ 0\rangle_e|1,-1\rangle_n\ \phi(R_1r_1;R_2r_2)\ \Phi^S(R_1R_2) \\ & - \frac{1}{\sqrt{2}}\cos\theta\,|1,-1\rangle_e|0,\ 0\rangle_n\ \phi(R_1r_1;R_2r_2)\ \Phi^{AS}(R_1R_2) \\ & + \frac{1}{\sqrt{2}}\sin\theta\,|0,\ 0\rangle_e|1,-1\rangle_n\ \phi(R_1r_1;R_2r_2)\ \Phi^{AS}(R_1R_2)\end{aligned} \qquad (1.22a.)$$

For completeness we also compare Ψ^c_{aa} and Ψ^c_{bb}:

$$\begin{aligned}\Psi^c_{aa}(R_1R_2r_1r_2) = {} & +\cos^2\theta\,|1,-1\rangle_e|1,\ 1\rangle_n\ \phi(R_1r_1;R_2r_2)\ \Phi^S(R_1R_2) \\ & - \frac{1}{2}\sin2\theta\,|1,\ 0\rangle_e|1,\ 0\rangle_n\ \phi(R_1r_1;R_2r_2)\ \Phi^S(R_1R_2) \\ & + \frac{1}{2}\sin2\theta\,|0,\ 0\rangle_e|0,\ 0\rangle_n\ \phi(R_1r_1;R_2r_2)\ \Phi^S(R_1R_2) \\ & + \sin^2\theta\,|1,\ 1\rangle_e|1,-1\rangle_n\ \phi(R_1r_1;R_2r_2)\ \Phi^S(R_1R_2)\end{aligned} \qquad (1.22b.)$$

and

$$\Psi^c_{bb}(R_1R_2r_1r_2) = |1,-1\rangle_e|1,-1\rangle_n\ \ \phi(R_1r_1;R_2r_2)\ \Phi^S(R_1R_2) \qquad (1.22c.)$$

Comparing equations (1.22.) with (1.19.) we observe that both sets of equations are identical except for the fact that the equations (1.22.) lack the exchange term $\phi(R_1 r_2; R_2 r_1)$. This is of course not surprising since electronic exchange is a consequence of the internal structure of the atom, which was not considered in deriving (1.22.). To the extent that hydrogen atoms satisfy (1.21.) we may call them bosons; according to (1.22.) and (1.19.) everywhere except in regions of direct electronic overlap.

So far we focused our attention on non-interacting H↓ atoms. What are the effects of the interactions? Unlike the non-interacting case, in an interacting system the effects of particle indistinguishability extend beyond the regions of direct overlap. The interactions cause the atoms to be scattered continuously. For the case of spin-zero bosons this gives rise to diffraction patterns characterized by even partial waves only. Many properties of a weakly interacting system are not very sensitive for these phenomena. Thermodynamic properties like pressure, internal energy, compressibility or specific heat, properties which are well defined also for non-interacting gases, are only affected modestly by the presence of the interaction. Other properties, however, only exist by virtue of the interactions, in particular transport phenomena. In these cases the properties depend critically on the nature of the scattering processes and thus indistinguishability effects may dominate the physics. A good example of the last class is presented by gaseous ^{3}He where polarization of the nuclear spin is expected to change the low temperature transport properties in a dramatic way. ^{3}He is a spin 1/2 fermion system. When both spin "up" and spin "down" atoms are present, the atoms may be scattered via s-waves, the only scattering channel which is energetically accesible at low temperature. This results in a finite viscosity. By spin polarizing the system s-wave scattering is inhibited by the fermion-nature of ^{3}He. As a result the viscosity is expected to vanish at low temperature.

We return to the case of H↓ with the aim to establish whether the atoms also behave like bosons in scattering processes, in spite of electronic overlap during collisions. Clearly the bosons defined by equation (1.21.) have a curious nature. We have decoupled total atomic spin states instead of electronic and nuclear spin states separately, i.e. atoms are exchanged in specific hyperfine states instead of electrons and protons with spin. Atomic hyperfine states are undefined when the atoms overlap as demonstrated

by the H_2 molecule in its ground state, where the hyperfine interaction is negligible. However, although the approach of equation (1.21.) is thus formally incorrect it may still be used to calculate many properties of the system if we replace the electrostatic interaction by an effective spin-dependent interaction between electrically neutral point-like atoms (i.e. remove $\phi(R_1 r_1; R_2 r_2)$ from (1.21.))[15]

$$V_{eff} = V(R_{12}) + J(R_{12})\ \vec{S}_1.\vec{S}_2 \qquad (1.23.)$$

where the first term is commonly referred to as the direct term [$V(R_{12}) \equiv 3/4\ V_T + 1/4\ V_S$] and the second term as the exchange term [$J(R_{12}) \equiv V_T - V_S$, V_T and V_S represent the triplet and singlet potentials respectively]. With this definition for the interatomic potential we implicitely account for electronic exchange effects and the point-like bosons experience the same potential as real hydrogen atoms. Heuristically this implies that the same partial waves undergo the same phase-shift in both cases and since the partial wave decompositions for both descriptions are asymptotically identical (i.e. outside regions of electronic overlap as shown by (1.19. and 1.22.)) the S-matrices coincide. It does not imply that the protons behave like bosons during the collision but only that the result of the complex quantum interference is Bose-like. Only at very high densities ($n \gtrsim 1.6 \times 10^{22}$ H↓/cm^3) this analysis breaks down. The atoms are then constantly in a state of collision and the problem becomes one of protons moving through a sea of electrons. The only way left to describe the translational states of the "atoms" is through the motion of the protons, which is not necessarily Bose-like as pointed out by Freed[16] using the Born-Oppenheimer approximation (e.g. see the fourth term of (1.19a.) or the third term of (1.19b.)). Fermi-like terms are absent in the fully spin-polarized case (corresponding to "b"-states only), where the protons behave as spin 1/2 bosons. However, for the general case of H↓ these terms only vanish in the limit of an infinitely high magnetic field.

Returning to lower densities we note that in an infinitely high magnetic field two interacting bosons described by (1.21.) and (1.23.) interact via the triplet potential as follows via (1.22.). In finite fields the situation is more complicated. The potential then depends on the hyperfine states involved in the collision

$$V_{eff}^{(aa)} = [\cos^4\theta + \frac{1}{4}\sin^2 2\theta + \sin^4\theta]\ V_T + \frac{1}{4}\sin^2 2\theta\ V_S$$

$$V_{eff}^{(bb)} = V_T$$

$$V_{eff}^{(ab)} = V_T \qquad \text{(scattering via } \Phi^S\text{)}$$
$$V_{eff}^{(ab)} = \cos^2\theta\, V_T + \sin^2\theta\, V_S \qquad \text{(scattering via } \Phi^{AS}\text{)} \tag{1.24.}$$

In the high field limit this reduces to

$$V_{eff}^{(aa)} \approx V_T + \varepsilon^2 V_S$$
$$V_{eff}^{(bb)} = V_T$$
$$V_{eff}^{(ab)} = V_T \qquad \text{(scattering via } \Phi^S\text{)} \tag{1.24b.}$$
$$V_{eff}^{(ab)} \approx V_T + \varepsilon^2 V_S \qquad \text{(scattering via } \Phi^{AS}\text{)}$$

Thus for a field of 10 Tesla, where $\varepsilon^2 \equiv \sin^2\theta = 10^{-5}$, one may assume $V_{eff} = V_T$ for all collisions. Some care is required since the triplet potential is much shallower than the singlet. For most internuclear separations the argument is trivial since $|V_S| \lesssim |V_T|$ everywhere except near the zero crossing of V_T. However, also the position of the crossing is not significantly affected by the $\varepsilon^2 V_S$ term because at the crossing $\varepsilon^2|V_S| \ll |V_T(R_{minimum})|$ (see section 1.1.1.).

Thus, assuming that the various arguments presented in this section may be generalized for a many-body system, an interacting gas of H↓ atoms in a high magnetic field behaves as a gas of chargeless point-like bosons interacting via the triplet potential for densities $\lambda_{th}^{-3} < n \ll 1.6 \times 10^{22}$ H↓/cm^3. However, since the H↓ atoms may exist in two different hyperfine states the statistics of this system differ from the well known spin-zero Bose-statistics. The properties of the gas will depend on the population of both spin states and in particular the (nuclear) relaxation between these states. For rapid relaxation the $|b\rangle$ state may be considered a spin excitation, whereas in the absence of nuclear relaxation the system behaves as a mixture of two distinguishable Bose systems.

1.2. PROPERTIES OF H↓

1.2.1. *Introduction*

Unlike ^{4}He the properties of H↓ are strongly influenced by the presence of magnetic field gradients. This affects the single particle properties -enabling us to spin polarize the system by spatial separation of H↓ and H↑ - but also affects the many-body behavior. This aspect of the H↓ problem is not only very interesting but also essential to understand the behavior of the system. Magnetic field inhomogeneities may be suppressed but can never be avoided completely under experimental conditions, so it is important to be aware of their consequences.

We introduce the basic concepts of the many-body theory on the basis of the experimental configuration used in our laboratory. It will be shown that the magnetic field gradients lead to a unique spatial separation between Bose condensate and normal fluid, which is most evident for the non-interacting gas {Sections (1.2.2) and (1.2.3)} but should remain an important identifying feature for Bose-Einstein condensation also in the presence of interactions {Sections (1.2.4) - 1.2.11)}. The presence of the nuclear spin and the hyperfine interaction do not just complicate the picture, but rather enrich the phenomena that can be observed once the system is brought into the Bose-condensed state. Some of these phenomena are discussed in Sections (1.2.12) - (1.2.14).

Clearly these properties, all associated with the spatial distribution of the gas in an inhomogeneous field, represent only a very specific class of phenomena that may be observed in H↓. They were selected in view of their relevance for the present thesis work (e.g. Chapter 4) and the recent interest in these phenomena in the literature. Moreover, the important class of thermodynamic properties has received a lot of theoretical interest in the past and has been reviewed extensively by Huang.[17]

Consider gaseous H↓ to be confined in a tube positioned along the axis of an axially symmetric magnetic field $B(x, r_\perp)$, which may be approximated over the region accessible to H↓ by the following expressions:

$$\begin{aligned} B(x,o) &= B_o[\,1 - (x/x_m)^2] \\ B(o,r_\perp) &= B_o[\,1 + \tfrac{1}{2}(x/x_m)^2\,] \end{aligned} \qquad (2.1.)$$

where $B_o \equiv B(o,o)$ is the central field and x_m sets the length scale. For the magnet used in our experiments B_o = 10 T and x_m = 51 mm. Neglecting

the nuclear spin the hamiltonian of the system is given by

$$\mathcal{H} = \sum_i \{-\frac{\hbar^2}{2m}\Delta_i + g\mu_\beta \vec{S}_i \cdot \vec{B}(\vec{r})\} + \frac{1}{2}\sum_{\substack{i,j \\ i\neq j}} V(r_{ij}) \qquad (2.2a.)$$

where $\hbar$ is Planck's constant, m the atomic mass, g the Landé-factor, μ_β Bohr's magneton and V the $^3\Sigma_u^+$ -potential. The Zeeman term is interpreted as an external single particle potential field so that the hamiltonian may be rewritten as:

$$\mathcal{H} = \sum_i \{-\frac{\hbar^2}{2m}\Delta_i + U_{ext}(\vec{r})\} + \frac{1}{2}\sum_{\substack{i,j \\ i\neq j}} V(r_{ij}) \qquad (2.2b.)$$

with an appropriate choice of the zero of energy and ignoring the radial field gradient

$$U_{ext}(\vec{r}) = \frac{1}{2} m\omega_o^2 x^2 \qquad (2.3a.)$$

with

$$\omega_o^2 = 2\mu_\beta B_o / (mx_m^2) \qquad (2.3b.)$$

Without the interaction term the hamiltonian reduces to the simple harmonic oscillator form for motion in the x-direction, whereas in the yz-direction the motion is free particle like if the radial field gradients are ignored.

1.2.2. *The non-interacting case*

Before addressing ourselves to the more realistic situation of the (weakly) interacting Bose gas some basic concepts in Bose systems are introduced for the non-interacting case. The attraction of this simple theory arises from its elegance and mathematical simplicity, but its presentation seems only justified in view of the results of more sophisticated treatments proving the model to give a correct qualitative description of various properties of H↓. An early discussion of Bose-condensation in inhomogeneous fields is given by De Groot et al.[18]

To calculate the density distribution we work with a grand ensemble constructed on the basis of the non-interacting hamiltonian $\hat{\mathcal{H}}_o$. The density distribution is then found as the ensemble average of the number density operator $\hat{\rho}(r)$

$$\rho(\vec{r}) = \ll \hat{\rho}(\vec{r}) \gg_o = \sum_k |\varphi_k(\vec{r})|^2 \langle n_k \rangle_o \qquad (2.4.)$$

$$\langle n_k \rangle_o = \frac{1}{e^{-\beta(\mu-\varepsilon_k)}-1} \qquad (2.4a.)$$

where $\langle n_k \rangle_o = \langle\langle \hat{n}_k \rangle\rangle_o$ is the Bose occupation function for the single particle eigenstates, with energy ε_k obtained from Schrödinger's equation

$$-\frac{\hbar^2}{2m}\nabla^2\varphi_k(\vec{r}) + U_{ext}(\vec{r})\,\varphi_k(\vec{r}) = \varepsilon_k\varphi_k(r) \qquad (2.5.)$$

μ is the chemical potential and $\beta = (k_B T)^{-1}$; n_k is obtained by evaluating the trace with the statistical operator $\hat{\rho}$ over all many-body eigenstates of the system

$$\langle\langle \hat{n}_k \rangle\rangle_o \equiv \mathrm{Tr}\,\langle \hat{\rho}\hat{n}_k \rangle_o \qquad (2.6.)$$

$$\hat{\rho} = \frac{1}{Z_{gr}} e^{\beta(\mu\hat{N} - \hat{\mathcal{H}})} \qquad (2.7.)$$

where Z_{gr} is the grand partition function, $\hat{N}$ the number operator. The symbol "$\hat{}$" is reserved to identify operators. The solutions of equation (2.5.) are straightforward. The motion of the particles perpendicular to the x-axis is free-particle-like, whereas the axial motion is oscillatory in nature. If we limit the yz motion to a $L \times L$ area near the symmetry axis we obtain

$$\varphi_k(\vec{r}) = \frac{1}{\sqrt{L}} e^{ik_y y} \cdot \frac{1}{\sqrt{L}} e^{ik_z z} \cdot \Psi_{n_x}(x) \qquad (2.8.)$$

$$\varepsilon_k = \frac{\hbar^2}{2m}(k_y^2 + k_z^2) + (n_x + \tfrac{1}{2})\hbar\,\omega_o \qquad (2.8a.)$$

Note that we have introduced periodic boundary conditions to treat the yz-motion. $\Psi_{n_x}(x)$ is an harmonic oscillator eigenstate.

The exact knowledge of the wave functions may be useful if we are interested in the details of a particular state. For our present purpose, carrying out summation (2.4.), it is more of a nuissance. Under typical experimental conditions $T \gg \hbar\omega_o / k_B \simeq 5 \times 10^{-8}$ K. Thus a large number of oscillator states is occupied and essentially all detail of the individual wave function will be averaged out by the summation. The problem may therefore be simplified by replacing the wave function by its quasi-classical approximation in terms of the normalized first order W K B solution to the Schrödinger equation. (The conditions for the W K B solution to be justified are discussed by Van den Bergh.[19]).

$$|\varphi_k(\vec{r})|^2 = \frac{1}{L^2}\left\{\frac{2m}{\hbar^2}\left[(n_x + \tfrac{1}{2})\hbar\omega_o - U_{ext}(\vec{r})\right]\right\}^{-\frac{1}{2}} \cdot \frac{m\omega_o}{\pi\hbar} \qquad (2.9.)$$

We are now set up to evaluate the summation. If we first assume $e^{\beta(\mu-\varepsilon_k)} < 1$

we may rewrite $\rho(\vec{r})$ as a fugacity expansion.

$$\rho(\vec{r}) = \sum_{\ell=1} z^{\ell} \sum_{k} e^{-\ell\beta\varepsilon_k} |\varphi_k(\vec{r})|^2 \qquad (2.10.)$$

where $z = e^{\beta(\mu-\varepsilon_o)}$ is the fugacity. $\varepsilon_o \equiv \frac{1}{2}\hbar\omega_o$. The summations over k_y and k_z are now readily carried out by replacing the sums by integrals. They each yield a factor $\lambda_{th}^{-1}\,\ell^{-1/2}$ where λ_{th} is the thermal wave length defined in section (1.1.3.). The sum over n_x requires a bit more care. Note that only those terms contribute to $\rho(x)$ for which x lies within the turning points of $\psi_{m_x}(x)$. This means that the first non-vanishing term in the series is related to x through the turning point condition

$$(n_x + \tfrac{1}{2})\,\hbar\omega_o = \tfrac{1}{2}m\omega_o^2\,x^2 \qquad (2.11.)$$

Again changing from summation to integration we obtain

$$\rho(\vec{r}) = \frac{1}{\sqrt{\pi}}\lambda_{th}^{-3} \sum_{\ell=1}^{\infty} \frac{z^{\ell}}{\ell^{3/2}} \int_{U_{ext}(\vec{r})}^{\infty} d\varepsilon\, e^{-\ell\beta\varepsilon}\,[\varepsilon - U_{ext}(\vec{r})]^{-\frac{1}{2}} \qquad (2.12.)$$

or

$$\rho(\vec{r}) = \lambda_{th}^{-3}\, g_{3/2}(z) \qquad (2.12a.)$$

where

$$g_{\alpha}(x) \equiv \sum_{\ell=1}^{\infty} \frac{x^{\ell}}{\ell^{\alpha}} \qquad (2.13.)$$

$$z \equiv \exp\{\beta\,[\mu - \varepsilon_o - U_{ext}(\vec{r})]\} \qquad (2.14.)$$

For a tube (of cross-sectional area A) the total number of particles follows by integration over the volume

$$\langle N\rangle = \frac{Ax_m}{\lambda_{th}^3}\left[\frac{\pi k_B T}{\mu_\beta B_o}\right]^{1/2} g_2(z) \qquad (2.15.)$$

Expression (2.12a) can also be obtained by assuming local homogeneity and requiring the chemical potential to be constant over the potential well. Such an approach fails once the quasi-classical approximation breaks down.

1.2.3. *Spatial Bose-Einstein condensation*

Bose-Einstein condensation (BEC) occurs once the system can lower its free energy by preferentially populating its ground state instead of maintaining a smooth distribution of the population over all states. This happens when the chemical potential (negative at low densities) approaches ε_o.

The relation for the critical temperature for BEC follows from equation (2.15.) by setting $z = 1$.

$$T_c = \left[\frac{6}{\pi^2} \cdot \left(\frac{2\pi\hbar^2}{mk}\right)^{\frac{3}{2}} \cdot \left(\frac{\mu_\beta B}{\pi k}\right)^{\frac{1}{2}} \cdot \frac{\langle N\rangle}{Ax_m}\right]^{\frac{1}{2}} \qquad (2.16.)$$

Equation (2.4.) still holds, but we have to separate out $\langle n_o\rangle$ before it is allowed to replace the sum by an integral

$$\rho(\vec{r}) = |\varphi_o(\vec{r})|^2 \langle n_o\rangle + \frac{1}{\lambda_{th}^3} g_{3/2}(z_c) \qquad (2.17.)$$

where

$$z_c \equiv \exp\left[-\beta U_{ext}(\vec{r})\right] \qquad (2.17a.)$$

Integrating (2.17.) over space we find

$$\langle N\rangle = \langle n_o\rangle + \frac{Ax_m}{\lambda_{th}^3} \left(\frac{\pi k_B T}{\mu_\beta B_o}\right)^{\frac{1}{2}} g_2(1) \qquad (2.18.)$$

Expressing the second term of (2.18.) in terms of T, T_c and $\langle N\rangle$ (using (2.16.) we obtain a relation for the ground state occupation below T_c

$$\langle n_o\rangle = \langle N\rangle \cdot \left[1-(T/T_c)^2\right] \qquad (2.19.)$$

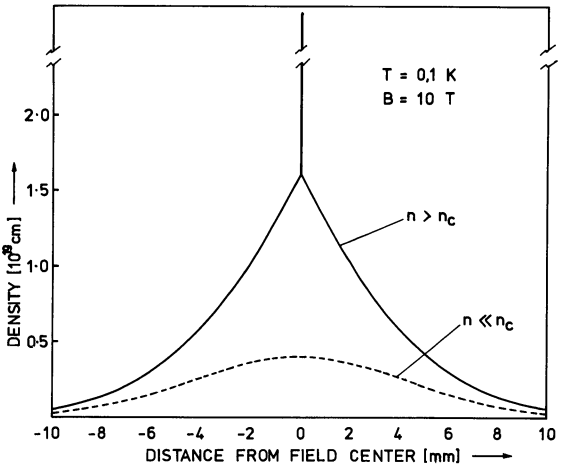

Fig. 3–Density distribution of H↓ along the axis of a magnetic field configuration as used in our experiments with B_o=10 T. The gas is treated as an ideal Bose gas. Above the critical density the condensate appears as a sharp spike in the density profile (solid line). Well below n_c the density profile has a gaussian shape (dashed line).

The presence of the external field causes BEC to occur in the narrow region of space defined by the oscillator ground state which has a width (between classical turning points) of $2(\hbar/m\omega_o)^{1/2} = 6 \times 10^{-4}$cm for our system operated at 10 Tesla, see Fig. 3.

1.2.4. *The interacting case*

Before we solve Schrödinger's equation for the interacting case it is useful to follow the approach of Goldman et. al.[20] and analyze the relative importance of the various characteristic energies involved and the associated lengths:

- The zero point energy $\varepsilon_{zp} = \frac{1}{2}\hbar\omega_o \approx 2.5 \times 10^{-5}$ mK
- The interaction energy $\varepsilon_{int} = \rho_o v_o \approx 0.4\ (\rho/10^{18})$mK
- The thermal energy $\varepsilon_{th} = kT_c \approx 16\ (\rho/10^{18})^{\frac{2}{3}}$ mK

where ρ_o is the density in the center of the field in units (H↓/cm^3); v_o is the interaction strength in the scattering length approximation, $v_o = 4\pi a\hbar^2/m$, a is the s-wave scattering length.[4] T_c is the (ideal gas) critical temperature for BEC. A field B_o = 10 T is assumed throughout this chapter.

The associated characteristic lengths are obtained by balancing the characteristic energies against the external field according to $\varepsilon_{ch} = \frac{1}{2}m\omega_o^2 x_{ch}^2$

- $x_{zp} = (\hbar/m\omega_o)^{\frac{1}{2}} \approx 3 \cdot 10^{-4}$ cm
- $x_{int} = (2\rho_o v_o/m\omega_o^2)^{\frac{1}{2}} \approx 0.04\ (\rho/10^{18})^{\frac{1}{2}}$ cm
- $x_{th} = (2kT_c/m\omega_o^2)^{\frac{1}{2}} \approx 0.2\ (\rho/10^{18})^{\frac{1}{2}}$cm

The significance of these figures is straightforward. Above T_c and for any experimentally conceivable density $\varepsilon_{th} \gg \varepsilon_{int}$. Hence the interactions may be neglected (as in the preceeding Section) or treated perturbatively in a weakly interacting Bose picture. Below T_c the ideal gas model predicts a macroscopic occupation of the oscillator ground state with energy ε_{zp}. However, $x_{int} \gg x_{zp}$ so that an enormous broadening of the ground state is to be expected (as discussed in chapter 4 and ref. 21). A natural way to account for this effect is to replace Schrödinger's equation (2.5.) by a self consistent set of coupled (Hartree-Fock) mean field equations as done by Goldman et al.[20] and Huse and Siggia.[22]

1.2.5. *Hartree-Fock approximation*

We first rewrite the hamiltonian (2.2b.) in terms of construction operators, approximating the interactions by shape independent pseudopotentials

$$\frac{1}{2}\sum_{\substack{i,j\\ i\neq j}} V(r_{ij}) = \frac{1}{2}v_o \sum_{\substack{i,j\\ i\neq j}} \delta(r_{ij}) \tag{2.20.}$$

We limit ourselves to the restricted set of terms of the operator density $\hat{\mathcal{H}}(\vec{r})$ required to calculate the diagonal matrix elements of a, so far, undetermined number representation $\{|n_\gamma>\}$

$$\hat{\mathcal{H}} = \int d\vec{r}\, \hat{\mathcal{H}}(\vec{r}) \tag{2.21a.}$$

We divide $\hat{\mathcal{H}}(\vec{r})$ in two parts, separating the single particle terms from the interaction terms:

$$\hat{\mathcal{H}}(\vec{r}) = \hat{\mathcal{H}}_1(\vec{r}) + \hat{\mathcal{H}}_2(\vec{r}) \tag{2.21b.}$$

where

$$\hat{\mathcal{H}}_1(\vec{r}) = \sum_k \varphi_k^*(\vec{r})\,[-\frac{\hbar^2}{2m}\nabla^2 + U_{ext}(\vec{r})]\,\varphi_k(\vec{r})\hat{n}_k \tag{2.21c.}$$

$$\hat{\mathcal{H}}_2(\vec{r}) = \frac{v_o}{2}\sum_k |\varphi_k(\vec{r})|^2 \cdot |\varphi_k(\vec{r})|^2\, \hat{n}_k(\hat{n}_k-1) + v_o \sum_{\substack{k,\ell\\ k\neq\ell}} |\varphi_k(\vec{r})|^2 \cdot |\varphi_\ell(\vec{r})|^2\, \hat{n}_k\,\hat{n}_\ell \tag{2.21d.}$$

The statistical variational principle

$$\Omega \leqslant \tilde{\Omega} \equiv \Omega_o + \ll \hat{\mathcal{H}} - \hat{\mathcal{H}}_o \gg_o \tag{2.22.}$$

enables us to obtain an upper limit for the thermodynamic potential Ω through variation of the trial ensemble defined by a trial hamiltonian $\hat{\mathcal{H}}_o$.
We choose for $\hat{\mathcal{H}}_o$ an arbitrary one-body trial hamiltonian $\hat{\mathcal{H}}_o = \sum_i \hat{H}(\vec{r}_i)$

$$\hat{H}(\vec{r}_i)\,\varphi_k(\vec{r}_i) = \varepsilon_k \varphi_k(\vec{r}_i) \tag{2.23.}$$

$$\hat{\mathcal{H}}_o(\vec{r}) = \sum_k \varepsilon_k |\varphi_k(\vec{r})|^2\, \hat{n}_k \tag{2.24.}$$

With the trial ensemble we find for $\tilde{\Omega}(\vec{r})$

$$\begin{aligned}\tilde{\Omega}(r) = {} & kT \sum_k |\varphi_k(\vec{r})|^2 \ln(1 - \ell^{\beta(\mu-\varepsilon_k)}) + \\ & + \sum_k \varphi_k^*(\vec{r})\,[-\frac{\hbar^2}{2m}\nabla^2 + U_{ext}(\vec{r}) - \varepsilon_k]\,\varphi_k(\vec{r}) \ll \hat{n}_k \gg_o + \\ & + \sum_k \varphi_k^*(\vec{r})\,[\frac{v_o}{2}\,|\varphi_k(\vec{r})|^2]\,\varphi_k(\vec{r}) \ll \hat{n}_k(\hat{n}_k - 1) \gg_o +\end{aligned} \tag{2.25.}$$

$$+ \sum_{\substack{k,\ell \\ k\neq\ell}} \varphi_k^*(\vec{r}) \left[v_o |\varphi_\ell(\vec{r})|^2 \right] \varphi_k(\vec{r}) \ll \hat{n}_k \hat{n}_\ell \gg_o$$

where

$$\ll \hat{n}_k \gg_o = \langle n_k \rangle_o \tag{2.26a.}$$

$$\ll \hat{n}_k \hat{n}_\ell \gg_o = \langle n_k \rangle_o \langle n_\ell \rangle_o \qquad k\neq\ell \tag{2.26b.}$$

$$\ll \hat{n}_k (\hat{n}_k - 1) \gg_o = 2 \langle n_k \rangle_o^2 \tag{2.26c.}$$

One notes that expression (2.26c.) becomes unphysical when $\langle n_k \rangle_o = O(N)$. This happens for the ground state $\varphi_o(\vec{r})$ in the case of Bose-Einstein condensation. Once a state becomes macroscopically occupied the ensemble leads to macroscopic fluctuations ($\Delta\rho_o$) in the density

$$\begin{aligned} \Delta\rho_o &= \frac{1}{V} \left[\ll \hat{n}_o^2 \gg_o - \ll \hat{n}_o \gg^2 \right]^{\frac{1}{2}} \\ &= \frac{1}{V} \left[\langle n_o \rangle_o (\langle n_o \rangle_o - 1) \right]^{\frac{1}{2}} \\ &= \frac{1}{V} O(N) \\ &= O(\rho) \end{aligned}$$

A well known procedure to avoid this phenomenon is to use the Bogoljubov ansatz[23] which is here equivalent with replacing the number operator $\hat{n}_o$ by a real number

$$\hat{n}_o = N_o \tag{2.27.}$$

1.2.6. *$T > T_c$*

We first assume the fluctuations to remain finite in the thermodynamic limit and minimize $\tilde{\Omega}$ by variation of the occupation numbers $\langle n_k \rangle_o$. This is particularly simple for the case of the grand ensemble since there is no restriction on the total number of particles

$$\begin{aligned} \frac{\partial \tilde{\Omega}(\vec{r})}{\partial \langle n_k \rangle} &= \varphi_k^*(\vec{r}) \left[-\frac{\hbar^2}{2m} \nabla^2 + U_{ext} - \varepsilon_k \right] \varphi_k(\vec{r}) + \\ &+ \varphi_k^*(\vec{r}) \left[\frac{v_o}{2} |\varphi_k(\vec{r})|^2 \right] \varphi_k(\vec{r}) \; 4 \langle n_k \rangle_o + \\ &+ 2 \sum_{\ell\neq k} \varphi_k^*(\vec{r}) \left[v_o |\varphi_\ell(\vec{r})|^2 \right] \varphi_k(\vec{r}) \langle n_\ell \rangle_o \end{aligned} \tag{2.28.}$$

The minimum[22] is found when $\frac{\partial \tilde{\Omega}}{\partial \langle n_k \rangle} = 0$ for all values of k or equivalently

$$\left[-\frac{\hbar^2}{2m} \nabla^2 + U_{ext}(\vec{r}) + 2 v_o \rho(\vec{r}) \right] \varphi_k(\vec{r}) = \varepsilon_k \varphi_k(\vec{r}) \tag{2.29.}$$

This relation represents a set of Hartree-Fock equations coupled through

expression (2.4.) for the density.

Since $\varepsilon_{th} \gg \varepsilon_{int}$ as discussed in Section (1.2.4.) the equations may be solved to a satisfactory degree of self consistency by an iterative procedure. First we set $\rho(\vec{r}) \equiv 0$ and obtain the harmonic oscillator solutions (2.8.) equivalent with the non-interacting density distribution (2.12a.). For simplicity we limit ourselves to the case that

$$g_{3/2}(z) \approx z = e^{\beta(\mu - \varepsilon_o - \frac{1}{2}m\omega_o^2 x^2)} \qquad (2.30.)$$

Furthermore , the strongest effects are to be expected in the center of the field where the density is highest. Thus it seems justified to further approximate $g_{3/2}$ for this analysis by a series expansion

$$\rho(\vec{r}) = \rho_o \left[1 - (x/x_o)^2 + \ldots.\right] \qquad (2.31.)$$

where ρ_o is the density in the center of the field (see Section (1.2.4.)) and x_o is the half-width of the (non-interacting) gaussian density distribution

$$x_o \equiv x_m (kT/\mu_\beta B_o)^{\frac{1}{2}} \qquad (2.32.)$$

With (2.31.) the effective single particle potential of equation (2.29.) reduces to

$$U_{ext} + 2v_o\rho = \\ = 2v_o\rho_o + \left[\frac{1}{2}m\omega_o^2 x_o^2 - \frac{1}{2}m\omega_o^2 x_{int}^2\right] \left(\frac{x}{x_o}\right)^2 + \ldots. \qquad (2.33.)$$

where the first term represents the first order shift of the energy levels due to the perturbation and we used a slightly different definition of x_{int}: ($2\, v_o\rho_o = \frac{1}{2}m\omega_o^2 x_{int}^2$; compare with Section (1.2.4.)). Since $x_{int} \ll x_o$ we note that one has obtained a rather good degree of self consistency after one iteration and that the ideal gas provides a remarkably good approximation to the density profile above T_c.

One may argue that in general the use of WKB-solutions to equation (2.29.) is justified if the (effective) potential varies sufficiently slow with position.[19,22] For our system this implies

$$\rho(\vec{r}) = \lambda_{th}^{-3}\, g_{3/2}\{\exp[\beta(\mu - 2v_o\rho(\vec{r}) - U_{ext}(\vec{r}))]\} \qquad (2.34.)$$

1.2.7. *$T < T_c$*

Below T_c we use the Bogoljubov ansatz (2.27.) and vary again with respect to the occupation numbers N_o and $\langle n_k \rangle$. For $[\partial\tilde{\Omega}(\vec{r})/\partial \langle n_k \rangle]$ $k \neq 0$ we obtain the same results as above T_c (2.28.), $[\partial\tilde{\Omega}/\partial \langle n_o \rangle]$ however becomes

$$\begin{aligned}\frac{\partial\tilde{\Omega}(\vec{r})}{\partial N_o} &= \varphi_o^*(\vec{r})\left[-\frac{\hbar^2}{2m}\nabla^2 + U_{ext}(\vec{r}) - \varepsilon_k\right]\varphi_o(\vec{r}) + \\ &+ \varphi_o^*(\vec{r})\left[\frac{v_o}{2}|\varphi_o(\vec{r})|^2\right]\varphi_o(\vec{r})\,(2N_o - 1) + \\ &+ 2\varphi_o^*(\vec{r})\left[v_o \sum_{k\neq o}|\varphi_k(\vec{r})|^2 \langle n_k\rangle_o\right]\varphi_o(\vec{r})\end{aligned} \tag{2.35.}$$

Thus below T_c (and putting $2N_o - 1 \approx 2N_o$) the Hartree-Fock equations for φ_o and φ_k are different:

$$\begin{aligned}&\left[-\frac{\hbar^2}{2m}\nabla^2 + U_{ext}(\vec{r}) + 2v_o\rho_n(\vec{r}) + v_o\rho_c(\vec{r})\right]\varphi_o(\vec{r}) = \varepsilon_o\varphi_o(\vec{r}) \\ &\left[-\frac{\hbar^2}{2m}\nabla^2 + U_{ext}(\vec{r}) + 2v_o\{\rho_n(\vec{r}) + \rho_c(\vec{r})\}\right]\varphi_k(\vec{r}) = \varepsilon_k\varphi_k(\vec{r}) \quad (k\neq 0)\end{aligned} \tag{2.36.}$$

where

$$\begin{aligned}\rho(\vec{r}) &= \rho_c(\vec{r}) + \rho_n(\vec{r}) \\ \rho_c(\vec{r}) &\equiv |\varphi_o(\vec{r})|^2 N_o \\ \rho_n(\vec{r}) &\equiv \sum_{k\neq o}|\varphi_k(\vec{r})|^2 \langle n_k\rangle_o\end{aligned} \tag{2.37.}$$

At first glance the new equations have a rather serious deficiency that violates the variational principle. We arrived at a result, where the ground state requires a different hamiltonian than the excited states resulting in non-orthogonality between ground state and excitations. However, in the quasi-classical approximation for $k \to \infty$

$$\int \varphi_o(\vec{r})\,\varphi_k(\vec{r})\,d\vec{r} \to 0$$

so that the problem only is serious for the first few excited states. Since this only affects a very restricted and finite set of equations it is plausible that the non-orthogonality is of little relevance for the results to be obtained. A more careful analysis of this problem has been made by Huse and Siggia[22] and by Goldman[20,24] and leads to a non-local term in the Hartree-Fock equations for $k \neq 0$ which can be shown to be of no consequence to the results.

1.2.8. *The zero temperature limit*

Before we continue with the self consistent solution to the Hartree-Fock equations for finite temperature we first analyze the zero temperature limit

$$[-\frac{\hbar^2}{2m}\nabla^2 + U_{ext}(\vec{r}) + v_o\rho_o(\vec{r})]\ \varphi_o(\vec{r}) = \varepsilon_o\varphi_o(\vec{r}) \qquad (2.38.)$$

This equation was first studied by Gross[25] and Pitaevskii[26] and may be solved approximatively (to obtain the density profile) by neglecting the kinetic energy completely (recall that $\varepsilon_{zp} \ll \varepsilon_{int}$):

$$U_{ext}(\vec{r}) + v_o\rho_o(\vec{r}) = \varepsilon_o \qquad (2.39.)$$

Since $\rho_o(r)$ must be positive, this may be rewritten as

$$\rho_o(\vec{r}) = \frac{1}{v_o}[\varepsilon_o - U_{ext}(\vec{r})]\ \theta[\varepsilon_o - U_{ext}(\vec{r})] \qquad (2.40.)$$

where θ is the unit-step-function. The single particle ground state energy, ε_o, follows from (2.40.) by setting $\vec{r} = 0$. After substituting the result $[\varepsilon_o = v_o\rho_o(o)]$ into (2.40.) we arrive at the result shown in Fig. 4A along with the effective one particle potential $U^{(o)}_{eff}(\vec{r}) \equiv U_{ext}(\vec{r}) + v_o\rho_o(\vec{r})$.

$$\rho_o(\vec{r}) = \frac{1}{v_o}[v_o\rho_o(o) - U_{ext}(\vec{r})]\ \theta(x_{zp} - x) \qquad (2.41.)$$

$$U^{(o)}_{eff}(\vec{r}) = \begin{cases} v_o\rho_o(o) & (\text{for } |x| \leq x_{int}) \\ U_{ext}(\vec{r}) & (\text{for } |x| > x_{int}) \end{cases}$$

This result is equivalent with the result of Walraven and Silvera (chapter 4). It shows that the condensate will distribute itself in such a way that the interaction energy is balanced by the external field.

A justification for the neglect of the kinetic energy term may be found in first order perturbation theory with respect to the ground state $[\varphi^{(o)}_o(\vec{r})]$ of the unperturbed (non-interacting) oscillator.

$$\varepsilon_o = \varepsilon^{(o)}_o + \varepsilon^{(1)}_o = \frac{1}{2}\hbar\omega_o + v_o\rho_o(o) \simeq v_o\rho_o(o) \qquad (2.42.)$$

where

$$\varepsilon^{(o)}_o = \int d\vec{r}\ \varphi^{(o)*}_o(\vec{r})\ [-\frac{\hbar^2}{2m}\nabla^2 + U_{ext}(\vec{r})]\ \varphi^{(o)}_o(\vec{r}) = \frac{1}{2}\hbar\omega_o$$

$$\varepsilon^{(1)}_o = \int d\vec{r}\ |\varphi^{(o)}_o(\vec{r})|^2\ v_o\rho_o(\vec{r}) \simeq v_o\rho_o(o)$$

Note that the result for $\varepsilon_o^{(1)}$ is only correct since the density does not vary significantly over the range of $\varphi_o^{(o)}(\vec{r})$ (recall that $x_{zp} \ll x_{int}$).

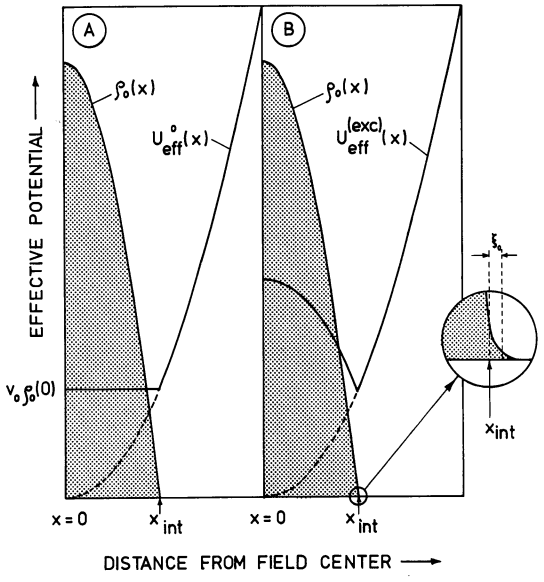

Fig. 4-Effective single-particle potentials at T=0K. A. Potential used to describe condensate. B. Potential used to describe the single-particle excitation spectrum. The distribution of the condensate along the axis of the magnet is also shown. The inset shows schematically how the condensate density falls off smoothly to zero over a healing length ξ_o.

1.2.9. *The excitation spectrum*

The single particle excitation spectrum follows from the Hartree-Fock equations by assuming $\langle n_\ell \rangle_o = 0$ for all states ℓ except $\varphi_{\ell=k}(\vec{r})$.

$$[-\frac{\hbar^2}{2m}\nabla^2 + U_{ext}(\vec{r}) + 2v_o\rho(\vec{r})]\ \varphi_k(\vec{r}) = \varepsilon_k\varphi_k(\vec{r}) \qquad (2.43.)$$

Since $\rho(\vec{r}) \simeq \rho_o(\vec{r})$ one notices immediately that there is a different effective potential for the excitations $U^{(exc)}_{eff}(\vec{r}) \equiv U_{ext}(\vec{r}) + 2v_o\rho(\vec{r})$; see Fig. 4B.

$$U^{(exc)}_{eff}(\vec{r}) = \begin{cases} v_o\rho_o(o) + v_o\rho_o(\vec{r}) & (|x| \leq x_{int}) \\ U_{ext}(\vec{r}) & (|x| > x_{int}) \end{cases}$$

We solve equation (2.43.) for ε_k using again first order perburtation theory as in the preceeding section:

$$\varepsilon_k = (n_k + \frac{1}{2})\,\hbar\omega_o + 2v_o \int d\vec{r}\, |\varphi_k^{(o)}(\vec{r})|^2 \rho(\vec{r}) \qquad (2.45.)$$

Limiting ourselves to the low-lying excitations and putting $\rho = \rho_o$ this expression reduces to

$$\varepsilon_k = (n_k + \frac{1}{2})\,\hbar\omega_o + 2v_o\rho_o(o) \qquad (2.45a.)$$

Note that the first order perburtation theory leads to a gap of size $v_o\rho_o(o)$ in the excitation spectrum:

$$\begin{aligned} E_o &= N\varepsilon_o \\ E_{o,k} &= (N-1)\varepsilon_o + \varepsilon_k \\ &= E_o + v_o\rho_o(o) + n_k\hbar\omega_o \end{aligned} \qquad (2.46.)$$

The gap is known[17] to be an artifact of the first order perturbation theory and may be avoided using a canonical transformation to quasi-particles - the Bogoljubov transformation. From Fig. 4B one expects the low-lying excitations to be localized at the minima of the effective potential. However, Huse and Siggia point out that within the Bogoljubov-Hartree-Fock approximation the low-lying excitations experience an effective potential almost identical to that seen by the condensate. This implies phonon-like excitations throughout the condensate as is the case for ^{4}He.

1.2.10. *The concept of healing length*

An obvious deficiency of the result of equation (2.40.), shown in Fig. 4, is the sharp edge of the condensate density at $x = x_{int}$ which is in contradiction with the omission of the kinetic energy term from the hamiltonian. A better approximation is shown in the inset of Fig. 4. where the condensate density falls off smoothly to zero, over a region ξ_o. This distance ξ_o, over which the wave function can adjust itself to a rapidly varying (effective) potential, is known as the healing length and studied in detail by Gross[27] in relation to the structure of vortices in liquid helium.

The healing length may be estimated by reducing the size of a cube of linear dimension until the kinetic energy of a single particle in its translational ground state equals the interaction energy due to the presence of other particles in the box:

$$\xi_o = (8\pi\rho v_o)^{-\frac{1}{2}}$$
$$= 2.3 \times 10^{-6} \ (10^{18}/\rho)^{\frac{1}{2}} \text{ cm} \qquad (2.47.)$$

Note that for typical experimental conditions $\xi_o \ll x_{int}$, so that the results of the mean field theory will be reliable as far as healing effects are concerned.

1.2.11. *Spatial separation of condensate and normal component at finite temperatures*

The solutions for the Hartree-Fock equations for T = 0 and T > T_c are readily generalized to obtain a coupled pair of equations that describe the density distributions of normal component and condensate at finite temperatures.

$$\rho_o(\vec{r}) = \frac{1}{v_o} \{\mu - 2v_o\rho_n(\vec{r}) - U_{ext}(\vec{r})\} \ \theta\{\mu - 2v_o\rho_n(\vec{r}) - U_{ext}(\vec{r})\} \qquad (2.48a.)$$

$$\rho_n(\vec{r}) = (1/\lambda_{th})^3 \ g_{3/2}\{\exp[\beta(\mu - 2v_o\rho_n(\vec{r}) - 2v_o\rho_o(\vec{r}) - U_{ext}(\vec{r}))]\} \qquad (2.48b.)$$

where we have replaced ε_o by μ since we are now interested in temperatures below T_c. The expression for $\rho_n(\vec{r})$ may be simplified by substituting equation (2.48a.) in (2.48b.). This leads to an expression for $\rho_n(\vec{r})$ which no longer depends explicitely on $\rho_o(\vec{r})$:

$$\rho_n(\vec{r}) = \lambda_{th}^{-3} \ g_{3/2}\{\exp -\beta|\mu - 2v_o\rho_n(\vec{r}) - U_{ext}(\vec{r})|\} \qquad (2.49.)$$

Returning to equation (2.48a.) we note once more, as in Section (1.2.8.), that the interactions tend to broaden the density profile until the interaction energy is balanced by the external potential. However, for a given density, the interaction energy is larger for the normal component than for the condensate as seen from the Hartree-Fock equations. Therefore, the normal component will tend to spread more which results in a spatial separation of the two components, although the effect is not complete. The equations (2.48a.) and (2.48b.) have been solved to self consistency by Goldman et. al. [20] and Huse and Siggia.[22] Although there is a slight disagreement between both results as far as the detailed density profile at the edge of the condensate is concerned, all authors agree that the condensate may be recognized as a distinct feature of the density profile and as such may be used to detect BEC as suggested by Walraven and Silvera (Chapter 4). The results

of Goldman et. al. are reproduced in Fig. 5.

Huse and Siggia suggest that the depression of the normal density (within the condensate), implicit to equation (2.49.), is an artifact that disappears with the use of the Bogoljubov-Hartree-Fock approximation without affecting the qualitative results for the density profiles presented above. Finally we note that for cross-sectional densities of at least $N/A = 10^{18}$ H↓/cm^2 the ideal Bose gas provides a remarkably good approximation for T_c. One finds [20] $T_c = 30.2$ mK for B = 10 T, whereas the mean field theory yields 29.34 mK for the same experimental conditions.

1.2.12. *Properties associated with the nuclear spin*

So far we neglected the possible influence of the atomic hyperfine structure on the collective properties of the gas. However, the nuclear spin affects the total number of accessible states and therefore has a direct influence on the onset, possibly also the nature, of BEC.

The nuclear relaxation rate which determines the time scale over which thermal equilibrium between the nuclear states is achieved is also important. If the nuclear relaxation proceeds slowly, i.e. at a rate negligible in comparison to the experimental time scale, the system behaves as a mixture of two distinguishable Bose systems (with separate chemical potentials) each of which may undergo BEC. On the other hand, in the case of rapid relaxation, one chemical potential is sufficient to describe the system and BEC only occurs for the spin configuration with the lowest energy (the $|a\rangle$ -state defined in section (1.1.2)).

1.2.13. *Rapid nuclear relaxation*

In the case of fast relaxation one expects spontaneous nuclear polarization, once the $|b\rangle$ -state (for definition of symbols in this section see (1.1.2.)) can no longer be populated thermally, thus for temperatures $T \lesssim T_{hfs}$ where $T_{hfs} \equiv (E_b - E_a)/k_B$ corresponds to the hyperfine splitting between the $|a\rangle$ - and $|b\rangle$ -states. In the high field limit $T_{hfs} \simeq (a/2 + g_N\mu_N B)/k_B \simeq 54$ mK at 10 T. The relevance of this nuclear polarization with respect to BEC is straightforward. By polarizing the nuclear spins we reduce the total number of accessible states by a factor 2 and therefore also the density required for BEC. Moreover, since T_{hfs} is field dependent, BEC may be induced at constant density by varying the magnetic field. Aspects of this nature have been discussed to some more detail by Mullin[28] for an ideal Bose gas of hydrogen atoms in a uniform external field.

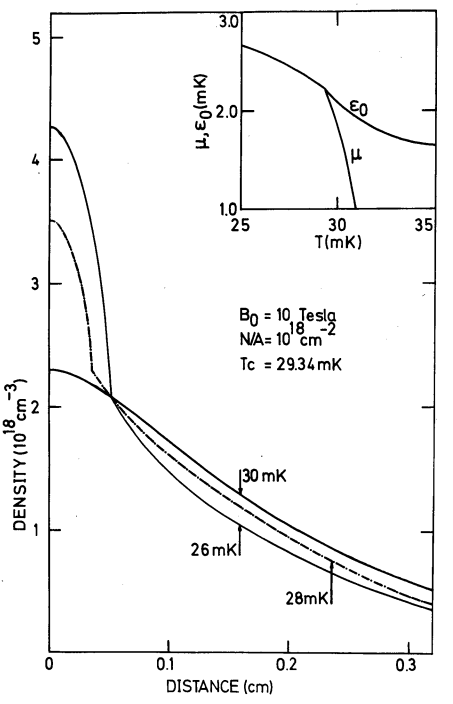

Fig.5-Axial density distribution of H↓ near the critical temperature for BEC (after ref. 20). The same field profile is assumed as in Fig. 3. The inset shows the temperature dependence of the chemical potential μ and the single particle ground state energy ε_0.

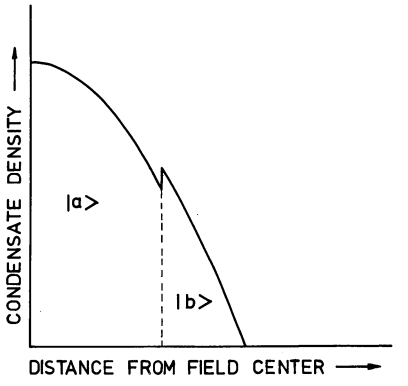

Fig.6-Phase separation in a two-compenent condensate, containing atoms in both |a> and |b> hyperfine states. A change in density at the interface accounts for the local pressure equilibrium.

1.2.14. *Slow nuclear relaxation - Phase separation between condensates*

The other limit, negligible nuclear relaxation, is more interesting. The system now behaves as a mixture of two distinguishable Bose systems, each of which may undergo BEC. In contrast to what might be expected, nuclear polarization can also occur in this limit. As pointed out by Statt and Berlinsky[29] this is to be the case if recombination dynamics are included in the picture. A discussion of these aspects of the problem, which may well turn out to be of most relevance to experiment, is postponed till section (1.4.).

The superfluid hydrodynamics of a Bose mixture have been studied by Siggia and Ruckenstein[30,31] but a discussion of their analysis falls outside the scope of this thesis, due to its rather specialized and detailed nature.

Here, we shall discuss one interesting feature of Bose mixtures: phase separation of the two condensates of a Bose mixture of $|a\rangle$ - and $|b\rangle$ -state hydrogen atoms in an inhomogeneous magnetic field. For this purpose we extend our variational analysis to allow for two condensates subject to the same interactions:

$$\hat{\mathcal{H}}_o = \sum_{\alpha,k} \varepsilon_{k\alpha} |\varphi_{k\alpha}(\vec{r})|^2 \hat{n}_{k\alpha} \tag{2.50.}$$

We obtain for $\tilde{\Omega}(\vec{r})$

$$\tilde{\Omega}(\vec{r}) = \sum_{\alpha} \tilde{\Omega}(\vec{r}) + \tilde{\Omega}_{ab}(\vec{r}) \tag{2.51.}$$

where $\tilde{\Omega}_{\alpha}$ has the same form as expression (2.25.), while

$$\tilde{\Omega}_{ab} \equiv v_o \sum_{k,\ell} |\varphi_{ka}(\vec{r})|^2 \cdot |\varphi_{\ell b}(\vec{r})|^2 \langle n_{ka}\rangle\langle n_{\ell b}\rangle .$$

Limiting ourselves to T = 0 equation (2.51.) leads to a pair of coupled Gross-Pitaevskii equations describing the two condensates

$$[-\frac{\hbar^2}{2m}\nabla^2 + U_{ext}^{(+)}(\vec{r}) + v_o\rho(\vec{r})]\ \varphi_a(\vec{r}) = \varepsilon_a\varphi_a(\vec{r}) \tag{2.52a.}$$

$$[-\frac{\hbar^2}{2m}\nabla^2 + U_{ext}^{(-)}(\vec{r}) + v_o\rho(\vec{r})]\ \varphi_b(\vec{r}) = \varepsilon_b\varphi_b(\vec{r}) \tag{2.52b.}$$

where φ_a and φ_b are the ground-state wave functions and ε_a, ε_b the ground-state energies per particle for atoms in the $|a\rangle$ and $|b\rangle$ hyperfine states. The total density is written as $\rho(\vec{r}) \equiv \rho_a(\vec{r}) + \rho_b(\vec{r})$.

Note that the external potential now also depends on the hyperfine state $U_{ext}^{(\pm)} \equiv \frac{1}{2}m\omega_{o\pm}^2 x^2$; $\omega_{o\pm}^2 = \mu^{(\pm)}B/(mx_m^2)$. [For definition of the various symbols see section (1.1.2.) and (1.2.1.)].

Calculating ε_a and ε_b to first order in perturbation theory we find

$$\varepsilon_a = \tfrac{1}{2}\hbar\omega_o^{(+)} + v_o\rho(o) \simeq v_o\rho(o) \qquad (2.53a.)$$

$$\varepsilon_b = \tfrac{1}{2}\hbar\omega_o^{(-)} + v_o\rho(o) \simeq v_o\rho(o) \qquad (2.53b.)$$

The Gross-Pitaevskii equations may now be solved, neglecting the kinetic energy terms as in Section (1.2.8.)

$$\rho(\vec{r}) = \frac{1}{v_o}\left[v_o\rho(o) - U_{ext}^{(+)}(\vec{r})\right] \qquad (2.54a.)$$

$$\rho(\vec{r}) = \frac{1}{v_o}\left[v_o\rho(o) - U_{ext}^{(-)}(\vec{r})\right] \qquad (2.54b.)$$

Trivially these equations are only meant to be valid as far as they predict ρ to be positive. Note that the solutions (2.54a.) and (2.54b.) seem to contradict each other. The only way to avoid the paradox is to assume that they apply to disjoint regions of space, as shown in Fig. 6. Near the center of the field we find the lowest hyperfine state ($\rho = \rho_a$), whereas near the surface of the condensate only the $|b\rangle$ -state is present ($\rho = \rho_b$). The discontinuity in the density at the interface is required to balance the pressure on both sides of the interface. The exact position of the interface depends on the relative concentrations of the two components. Of course a sharp interface is physically not realistic. A proper treatment of the kinetic energy would show gradual changes of the condensate densities over distances of the order of the (local) healing length.

1.3. INTERACTION OF H↓ WITH SURFACES

1.3.1. *Introduction*

Knowledge of the bulk properties of H↓ as discussed in sections (1.1.) and (1.2.) is not enough to understand the behaviour of the system under real experimental conditions. This is caused by the gaseous nature of H↓ that requires containment at all temperatures. Unfortunately pure electro-magnetic confinement is not very promissing so that walls of rigid materials are required. However, since gaseous H↓ itself is the most weakly interacting atomic system known, the presence of a different material leads to an important perturbation of the system. Especially at low temperatures, where the most fascinating properties of H↓ are to be expected, this leads to strong surface adsorption followed by rapid recombination. In view of these considerations it is not surprising that the main experimental effort initially has been concentrated on minimizing these surface effects. In this context the first experimental demonstration that helium covered walls at $T \approx 300$ mK provide an enhanced lifetime of approximately eight orders of magnitude, as presented in chapter (3), is to be considered as a breakthrough. Subsequently the experimental effort was concentrated, as far as the surface problem is concerned, on the determination of the adsorption energies of H on the surfaces of ^{3}He and ^{4}He. Here the publication of a study of spin polarized atomic deuterium, presented in chapter (6), provided the first comparison of experimental and theoretical values for an adsorption energy and secondly establised that surface recombination is the dominant loss mechanism for the hydrogen isotopes at low temperatures. For completeness we note that the adsorption energies of H on ^{4}He and ^{3}He ($\varepsilon_a \approx 1$ K and $\varepsilon_a \approx 0.4$ K respectively) are also known. They were obtained essentially simultaneously and by different experimental techniques by groups at the University of British Columbia[32,33] and the University of Amsterdam.[34,35] However, this work falls outside the scope of this thesis.

In this section we first briefly present theoretical estimates for the adsorption energies. Then we discuss the interaction between bulk gas and surfaces in relation with BEC using a theory for the surface adsorption isotherm.

1.3.2. *H↓ in contact with the surface of liquid helium*

With the knowledge that H↓ may condense onto the surface of liquid helium we have to reconsider our analysis of the weakly interacting Bose gas

and find out how the model is affected by surface adsorption. In this section we will show that such an analysis (technically a calculation of the surface adsorption isotherms)leads to two main conclusions. First the existence of a saturation coverage, i.e. only a limited amount can be in the adsorbed state, and secondly that the surface has to be saturated before BEC becomes possible in the bulk. Moreover, the saturation coverage will be found to be essentially independent of temperature, so that there is little preference to try and achieve BEC at low or high temperature as far as the surface coverage is concerned.

The Hartree-Fock approximation presented in section (1.2.5.) may also be used to study the atomic hydrogen system in contact with the surface of liquid helium. For convenience we shall neglect recombination and limit ourselves to a configuration with uniform external field. We shall also suppress the additional degree of freedom provided by the nuclear spin, which may supply some interesting features to the problem, but does not affect the main conclusions of our analysis. These considerations have been discussed by Goldman and Silvera.[36] Finally we shall neglect any direct interaction between atoms in the gas and the adsorbate.

To allow for surface adsorption we have to extend the Hartree-Fock equations by a set of equations for the surface states $\varphi_{Sq}(\vec{r})$. Only allowing for BEC in the bulk we obtain

$$[-\frac{\hbar^2}{2m}\nabla^2 + 2v_3\rho_3]\,\varphi_k(\vec{r}) = \varepsilon_k^{(3)}\varphi_k(\vec{r}) \qquad k\neq o \qquad (3.1a.)$$

$$[-\frac{\hbar^2}{2m}\nabla^2 + 2v_3\rho_3^{(n)} + v_3\rho_3^{(o)}]\,\varphi_o(\vec{r}) = \varepsilon_o^{(3)}\varphi_o(\vec{r}) \qquad (3.1b.)$$

$$[-\frac{\hbar^2}{2m}\nabla^2 + 2v_S\rho_S(\vec{r}) + U_S(\vec{r})]\,\varphi_{Sq}(\vec{r}) = \varepsilon_q^{(2)}\varphi_{Sq}(\vec{r}) \qquad (3.1c.)$$

where ρ_3, $\rho_3^{(n)}$ and $\rho_3^{(o)}$ are the total, normal and condensate densities in the bulk respectively, v_3 and v_S are the bulk and surface scattering amplitudes, $U_S(\vec{r})$ represents the surface adsorption potential and $2v_S\rho_S$ is the interaction energy due to a finite density of adsorbate $[\rho_S(\vec{r})]$ on the surface. We shall assume

and
$$v_S = v_3 \qquad (3.2.)$$

$$U_S(\vec{r}) = U(z) \qquad (3.3.)$$

Considerations concerning the validity of these two approximations are discussed, in a slightly different context, by Edwards and Mantz.[37] The use of

the bulk scattering amplitude v_3 is only justified if the interatomic potential is not significantly changed by the presence of the helium surface. Also the use of a uniquely defined adsorption potential U(z) is associated with this point, since it assumes the surface potential to be independent of the distance of neighboring atoms which implies that the surface of the liquid is not distorted by their presence. Both approximations are quite reasonable in view of Mantz and Edwards[38] analysis of the adsorption problem where the wave function was found to extend quite far above the helium surface.

The main aspect of equations (3.1.) that seems to be questionable is the very concept of a mean field, which neglects any correlation in the motion of the atoms. Although the mean field approach was well suited for the macroscopic external fields of section (1.2.) it seems to be less appropriate to treat the interactions within the monolayer of adsorbate, having a "thickness" comparable to the range of the interatomic potential. However, an alternative treatment of the interactions is not available in the literature undoubtedly due to the strong anisotropy of the scattering problem on these helium surfaces.

1.3.3. *Further simplifications*

In order to solve equations (3.1.) within the approximations (3.2.) and (3.3.), we note that the two-dimensional translational invariance of the surface mean field hamiltonian enables us to decompose the adsorbate wave function in components normal (= z) and transverse (= xy) to the surface.

$$\varphi_{Sq}(\vec{r}) = \phi(z)\ \Psi_q(\vec{r}_\perp) \tag{3.4.}$$

$$\rho_S(\vec{r}) = \phi^2(z)\ \rho_2 \tag{3.5.}$$

where $\phi(z)$ is real and positive and will be referred to as the "bound state wave function", normalized to unity

$$\int dz\ \phi^2(z) = 1 \tag{3.6.}$$

ρ_2 is the two-dimensional density of hydrogen atoms, i.e. the number of atoms per unit area. To further simplify the adsorbate equations we integrate over the bound state wave function

$$\left[-\frac{\hbar^2}{2m}\nabla_\perp^2 + 2v_3\rho_2 \int dz\ \phi^4(z) - \varepsilon_a\right] \Psi_q(\vec{r}_\perp) = \varepsilon_q^{(2)}\Psi_q(\vec{r}_\perp) \tag{3.7.}$$

ε_a, the mean field solution to the adsorption energy is defined as

$$\varepsilon_a = \int dz\ \phi(z)\ [+\frac{\hbar^2}{2m}\nabla^2 - U(z)]\,\phi(z) \qquad (3.8.)$$

Returning to the line of thought of Edwards and Mantz[37] we assume $\phi(z)$ to be independent of coverage so that the bound state wave function $\phi_1(z)$ for one single atom adsorbed on the helium surface may be used and equation (3.7.) reduces to

$$[-\frac{\hbar^2}{2m}\nabla_\perp^2 + 2v_2\rho_2 - \varepsilon_a\ ]\ \Psi_q(\vec{r}_\perp) = \varepsilon_q^{(2)}\Psi_q(\vec{r}_\perp) \qquad (3.9.)$$

where $v_2 \equiv v_3 \int dz\ \phi_1^4(z)$. The integral has been evaluated by Edwards and Mantz, who find

$$\int dz\ \phi_1^4(z) = 0.095\ \text{Å}^{-1} \qquad (3.10.)$$

The interpretation of this approximation is straightforward within the mean field picture. The bound state wave function is not allowed to broaden, when the surface density increases. Such a broadering leads to an increase in kinetic energy perpendicular to the surface (i.e. ε_a becomes smaller), but also to a reduction of v_2. Thus broadening of $\phi(z)$ will become energetically favorable if the surface density is high enough. It remains to be seen however whether a further minimization of the mean field energy would provide a better approximation to the physical problem in view of the total neglect of correlation energy.

We have now arrived at a point where the Hartree-Fock equations have been simplified far enough to enable a solution, but before proceeding in this direction we note that one may also start out from the beginning with equation (3.9.) through the ansatz of pure two-dimensional surface states and a calculation of v_2 in two dimensions. This approach, which tends to overestimate the interaction energy due to phase space limitations, has been taken by Silvera and Goldman[39] and results in

$$v_2 = 2.9\ \hbar^2/2m \qquad (3.11a.)$$

which is to be compared with the result of Edwards and Mantz[37]

$$v_2 = 2.1\ \hbar^2/2m \qquad (3.11b.)$$

who based their results on the Monte Carlo calculations of Etters, Danilowicz and Palmer.[8] Using only the s-wave scattering length[4] one obtains

$$v_2 = 1.7\ \hbar^2/2m$$

1.3.4. *Saturation of the surface coverage*

Solving the Hartree-Fock equations separately to first order in perturbation theory as in section (1.2.) we obtain

$$\varepsilon_k^{(3)} = \frac{\hbar^2 k^2}{2m} + 2v_3\rho_3 \tag{3.12a.}$$

$$\varepsilon_o^{(3)} = 2v_3^{(n)}\,\rho_3^{(n)} + v_3\rho_3^{(o)} \tag{3.12b.}$$

$$\varepsilon_q^{(2)} = \frac{\hbar^2 q^2}{2m} + 2v_2\rho_2 - \varepsilon_a \tag{3.12c.}$$

For coverages

$$\rho_2 > (\varepsilon_a/2v_2) \equiv \rho_{sat} \tag{3.13.}$$

the single-particle surface energies $\varepsilon_q^{(2)}$ become positive in the mean field picture and one expects the surface coverage to saturate. Indeed, ρ_2 does not grow much above ρ_{sat} as was established by a calculation of the adsorption isotherms (see section (1.3.6.)). Both Silvera and Goldman[39] and Edwards and Mantz[37] did not take into account exchange effects between identical particles, which give rise to the factors 2 in expressions (3.12.) and (3.13.). The publication by Goldman and Silvera[36] corrects for this effect. Here we estimate $\rho_{sat} = 1.2 \times 10^{14}$ cm^{-2} for an adsorption energy $\varepsilon_a = 1$ K and $a = 0.72$ Å using equations (3.11c.) and (3.13.).

1.3.5. *BEC in the presence of surfaces*

With the procedure of section (1.2.11.) we find expressions for the bulk and surface densities in terms of μ and T

$$\rho_3 = \rho_3^{(o)} + (1/\lambda_{th})^3\, g_{3/2}\{\exp[-\beta(\mu - 2v_3\rho_3)]\} \tag{3.14.}$$

$$\rho_2 = (1/\lambda_{th})^2\, g_1\{\exp[\beta(\mu - 2v_2\rho_2 + \varepsilon_a)]\} \tag{3.15.}$$

We first note from equation (3.15.) that the adsorbate cannot Bose condense due to the divergence of the $g_1(z)$ function (for $z \to 1$), as discussed by De Groot et. al.[18] (see also the book by Band[40]). Furthermore the same divergence implies

$$\mu < 2v_2\rho_2 - \varepsilon_a \tag{3.16.}$$

Then, to achieve BEC in the bulk one must satify

$$\mu = 2v_3\rho_3 \tag{3.17.}$$

Noting that this value is non-negative one may combine equations (3.16.) and (3.17.) to obtain a general condition for BEC in the presence of surfaces

$$o \leqslant 2v_3\rho_3 < 2v_2\rho_2 - \varepsilon_a \qquad (3.18.)$$

From this inequality one may draw two conclusions:

- A non-interacting Bose gas ($v_2=v_3=0$) does not display BEC in the presence of surfaces if a surface bound exists ($\varepsilon_a>0$).
- To observe BEC in an interacting Bose gas in contact with surfaces, these surfaces have to be "saturated"

$$\rho_2 > \rho_{sat} + (v_3/v_2)\,\rho_3 \qquad (3.18a.)$$

Over the range of densities of experimental interest the second term may be neglected ($v_3/v_2 \approx 3.7 \times 10^{-8}$ cm).[36]

1.3.6. *Surface adsorption isotherms*

The adsorption isotherms, relating bulk and adsorbate densities at constant temperature, are now readily obtained by eliminating the chemical potential from the expressions (3.14.) and (3.15.) for ρ_3 and ρ_2. This was done numerically by Silvera and Goldman[39] and, properly taking into account the nuclear spin and exchange effects, by Goldman and Silvera.[36] Results of this last publication are reproduced in Fig. 7.

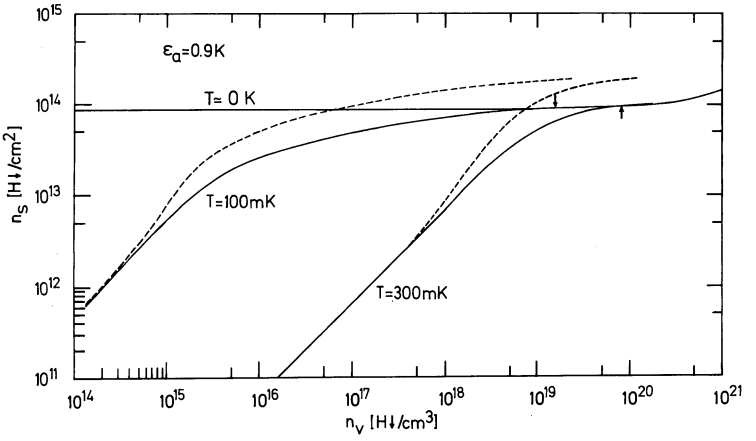

Fig.7-Adsorption isotherm for H↓ on a ^{4}He surface, (ε_a= 0.9 K; after ref. 36). The surface density n_s is plotted vertically, the bulk density n_v horizontally. The neglect of exchange effects leads to the dotted curves. The arrows indicate the critical densities for BEC.

Edwards and Mantz[37] present explicit equations for the surface and bulk chemical potentials which are correct to first order in the interaction. Here we shall limit ourselves to some useful expressions that apply for $T \gg T_c$. Then the functions $g_{3/2}$ and g_1 represent simple exponents and by eliminating μ we obtain a high temperature expression for the adsorption isotherms

$$\rho_2 = \lambda_{th}\rho_3 \exp\left[\beta(2v_3\rho_3 - 2v_2\rho_2 + \varepsilon_a)\right] \qquad (3.19.)$$

which reduces in the low density limit to the well known ideal gas result[40]

$$\rho_2 = \lambda_{th}\rho_3 \exp\left(\beta\varepsilon_a\right) \qquad (3.20.)$$

This expression will be used in section (1.4.8.) where a phenomenological theory for surface recombination is presented.

1.4. THE STABILITY OF H↓

1.4.1. *Introduction*

In any experimental study of the properties of atomic hydrogen one cannot escape being confronted at some stage with the kinetics of the recombining gas. For this reason it seems appropriate to consider here recombination in some detail. The hydrogen recombination reaction is one of the most fundamental chemical reactions and has been extensively studied, both theoretically and experimentally for more than fifty years.[41]

Here, we do not aim at a detailed description of the various known recombination processes, but rather emphasize the physics of recombination at low temperature. In particular we shall analyze the magnetic field dependence and in this way explain the remarkable stability of the gas in high magnetic fields. Also the dependence of the recombination rate on the various hyperfine states of the collision partners will be discussed.

The most likely process for the formation of a hydrogen molecule is a three-body process

$$H + H + X \rightarrow H_2 + X \qquad (4.1.)$$

where X may be another hydrogen atom or an atom of a different gas. The two-body radiative process

$$H + H \rightarrow H_2 + h\nu \qquad (4.2.)$$

was shown to be completely negligible on a laboratory time-scale by Jones et al.[42] Reaction (4.1.) may also proceed in two steps

$$\begin{aligned} H + X &\rightarrow (HX)^* \\ (HX)^* + H &\rightarrow H_2 + X \end{aligned} \qquad (4.3a.)$$

where $X \neq H$ and the symbol * is used to indicate that the intermedeate state is meta-stable. This process is known as an exchange process, because the final step involves $H \rightleftharpoons X$ exchange to form H_2. Another two-step reaction requires an energy transfer mechanism to stabilize the molecule:

$$\begin{aligned} H + H &\rightarrow H_2^* \\ H_2^* + X &\rightarrow H_2 + X \end{aligned} \qquad (4.3b.)$$

The third body "X" may also be another hydrogen atom and just serves to carry away the excess energy from the intermedeate state H_2. At low temperatures (T < 1 K) the exchange process may be excluded since the only materials, with a non-negligible vapor pressure at these temperatures (^{4}He and ^{3}He), do not form a (meta-) stable bound state with H.

The case of the energy transfer mechanism is more subtle. For a pair of H-atoms having singlet character in their interaction, scattering resonances may lead to the population of meta-stable H_2 complexes (quasi-bound states). It was shown by Roberts, Bernstein and Curtiss[43,44] that for some of these complexes thermal equilibrium is achieved, which strongly enhances their relative importance and simplifies calculation. The theory for these processes reduces to an effective two-body theory, where one has to calculate the probability that the complex is stabilized in a collision. However, at low temperatures the resonances no longer can be populated thermally. As a result the energy transfer mechanism is thought to be of negligible importance below 1 K.

As pointed out by Stwalley[45,46] some care is required if one applies a magnetic field. With growing field the $^3\Sigma_u^+$, $M_S = -1$ is pushed below the singlet (see Fig. 1.) and may be tuned to induce resonant transitions to one of the bound vibration-rotation levels of the $^1\Sigma_g^+$ -potential. Scattering resonances of this nature require a non-vanishing triplet-singlet transition probability which is provided, for the H-H case, by the hyperfineinteraction.[46]
In Fig. 8. we show the vibration-rotation spectrum[47] of singlet H_2 near

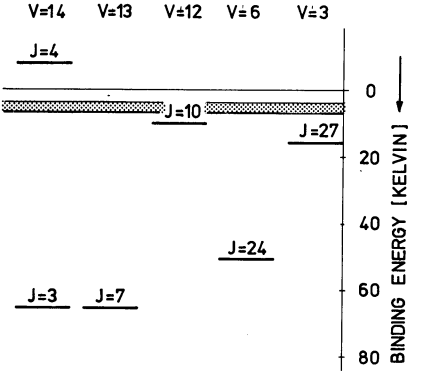

Fig. 8-Vibration-rotation spectrum of H_2 near the dissociation limit. The cross-hatched zone indicates a band of thermally accessible energies (with $exp[E/k_BT] < 10^{-6}$).

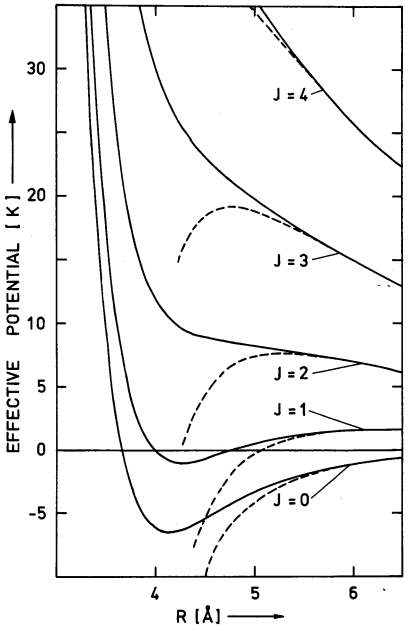

Fig.9-Effective interaction potential of two H atoms as function of particle separation R. Solid line: particles interacting via the $^3\Sigma_u^+$ *-potential. Dashed line: atoms interacting via the* $^1\Sigma_g^+$ *-potential*

the dissociation limit along with a band of thermally accessible energies for B = 10 T. Note that low J resonances (J < 4) are well below threshold. Although the v = 14, J = 4 vibration-rotation state may be tuned above threshold it also turns out to be inaccessible at low temperatures. This may be illustrated using Fig. 9, where we have plotted the effective interatomic potential $v_J(r)$ of two H-atoms for various values of relative angular momentum (J = 0,1,2,3,4). $V_J(r)$ appears in the radial Schrödinger equation for the pair:

$$[-\frac{\hbar^2}{2\mu}\frac{d^2}{dr^2} + V_J(r)]\ y_J(r) = E\ y_J(r) \qquad (4.4a.)$$

$$V_J(r) \equiv V(r) + J(J+1)\frac{\hbar^2}{2\mu r^2} \qquad (4.4b.)$$

where V(r) may be the triplet potential (solid curve in Fig. 9.) or the singlet potential (dashed line in Fig. 9.) depending on the spin state of the pair, $\mu = m/2$ is the reduced mass and $r \equiv |\vec{r}_1 - \vec{r}_2|$.

For all but the lowest states of relative angular momentum the effective potential provides a barrier (rotational barrier) to the radial motion of the pair, high in comparison to accessible energies at low temperatures. The probability to tunnel through the barrier into the v = 14; J = 4 state may be shown to be negligibly small for energies $E/k_B \lesssim 0.25$ K.

We note that the absence of resonant recombination for H_2 is somewhat fortunate. For D-D collisions a resonance, associated with the v = 21; J = 0 vibrational state of D_2 exists at ~ 1.7 cm^{-1} below the dissociation limit,[3,46] which may give rise to enhanced recombination in fields above ~ 1.9 Tesla. However, for the hydrogen case the non-resonant direct process will be dominant.

1.4.2. *The direct three-body process*

The rate of recombination for the direct process

$$H + H + He \rightarrow H_2 + He \qquad (4.5.)$$

has been calculated by Greben, Thomas and Berlinsky[48] (GTB), using a fully quantum mechanical three-body scattering approach. Although the theory was developed in relation to experiments by Hardy and coworkers,[49] who studied the recombination of hydrogen atoms at $T \approx 1$ K in zero field, the results are more generally applicable. In particular the theory is very useful to understand the origin of the B^{-2} field dependence of the recombination rate in high fields. The fundamentals of the method also apply to surface recombination, dominant at low temperature,[32-35] where the surface effectively acts as a third body.

We define the recombination problem by considering an ensemble of initial states $|\Psi_o\rangle$, composed of all (unsymmetrized) non-interacting atomic three-body states

$$|\Psi_o\rangle = |\vec{k}_1 h_1, \vec{k}_2\ h_2; \vec{k}_3\rangle \qquad (4.6a.)$$

where $\vec{k}_1$ and $\vec{k}_2$ represent the momenta of H-atoms in hyperfine states h_1 and h_2 respectively and $\vec{k}_3$ represents the momentum of the He-atom. All three atoms are assumed to be in the electronic ground state. The final states $|\phi_3\rangle$ consist of two particles, a hydrogen molecule with momentum $\vec{p}_{12}$ and a He-atom with momentum $\vec{p}_3$:

$$|\phi_3\rangle = |\vec{p}_{12},\ v,\ LM_L,\ IM_I;\ \vec{p}_3\rangle \qquad (4.6b.)$$

The internal state of the molecule is represented by the vibrational (v), rotational (L,M_L) and nuclear-spin (I,M_I) quantum numbers. L+I must be even, as required by symmetry. Also in the final state only electronic ground states are relevant for the present problem.

At this point one may raise the question if it is justified to use an initial state which is not symmetrized with respect to exchange of the hydrogen atoms? Applying the general considerations of section (1.1.3.) we note that in the low density regime, where the atomic wave functions do not overlap (i.e. for densities $n \ll \lambda_{th}^{-3}$, symmetrized and non-symmetrized pair states lead to similar spatial distributions of pairs. Then symmetrization is of no practical consequence, and thus not required, for the initial states. The validity of the GTB theory is thus restricted to the low density (or high temperature) regime. But even at low densities the atomic or even electronic wave functions will overlap during the scattering process. This will be accounted for by decomposing the initial state (4.6a.) into states which are properly symmetrized with respect to the exchange of both electrons and protons.

The rate equation describing the reaction kinetics of process (4.5.) in the absence of the reverse reaction, is given by

$$\frac{dn_H}{dt} = - k\, n_H^2\, n_{He} \qquad (4.7.)$$

k is the rate constant for the reaction and follows[51] from a quantum mechanical evaluation of the transition rate from three-body initial states (i) to two-body final states (f):

$$k = (2\pi)^7 \sum_{i,f} P_i \, |T_{if}|^2 \, \delta(\vec{p}_i - \vec{p}_f) \, \delta(E_i - E_f) \qquad (4.8.)$$

Here P_i is the statistical probability that an initial state is occupied, T_{if} represents the amplitude for the i→f transition and the δ-functions enforce conservation of momentum and energy.

1.4.3. *The three-body scattering amplitude* T_{if}

The three-body scattering amplitudes T_{if} represent a generalization of the more familiar scattering amplitudes for the two-body case. Although a formal expression for T_{if} is easily obtained (and will be discussed later in this section) any practical evaluation involves, as one might expect, some kind of decomposition into two-body scattering terms. Before discussing the scattering amplitudes in more detail we first introduce a notation that

enables such a decomposition in the next section.

Dropping the symbol "^", used in the foregoing sections to identify operators, the three-body hamiltonian is written as

$$\mathcal{H} = \mathcal{H}_o + V_1 + V_2 + V_3 \qquad (4.9.)$$

$\mathcal{H}_o$ describes the non-interacting three-body system with atoms labeled 1, 2 and 3. V_i represents the interaction between particles j and k [$i \neq j = k \neq i$; $i,j,k \in (1,2,3)$], thus i is the "spectator" index. For convenience of presentation pure three-body forces will be neglected. The hamiltonian may be rewritten for specific "channels"

$$\mathcal{H} = \mathcal{H}_i + V^i \qquad (4.10.)$$

where

$$\mathcal{H}_i \equiv \mathcal{H}_o + V_i \qquad (4.11a.)$$

$$V^i \equiv \sum_{\substack{j=0 \\ j\neq i}}^{3} V_j \qquad \text{with } V_o \equiv 0 \qquad (4.11b.)$$

$\mathcal{H}_{i\neq 0}$ is the three-body hamiltonian, where only particles j and k interact. V^i represents the interaction of j and k with the spectator (i). By including j = 0 in the summation the notation conserves the flexibility to separate $\mathcal{H}_o$ from the interactions. More specifically, if particle 3 is the helium atom, as we assume from this point, then $\mathcal{H}_3$ is the hamiltonian of an interacting pair of hydrogen atoms and a free helium atom. Note that the hydrogen atoms may be paired into a molecule or be in a continuum state. The time development of the unperturbed initial and final states $\Psi_o(t)$ and $\Phi_3(t)$ is defined by

$$-\frac{\hbar}{i}\frac{\partial}{\partial t}\Psi_o(t) = \mathcal{H}_o\,\Psi_o(t) \qquad \Psi_o(o) = \Psi_o \qquad (4.12.)$$

$$-\frac{\hbar}{i}\frac{\partial}{\partial t}\Phi_3(t) = \mathcal{H}_3\,\Phi_3(t) \qquad \Phi_3(o) = \phi_3 \qquad (4.13.)$$

The dynamics of the state $\Psi_o^+(t)$, that evolved from $\Psi_o(t)$ (and has the same energy as Ψ_o) is governed by the full hamiltonian

$$-\frac{\hbar}{i}\frac{\partial}{\partial t}\Psi_o^+(t) = \mathcal{H}\;\Psi_o^{(+)}(t) \qquad \Psi_o^+(o) = \Psi_o^+ \qquad (4.14.)$$

The relation between Ψ_o^+ and Ψ_o has been studied extensively in the literature.[50,51] We limit ourselves to using the results:

$$|\Psi_o^+\rangle = \lim_{\eta\downarrow o} i\eta G(z)|\Psi_o\rangle \qquad (4.15.)$$

where

$$G(z) \equiv \frac{1}{z-\mathcal{H}} \quad ; \quad z \equiv E + i\eta \tag{4.16a.}$$

We shall use more generally

$$G_i(z) \equiv \frac{1}{z-\mathcal{H}_i} \tag{4.16b.}$$

Analogously one writes

$$|\phi_3^-\rangle = \lim_{\eta \downarrow o} - i\eta\, G^-(z)|\phi_3\rangle \tag{4.17.}$$

In view of equations (4.12.) and (4.13.) it is attractive to evaluate the transition rate in the interaction picture of $\mathcal{H}_o$ or $\mathcal{H}_3$. This leads to two expressions for $T_{if} \equiv T_{30}$ (see ref. 51 for a detailed derivation)

$$T_{30} = \langle\phi_3| \; V^3 \; | \; \Psi_o^+\rangle \tag{4.18a.}$$

$$T_{30} = \langle\phi_3^-| \; V^o \; | \; \Psi_o\rangle \tag{4.18b.}$$

Equations (4.18a.) and (4.18b.) represent remarkable matrix elements in the sense that they involve a mixed representation. As one expects initial and final states are connected by a perturbation operator, describing the interaction between particles. However, the interaction in the initial state, where three essentially free atoms interact (via V^o) is quite different from the interaction in the final state, where only two particles interact (via V^3), the H_2 molecule and the He atom. Remarkably enough (4.18a.) only contains the final state interaction explicitely. This feature suggests a very convenient approximation where V^3, the interaction between the H atoms, is completely eliminated.

1.4.4. *The Faddeev equations and the AGS theory*

To evaluate the scattering amplitude (4.18a.) we have to rely on a perturbative expansion for $|\Psi_o^+\rangle$ or G. We discuss the decomposition of G in terms of the propagators G_i. This point is not straightforward because the various two-body scattering processes mutually influence each other. Mathematically this leads to a set of coupled scattering equations, the Faddeev equations.

We first decompose G in analogy with the two-body case

$$G = G_i + G_i V^i G \tag{4.19.}$$

with i = o this forms the ansatz for the Born approximation in a Lippmann-Schwinger picture, while i≠o would lead to a distorted wave Born approximation. The Faddeev decomposition of G involves four components

$$G = G_o + \sum_{i=1}^{3} G^i \tag{4.20.}$$

where

$$G^i \equiv G_o V_i G \tag{4.21.}$$

Equations (4.19.) and (4.20.) are easily shown to be equivalent. Note that the G^i are interdependent. Substituting (4.19.) into (4.21.) we find

$$G^i = G_o V_i G_i + G_o V_i G_i V^i G \tag{4.22.}$$

Using the operator identity

$$G_i = G_o + G_o V_i G_i \tag{4.23a.}$$

$$= G_o + G_o t_i G_o \tag{4.23b.}$$

which defines the two-body scattering problem in the presence of a non-interacting spectator (i), one obtains the Faddeev equations for G^i

$$G^i = (G_i - G_o) + G_o t_i (G^j + G^k) \tag{4.24.}$$

where t_i is a two-body transition operator. It may be shown[50] that for integral equations of the Lippmann-Schwinger type a unique solution does not exist in the three-body case. This problem does not arise for the Faddeev decomposition if one requires equation (4.24.) to be satisfied.

Returning to (4.18.) for the transition amplitude we conclude that in the evaluation of T_{30} Faddeev-like equations have to be enforced. This is most elegantly done by the method of Alt, Grassberger and Sandhas (AGS)[52] who expressed G in terms of scattering amplitudes U_{ij} defined by

$$G = G_i \delta_{ij} + G_i U_{ij} G_j \qquad i,j \in (0,1,2,3) \tag{4.25.}$$

where

$$U_{ij} = (1-\delta_{ij}) G_0^{-1} + \sum_{\ell \neq i} t_\ell G_o U_{\ell j} \tag{4.26.}$$

We thus ask for T_{30} in terms of the U_{ij}.

$$\langle \phi_3 | V^3 | \Psi_o^+ \rangle = \lim_{\eta \downarrow o} i\eta \langle \phi_3 | V^3 G(z) | \Psi_o \rangle \tag{4.27a.}$$

$$= \lim_{\eta \downarrow o} i\eta \, \langle \phi_3 | G_3^{-1} G - 1 | \Psi_o^+ \rangle \qquad (4.27b.)$$

Now substituting (4.26.) with i=3 and j=0 we obtain in the limit $\eta \downarrow 0$ the simple relation

$$\langle \phi_3 | V^3 | \Psi_o^+ \rangle = \langle \phi_3 | U_{30} | \Psi_o^+ \rangle \qquad (4.28.)$$

With this equation the three-body transition amplitude may be expressed as a multiple scattering expansion only requiring G_o and the two-body transition operators t_ℓ. Moreover, the mathematical requirements as formulated by Faddeev are enforced implicitely through (4.26.). For our problem (4.26.) becomes

$$U_{30} = G_o^{-1} + \sum_{\ell=1}^{2} t_\ell G_o U_{\ell o} \qquad (4.29a.)$$

which may be expanded by iteration to yield

$$U_{30} = G_o^{-1} + (t_1 + t_2) + \sum_{\ell=1}^{2} t_\ell G_o (t_1 + t_2) + \ldots . \qquad (4.29b.)$$

Following GTB we note that $G_o^{-1} | \Psi_o^+ \rangle = 0$ and thus G_o^{-1} does not contribute to the (energy conserving) scattering amplitude. Neglecting furthermore all multiple scattering terms we deal with the impulse approximation

$$U_{30} = t_1 + t_2 \qquad (4.29c.)$$

We note that in this approximation t_3, involving the interaction potential between the H atoms does not contribute! Physically this means that recombination occurs always when two hydrogen atoms, having some singlet character in their interaction, collide in the presence of a helium atom. The only role of the helium atom is to enable the reaction by conserving energy and momentum in the process. The main justification for the use of the impulse approximation by GTB seems to be the reasonable agreement with experiment. The essence of this physical picture in relation to the field dependence of $H\downarrow$-atom recombination in high fields was first pointed out by Silvera[53] and published by Silvera and Walraven[54] using a rough approximation to (4.18b.)

1.4.5. *Decomposition of the initial states*

In the detailed discussion of three-body scattering, in relation to the Faddeev theory and the multiple scattering expansion, the point of indistinguishability of identical particles was not raised. In general this aspect can be accounted for by properly symmetrizing all states involved.

For our case GTB decomposed the initial states (4.6a.) into states which are properly symmetrized with respect to exchange of the electrons and protons of the H atoms. The helium atom is treated as a distinguishable third body. The final state consists of two distinguishable particles, an H_2 molecule and a helium atom. Although, in principle, one also has to symmetrize all relevant intermediate states this is, as usually, of no practical consequence because both the transition operators t_i and the propagator G_o are symmetric under exchange of identical particles, implying that only the properly symmetrized intermediate states can contribute. These concepts are reviewed by Afnan and Thomas[50] and, more in detail, by Goldberger and Watson.[51]

We first consider the non-symmetrized initial state $|\Psi_o>$ more closely. Although $\vec{f} \equiv \vec{i}+\vec{s}$ is a good quantum number only for H in zero magnetic field, the $\vec{f}$ representation also may be used to characterize the atomic hyperfine states $|h>$ in non-zero fields. To express the field dependence we specify the field explicitely.

$$|h> \equiv |B;\ f,m> \tag{4.30.}$$

Within this representation the hyperfine states become $|a> \equiv |B;\ o,o>$, $|b> \equiv |B;\ 1,-1>$, $|c> \equiv |B;\ 1,o>$ and $|d> \equiv |B;\ 1,1>$ and the unsymmetrized H atom pair wave function, which is part of the initial state $|\Psi_o>$ (4.6a.) may be written as

$$<\vec{R}_1\vec{r}_1\vec{R}_2\vec{r}_2|\vec{k}_1h_1,\vec{k}_2h_2> =$$
$$= |B;\ f_1m_1,\ f_2m_2)\ \varphi(\vec{R}_1\vec{r}_1)\ \varphi(\vec{R}_2\vec{r}_2)\ e^{i\vec{k}_1\cdot\vec{R}_1}\ e^{i\vec{k}_2\cdot\vec{R}_2} \tag{4.31.}$$

where φ represents an 1 s electronic wave function. To decompose (4.31.) in fully symmetrized wave functions we first decompose the orbital, electronic and spin parts separately.

The decomposition of the orbital wave function is done after transformation to the relative coordinate system

$$e^{i\vec{k}_1\cdot\vec{R}_1}\ e^{i\vec{k}_2\cdot\vec{R}_2} =$$
$$= \frac{1}{\sqrt{2}} e^{i\vec{Q}(\vec{R}_1+\vec{R}_2)/2}\ [\Phi^{(even)}(\vec{R}_1\vec{R}_2) + \Phi^{(odd)}(\vec{R}_1\ \vec{R}_2)] \tag{4.32.}$$

$$\Phi^{(\alpha)}(R_1R_2) \equiv \frac{1}{\sqrt{2}}\left[e^{i\vec{q}\cdot(\vec{R}_1-\vec{R}_2)} + (-1)^{\alpha} e^{-i\vec{q}\cdot(\vec{R}_1-\vec{R}_2)}\right] \tag{4.33.}$$

where α is even or odd, $\vec{Q} \equiv \vec{k}_1 + \vec{k}_2$ and $\vec{q} \equiv \frac{1}{2}(\vec{k}_1 - \vec{k}_2)$ represent the center of mass momentum and relative momentum respectively. The spin part is decomposed by a transformation to the coupled representation of I and S

$$|B;f_1m_1,f_2m_2\rangle = \sum_{IMSN} |IMSN\rangle \langle IMSN| B;f_1m_1,f_2m_2\rangle \tag{4.34.}$$

The coefficient may be expressed in terms of Clebsch-Gordon coefficients[14] and may be conveniently written as

$$A(B;f_1m_1,f_2m_2;IMSN) \equiv \delta_{(m_1+m_2),(M+N)} \langle IMSN|B;f_1m_1,f_2m_2\rangle \tag{4.35.}$$

Values for A are tabulated in Table 1. The electronic product wave function finally is decomposed in terms of bonding and anti-bonding electronic wave functions:

$$\varphi(R_1r_1)\,\varphi(R_2r_2) = \frac{1}{\sqrt{2}}\left[\phi^{(even)}(R_1R_2r_1r_2) + \phi^{(odd)}(R_1R_2r_1r_2)\right] \tag{4.36.}$$

with

$$\phi^{(\alpha)} \equiv \frac{1}{\sqrt{2}}\left[\varphi(R_1r_1)\,\varphi(R_2r_2) + (-1)^{\alpha}\varphi(R_1r_2)\,\varphi(R_2r_1)\right] \tag{4.37.}$$

α being even or odd.

Substituting (4.32.), (4.34.) and (4.36.) into (4.31.) and retaining only the terms consistent with the Fermi nature of the electrons and protons we have completed the decomposition of (4.31.) in terms of properly symmetrized H atom pair wave functions. With an obvious generalization to include $\vec{k}_3$ the decomposition of $|\Psi_o\rangle$ (4.6a.) is written as

$$|\Psi_o\rangle = \frac{1}{2}\sum_{IMSN} |\vec{Q},\vec{q};IMSN;\vec{k}_3\rangle A(B;f_1m_1,f_2m_2;IMSN) \tag{4.38.}$$

In the position representation the fully symmetrized two H atom pair state is given by

$$\langle\vec{R}_1\vec{R}_2\vec{r}_1\vec{r}_2|\vec{Q},\vec{q};IMSN\rangle = |IMSN\rangle\,\phi^{(S)}(R_1R_2r_1r_2)\,\Phi^{(I+S)}(R_1R_2)\,e^{i\vec{Q}(\vec{R}_1+\vec{R}_2)/2} \tag{4.39.}$$

Note the normalization $N \equiv \langle\vec{Q},\vec{q};IMSN|\vec{Q},\vec{q};IMSN\rangle = 1$

S	N	I	M	aa	ba ab	ca ac	da ad	bb	cb bc	db bd	cc	dc cd	dd
0	0	0	0	$\sin\theta\cos\theta$	0	$\frac{1}{2}(\cos^2\theta-\sin^2\theta)$	0	0	0	$\frac{1}{2}$	$-\sin\theta\cos\theta$	0	0
0	0	1	1	0	0	0	$\mp\frac{1}{\sqrt{2}}\cos\theta$	0	0	0	0	$\pm\frac{1}{\sqrt{2}}\sin\theta$	0
0	0	1	0	0	0	$\mp\frac{1}{2}$	0	0	0	$\pm\frac{1}{2}$	0	0	0
0	0	1	-	0	$\mp\frac{1}{\sqrt{2}}\sin\theta$	0	0	0	$\mp\frac{1}{\sqrt{2}}\cos\theta$	0	0	0	0
1	1	0	0	0	0	0	$\pm\frac{1}{\sqrt{2}}\sin\theta$	0	0	0	0	$\pm\frac{1}{\sqrt{2}}\cos\theta$	0
1	1	1	1	0	0	0	0	0	0	0	0	0	1
1	1	1	0	0	0	0	$+\frac{1}{\sqrt{2}}\sin\theta$	0	0	0	0	$\frac{1}{\sqrt{2}}\cos\theta$	0
1	1	1	-	$\sin^2\theta$	0	$\sin\theta\cos\theta$	0	0	0	0	$\cos^2\theta$	0	0
1	0	0	0	0	0	$\pm\frac{1}{2}$	0	0	0	$\pm\frac{1}{2}$	0	0	0
1	0	1	1	0	0	0	$-\frac{1}{\sqrt{2}}\cos\theta$	0	0	0	0	$\frac{1}{\sqrt{2}}\sin\theta$	0
1	0	1	0	$-\sin\theta\cos\theta$	0	$-\frac{1}{2}(\cos^2\theta-\sin^2\theta$	0	0	0	$\frac{1}{2}$	$\sin\theta\cos\theta$	0	0
1	0	1	-	0	$\frac{1}{\sqrt{2}}\sin\theta$	0	0	0	$\frac{1}{\sqrt{2}}\cos\theta$	0	0	0	0
1	-	0	0	0	$\pm\frac{1}{\sqrt{2}}\cos\theta$	0	0	0	$\mp\frac{1}{\sqrt{2}}\sin\theta$	0	0	0	0
1	-	1	1	$\cos^2\theta$	0	$\sin\theta\cos\theta$	0	0	0	0	$\sin^2\theta$	0	0
1	-	1	0	0	$-\frac{1}{\sqrt{2}}\cos\theta$	0	0	0	$\frac{1}{\sqrt{2}}\sin\theta$	0	0	0	0
1	-	1	-	0	0	0	0	1	0	0	0	0	0

Table 1-The table contains the coefficients $A(B;f_1m_1,f_2m_2;IMSN)$; $|h_i\rangle = |B;\ f_im_i\rangle$; $|a\rangle = |B;0,0\rangle$, $|b\rangle = |B;1,-1\rangle$, $|c\rangle = |B;1,0,\rangle$ *and* $|d\rangle = |B;1,1\rangle$

1.4.6. *State dependence for recombination*

With equations (4.38.) and (4.39.) we arrived at a point where the formalism is developed sufficiently to derive some specific results. These results are of basic importance to understand the properties of the recombining gas. In the first place we shall discuss how the probability of the recombination depends on the hyperfine states of the incoming atoms. The next section deals with the field dependence of the three-body recombination rate.

To calculate the state-dependent recombination probability we ask for $|T_{30}|^2$ starting from an initial state containing two H atoms in specific hyperfine states. Obviously, in evaluating $|T_{30}|^2$ only those terms of (4.38.) have to be taken into account that may lead to the formation of a molecule. In view of the fact that t_1 and t_2 are spin-independent this implies that only initial states with electronic "singlet"-character can contribute, i.e. S=0, N=0 and thus $M = m_1 + m_2$.

$$\begin{aligned} |T_{30}|^2 &\approx |\langle\phi_3|t_1 + t_2|\Psi_o\rangle|^2 \\ &= \frac{1}{4} \sum_I |A(B;f_1m_1,f_2m_2;I,m_1+m_2,o,o)|^2 \times \\ &\times |\langle\phi_3|t_1 + t_2|\vec{Q},\vec{q};I,m_1+m_2,o,o;\vec{k}_3\rangle|^2 \end{aligned} \qquad (4.40.)$$

Note that the spin-dependence of t_1 and t_2 leads to a simple separation of (4.40.) into two terms, one for recombination to para hydrogen (I=0), the other for recombination to the ortho molecular state (I=1).

We evaluate (4.40.) for three different combinations of hyperfine states entering in $|\Psi_o\rangle$:

-The a-a case ($f_1 = f_2 = 0$; $m_1 = m_2 = 0$):
Using table 1 we find

$$|\langle\phi_3|t_1+ t_2|\Psi_o^{aa}\rangle|^2 = \frac{1}{4} \sin^2\theta \cos^2\theta |\langle\phi_3|t_1+t_2|\vec{Q},\vec{q};o,o,o,o;\vec{k}_3\rangle|^2 \qquad (4.41.)$$

i.e. only para-H_2 results.

-The a-b case ($f_1 = 0$, $m_1 = 0$; $f_2 = 1$, $m_2 = -1$):
Again using table 1 one finds

$$|\langle\phi_3|t_1+ t_2|\Psi_o^{ab}\rangle|^2 = \frac{1}{8} \sin^2\theta |\langle\phi_3|t_1+t_2|\vec{Q},\vec{q};1,-1,o,o;\vec{k}_3\rangle|^2 \qquad (4.42.)$$

i.e. only ortho-H_2 results.

- The b-b case ($f_1 = f_2 = 1$; $m_1 = m_2 = -1$):
  Table 1 leads to

$$|\langle\phi_3|t_1 + t_2|\psi_o^{bb}\rangle|^2 = 0 \qquad (4.43.)$$

Equation (4.43.) shows that the GTB theory satisfies the intuitive picture that collisions between fully polarized ($|b\rangle$ -state) atoms should not lead to recombination. This implies preferential recombination for the $|a\rangle$ -state. As pointed out by Statt and Berlinsky[29] this leads, in the limit of high magnetic fields and negligible relaxation between the hyperfine levels, to a depletion of the $|a\rangle$ -state and thus to the formation of a doubly-polarized gas ($H\downarrow\mp$) of only $|b\rangle$ -state atoms. $H\downarrow\mp$ has been observed by Cline, Greytak and Kleppner[55] as well as by Sprik, Walraven, Van Yperen and Silvera.[56] As far as the experiments for this thesis are concerned we have been working in a regime of *rapid* relaxation, implying thermal equilibrium between the $|a\rangle$ - and $|b\rangle$ -state occupations.

Comparing (4.41.) and (4.42.) we note that they differ not only in θ-dependence but also in the orbital matrix elements. According to GTB this leads to a significant difference in temperature dependence between the a-a (para) and a-b (ortho) recombination probability, with the a-b recombination rate vanishing in the low temperature limit. A difference in recombination rates for a-a and a-b collisions has been observed experimentally by Sprik et al.[56] but a discussion of their results falls outside the scope of this thesis.

1.4.7. *The magnetic field dependence of recombination*

The field dependence of the recombination rate may be obtained by summing over the various hyperfine initial states:

$$\sum_{h_1 h_2} n_{h_1} n_{h_2} |\langle\phi_3|t_1 + t_2|\psi_o(h_1,h_2)\rangle|^2 =$$

$$= \sum_{I=0}^{1} f_I \cdot |\langle\phi_3|t_1 + t_2|\vec{Q},\vec{q};I,m_1+m_2,o,o;\vec{k}_3\rangle|^2 \qquad (4.44.)$$

where f_I represents the, field dependent, probability that the scattering proceeds through the channel under consideration, f_1, for recombination to ortho-H_2 and f_0 for recombination to para-H_2.

$$f_I(B) = \sum_{h_1 h_2} n_{h_1} n_{h_2} |A(B;f_1 m_1, f_2 m_2; I_1, m_1+m_2, o, o)|^2 \qquad (4.45.)$$

With the aid of table 1 equation (4.45.) is evaluated for I=0 and I=1, yiel-

ding

$$f_o(\theta) = \frac{1}{4}\left[(n_a^2 + n_c^2) \sin^2 2\theta + 2n_a n_c \cos^2 2\theta + 2n_b n_d \right] \qquad (4.46a.)$$

$$f_1(\theta) = \sin^2\theta(n_a n_b + n_c n_d) + \cos^2\theta(n_a n_d + n_b n_c) + \frac{1}{2}(n_a n_c + n_b n_d) \qquad (4.46b.)$$

In particular we find for a 50/50 $|a>/|b>$ mixture of H↓ in the high field limit ($n_a = 1/2$, $n_b = 1/2$, $\theta \to 0$)

$$f_o(\varepsilon) \approx \frac{1}{4}\varepsilon^2 \qquad (4.47a.)$$

$$f_1(\varepsilon) \approx \frac{1}{4}\varepsilon^2 \qquad (4.47b.)$$

where $\varepsilon^2 \sim B^{-2}$ as seen in (1.3a.). Since the field dependence of (4.44.) is determined by the $f_I(\theta)$ alone the rate of recombination scales, for a given temperature and density, inversely proportional with the square of the magnetic field. For the zero field case with equal occupation of the four hyperfine levels ($n_a = n_b = n_c = n_d = 1/4$, $\theta = \pi/4$) we obtain

$$f_o(B=0) = \frac{1}{16} \qquad (4.48a.)$$

$$f_1(B=0) = \frac{3}{16} \qquad (4.48b.)$$

In fact this result holds, more generally, for equal occupation of all hyperfine levels independent of the magnetic field. With the assumption that all orbital matrix elements are approximately the same, the ratio of high field and zero field recombination rates is given by $2\varepsilon^2$. For a 10 T field this implies that the recombination proceeds $\sim 10^5$ times slower than in zero field! This feature of the theory is believed to remain unchanged for surface recombination and, in fact, only has been studied under surface limited conditions. Clearly the GTB theory provides an explanation for the remarkable stability of H↓ in high fields, as discussed in chapters 3, 4 and 5, in comparison to the zero field results of Morrow et al.[32] The B^{-2} field dependence was established experimentally by Matthey, Walraven and Silvera[34], but a description of these experiments falls outside the scope of this thesis. Finally we note that (4.47.) and (4.48.) suggest a difference in the rate of formation of ortho- and para-H_2 between high and low fields. This feature of the theory has not yet been investigated experimentally.

1.4.8. *A simple phenomenological recombination model*

In this section we present a very simple hard sphere recombination model that has proved to be very useful to describe second order volume and surface recombination. The model is believed to fairly accurately describe both the temperature and field dependence of these processes for various kinds of "third bodies" (^{3}He, ^{4}He, H_2 -but not H) and surfaces (^{3}He, ^{4}He, H_2).

We write for the phenomenological rate equation for second order recombination

$$\frac{d\rho_i}{dt} = -2f(B)\,\frac{1}{2}\,\rho_i \dot{N}_i P_i \qquad (4.49.)$$

where i = 3 refers to the volume process and i = 2 to the surface case, ρ_i is the H atom density, $f(B) = \sum_{I=1}^{2} f_I(B)$ is defined by (4.45.) and refers to the, field dependent, probability of recombination per 3-body collision, $1/2\ \rho_i \dot{N}_i$ is the total number of H-H collisions per unit volume (area) and time, $\dot{N}_i$ is the number of H-H collisions per H-atom and unit time and P_i is the probability that a He atom is found within the interaction range of two interacting H atoms. The factor 2 appears because every recombination results in the loss of 2 H atoms. For surface recombination we assume the third body always to be present ($P_2 = 1$), whereas for the three-dimensional case we write $P_3 = \rho_3^{He}\Omega$; Ω is a reaction volume. For $\dot{N}_i$ we use the well known expression from kinetic theory for the -classical- hard sphere (disc) model

$$\dot{N}_i = \sqrt{2}\,\rho_i\,\bar{v}_i\,\sigma_i \qquad (4.50.)$$

$\bar{v}_i$ and σ_i are the average velocity and cross-section respectively.

$$\bar{v}_3 = \left(\frac{8kT}{\pi m}\right)^{\frac{1}{2}} \quad ; \quad \bar{v}_2 = \left(\frac{\pi kT}{2m}\right)^{\frac{1}{2}} \qquad (4.51.)$$

$$\sigma_3 = \pi\delta_o^2 \quad ; \quad \sigma_2 = 2\delta_o \qquad (4.52.)$$

Substituting (4.50.), (4.51.) and (4.52.) into (4.49.) we obtain

$$\frac{d\rho_3}{dt} = -K_3\,\rho_3^2\,\rho_3^{(He)} \quad ; \quad \frac{d\rho_2}{dt} = -K_2\rho_2^2 \qquad (4.53.)$$

with

$$K_3 \equiv \pi\sqrt{2}\,f(B)\,\delta_o^2\,\bar{v}_3\Omega \qquad (4.54a.)$$

$$K_2 \equiv 2\sqrt{2}\,f(B)\,\delta_o\,\bar{v}_2 \qquad (4.54b.)$$

If we assume the recombination to proceed slow in comparison to the rate at which thermal equilibrium is achieved we may use the adsorption isotherm to relate ρ_2 and ρ_3. In the low density limit, relevant for the experiments described in this thesis, the adsorption isotherm is given by equation (3.20.) and the rate equation for surface recombination may be transformed to show the effects of surface recombination on ρ_3.

$$\frac{d\rho_3}{dt} = - K_2^{eff} \rho_3^2 \qquad (4.55.)$$

where

$$K_2^{eff} \equiv 2\sqrt{2} \frac{A}{V} f(B) \delta_o \bar{v}_2 \lambda_{th}^2 e^{2\varepsilon_a/kT} \qquad (4.56.)$$

Combining (4.53.) and (4.56.) the overall rate equation for second order recombination becomes

$$\frac{d\rho_3}{dt} = - K_3 \rho_3^2 \rho(He) - K_2^{eff} \rho_3^2 \qquad (4.57.)$$

By working at low temperatures ($T < 0.6$ K) the helium vapor pressure can be made negligible and (4.57.) reduces to

$$\frac{d\rho}{dt} = - K_2^{eff} \rho_3^2 \qquad (4.58.)$$

K_2^{eff} may be determined experimentally as a function of temperature. If one then assumes δ_o to be temperature independent (4.56.) may be used to determine ε_a. This method has been used to dertermine the adsorption energy of atomic deuterium and is discussed in chapter 6.

REFERENCES

1. W. Kolos and L. Wolniewicz, J. Chem. Phys. 43, 2429 (1965).
2. W. Kolos and L. Wolniewicz, Chem. Phys. Lett. 24, 457 (1974).
3. W. Kolos and L. Wolniewicz, J. Mol. Spectr. 54, 303 (1975).
4. $a \approx 0.72$ Å. See D.G. Friend and R.D. Etters, J. Low Temp. Phys. 39, 409 (1980). The s-wave scattering length has been calculated by a number of authors yielding slightly different results. For a detailed account of the calculation see Y.H. Uang and W.C. Stwalley, J. de Phys. 41, C7 - 33 (1980).
5. C.E. Hecht, Physica 25, 1159 (1959).
6. J.V. Dugan and R.D. Etters, J. Chem. Phys. 59, 6171 (1973).
7. R.D. Etters, J.V. Dugan and R.W. Palmer, J. Chem. Phys. 62, 313 (1975).
8. R.D. Etters, R.L. Danilowicz and R.W. Palmer, J. Low Temp. Phys. 33, 305 (1978).
9. L.H. Nosanow, J. de Phys. 41, C7 - 1 (1980) and references therein.
10. G. Breit and I.I. Rabi, Phys. Rev. 38, 2082 (1931).
11. J.T.M. Walraven, E.R. Eliel and I.F. Silvera, Phys. Lett. 66A, 247 (1978).
12. A valuable discussion concerning particle indistinguishability is presented in N.F. Mott and H.S.W. Massey, *The Theory of Atomic Collisions*, 3rd edition, chapter XI, Clarendon Press, Oxford 1965.
13. A detailed analysis of the statistical nature of the hydrogen atom in relation to its composite structure is presented by M.D. Girardeau, J. Math. Phys. 16, 1901 (1975).
14. V. Heine, *Group Theory in Quantum Mechanics*, Pergamon Press, Oxford 1960.
15. In writing this expression for the effective potential we neglect the presence of the nuclear-electronic spin interaction and relativistic terms in the diatomic hamiltonian. These terms may give rise to singlet-triplet transitions, but are of no consequence for the H↓-H↓ case since relevant quasi-bound states are inaccessible at low temperature. For a discussion of the hyperfine potential energy curves see ref. 46 and references therein.
16. J.H. Freed, J. Chem. Phys. 72, 1414 (1980).
17. K. Huang, *Statistical Mechanics*, John Wiley & Sons, New York 1963; K. Huang in *Studies in Statistical Mechanics II*,

J. De Boer and G.E. Uhlenbeck, eds. North-Holland Publ. Co. Amsterdam 1964.

18. S.R. De Groot, G.J. Hooyman and C.A. Ten Seldam, Proc. Roy. Soc. A 203, 266 (1950).
19. M. Van den Bergh, Phys. Lett. 78A, 88 (1980)
20. V.V. Goldman, I.F. Silvera and A.J. Leggett, Phys. Rev. B, 24, 2870 (1981).
21. J.T.M. Walraven and I.F. Silvera, Journal de Physique, 41, C7-147, (1980).
22. D.A. Huse and E.D. Siggia, J. Low Temp. Phys. 46, 137 (1982).
23. N.N. Bogoljubov, J. Phys. USSR, 11, 23 (1947).
24. Private communication.
25. E.P. Gross, Nuovo Cimento, 20, 454 (1961).
26. L.P. Pitaevskii, Sov. Phys. - JEPT 13, 451 (1961).
27. E.P. Gross, J. Math. Phys. 4, 195 (1963).
28. W.J. Mullin, Phys. Rev. Lett. 44, 1420, (1980).
29. B.W. Statt and A.J. Berlinsky, Phys. Rev. Lett. 45, 2105 (1980).
30. E.D. Siggia and A.E. Ruckenstein, Phys. Rev. Lett. 44, 1423 (1980).
31. E.D. Siggia and A.E. Ruckenstein, Phys. Rev. B, 23, 3580 (1981).
32. M. Morrow, R. Jochemsen, A.J. Berlinsky and W.N. Hardy, Phys. Rev. Lett. 46, 195 (1981); erratum Phys. Rev. Lett. 47, 455 (1981).
33. R. Jochemsen, M. Morrow, A.J. Berlinsky and W.N. Hardy, Phys. Rev. Lett. 47, 852 (1981).
34. A.P.M. Matthey, J.T.M. Walraven and I.F. Silvera, Phys. Rev. Lett. 46, 668 (1981).
35. G.H. Van Yperen, A.P.M. Matthey, J.T.M. Walraven and I.F. Silvera, Phys. Rev. Lett. 47, 800 (1981).
36. V.V. Goldman and I.F. Silvera, Proceedings LT - 16, Physica 107B, 515 (1981).
37. D.O. Edwards and I.B. Mantz, J. de Phys. 41, C7, 257 (1980).
38. I.B. Mantz and D.O. Edwards, Phys. Rev. B, 20, 4518 (1979).
39. I.F. Silvera and V.V. Goldman, Phys. Rev. Lett. 45, 915 (1980).
40. W. Band, *An Introduction to Quantum Statistics*, D. Van Nostrand, Princeton 1955.
41. Classic investigations were done by I. Amdur and coworkers. See J. Am. Chem. Soc. 55, 1395 (1933); 57, 856 (1935); 60, 2347 (1938).
42. J.T. Jones, M.H. Johnson, H.L. Mayer and R.S. Wright, Aeronutronic Systems Inc. Publ. No U-216 (1958).

43. R.E. Roberts, R.B. Bernstein and C.F. Curtiss, J. Chem. Phys. 50, 5163 (1969).
44. See also R.J. Le Roy and R.B. Bernstein, J. Chem. Phys. 54, 5114 (1971).
45. W.C. Stwalley, Phys. Rev. Lett. 37, 1628 (1976).
46. Y.H. Uang and W.C. Stwalley, Phys. Rev. Lett. 45, 627 (1980). Y.H. Uang, R.F. Ferrante and W.C. Stwalley, J. Chem. Phys. 74, 6256 (1981).
47. T.G. Waech and R.B. Bernstein, J. Chem. Phys. 46, 4905 (1967). These values are known to be approximately 4 cm^{-1} too high, see ref. 44 and ref. 3.
48. J.M. Greben, A.W. Thomas and A.J. Berlinsky, Can. J. Phys. 59, 945 (1981).
49. W.N. Hardy, M. Morrow, R. Jochemsen, B.W. Statt, P.R. Kubrik, R.M. Marsolais, A.J. Berlinsky and A. Landesman, Phys. Rev. Lett. 45, 453 (1980); J. de Phys. 41, C7 157 (1980).
50. For a concise review of the three-body scattering theory and the Faddeev formalism see I.R. Afnan and A.W. Thomas in *Modern Three Hadron Physics*, A.W. Thomas (ed.), Springer Verlag Berlin 1977.
51. M.L. Goldberger and K.M. Watson, *Collision Theory*, John Wiley & Sons, New York 1964.
52. E.O. Alt, P. Grassberger and W. Sandhas, Nucl. Phys. B 2, 167 (1967).
53. I.F. Silvera, Finish Low Temperature Winter School, Lammi. Finland, Jan. 1979, unpublished.
54. I.F. Silvera and. J.T.M. Walraven, *Recent Developments in Condensed Matter Physics*, J.T. Devreese (ed.), Volume 1, 29, Plenum Press, New York (1981).
55. R.W. Cline, T.J. Greytak and D. Kleppner, Phys. Rev. Lett. 47, 1195(1981).
56. R. Sprik, J.T.M. Walraven, G.H. Van Yperen and I.F. Silvera, to be published.

CHAPTER 2

EXPERIMENTAL CONSIDERATIONS

2.1. THE PRODUCTION AND COOLING OF ATOMIC HYDROGEN

A Helium-Temperature Beam Source of Atomic Hydrogen

J.T.M. Walraven and Isaac F. Silvera

Natuurkundig Laboratorium der Universiteit van Amsterdam,

Valckenierstraat 65, 1018 XE Amsterdam, The Netherlands

(accepted for publication by the Review of Scientific Instruments)

Abstract

We describe a technique for producing a high flux beam of atomic hydrogen with a velocity distribution corresponding to liquid helium temperatures. We have studied how a gas of hydrogen atoms (H) may be cooled to low temperatures through interaction with cold walls. The gas was analyzed by forming an atomic beam. We obtained fluxes $\phi_H \simeq 2.4 \times 10^{16}$ atoms/sec at $T \simeq 8$ Kelvin, which corresponds to an increase in flux of low velocity atoms by a factor 20 over that of the same source operated at room temperature. The degree of dissociation and the translational temperature of the gas were determined using a quadrupole mass-spectrometer and time of flight techniques. A beam modulation technique advantageous for such a system is discussed and analyzed. General design considerations for the transport and cooling of H are presented and illustrated with examples. The methods of data analysis are discussed in detail.

1. Introduction

In this paper we discuss a method by wich atomic hydrogen (H), produced at room temperature, is cooled to helium temperature through interaction with cold walls, providing a high flux source. Although there exists an extensive literature on sources of H, only very recently have there been any reports of sources of liquid helium temperature H.[1,2,3] The work described here has been motivated by our endeavors to produce a stable gas of atomic hydrogen at low temperature for studies of its predicted properties as a weakly interacting Bose gas.[4] However, the source is not limited to this type of research and should have potential applications in many areas. As a time and frequency standard the hydrogen maser can be improved by low temperature operation.[5,6] Low velocity H beams are required to study the well-region of the interaction potential of (for instance) the $H+H_2$ system.[7] Considerable interest also exists in high energy physics where low velocity atoms are of interest to improve the intensity of polarized proton sources and targets.[8,9,10,11]

The feasability of cooling H to helium temperature has been demonstrated in numerous experiments where gaseous mixtures of H, H_2 and (often) inert gases are rapidly condensed onto a cold substrate in order to matrix isolate the H atoms.[12,13] However, these experiments yield little information about the efficiency of the cooling process. The present work is aimed towards the study of the experimental conditions by which H can be cooled to low temperatures and the efficiency of this process with respect to recombination. Our experimental approach is to run H through a short cylindrical tube of variable temperature, the walls of which act as an accommodator. The gas emerging from the accommodator forms an atomic beam and is analysed using standard beam techniques. In this way we determine the atomic flux, degree of dissociation and translational temperature of the gas. The measurements also enable an estimate of the average density of H in the accommodator. Although the paper gives an account of these measurements, we have tried to emphasize design and measurement technique considerations, in particular the transport of a recombining gas of hydrogen. The advantages and use of an equal segmented chopper-blade for time of flight measurements of hydrogen, rather than the usual narrow slit chopper, are discussed in detail. To our knowledge this technique has not been discussed in the literature.

We have divided this paper into three main sections. First (Section 2) we discuss our experimental apparatus along with design considerations. Sec-

tion 3 is devoted to the procedures employed in the measurements and the results are presented and discussed in Section 4.

2. The Experimental Apparatus

Overview

A schematic diagram of the apparatus is given in Fig. 1. H is produced at the left in a water cooled fused quartz discharge tube inserted into a microwave dissociator operated at 2450 MHz. The discharge pressure is adjusted in the range 0.5 - 1.5 torr using a needle-valve which also serves to limit the total flow through the system. Typically the dissociated fraction is 90%. The atoms flow through a small orifice into a teflon tube which serves to guide the atoms towards a cylindrical accommodator (4 mm ID, 20 mm long) intended to cool the H-gas to liquid helium temperature. For this

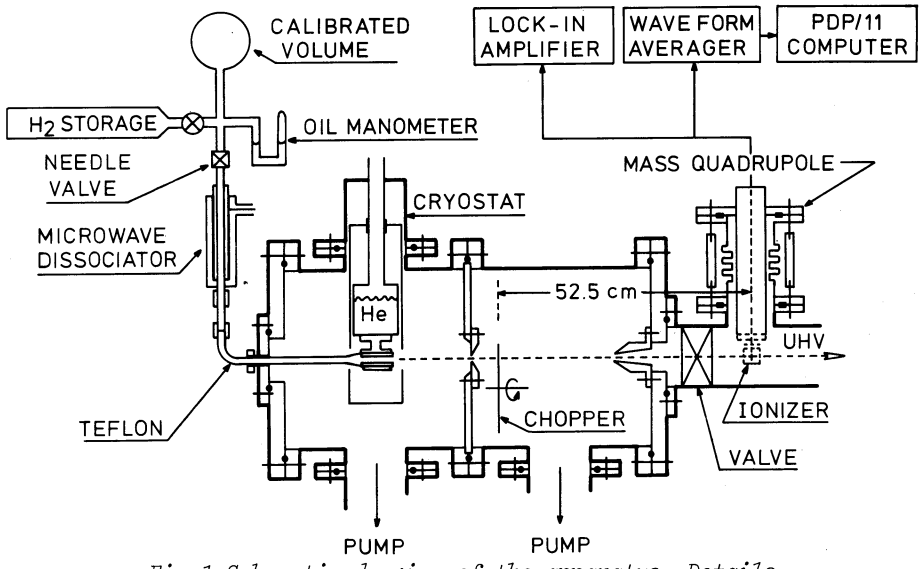

Fig. 1-Schematic drawing of the apparatus. Details of the dissociator, etc. are given in subsequent figures.

purpose a small He cryostat with vapor cooled shielding is incorporated in the system. The beam emerging from the accommodator is differentially pumped in three stages to obtain pressures of order 10^{-9} torr in the last stage where a quadrupole mass spectrometer is used as a detector. The beam intensity is modulated in the second stage using an equal segmented chopper-blade. The distance between chopper and detector (52.5 cm) enables a time

of flight (TOF) analysis of the beam, using a waveform averager and a PDP/11 computer for signal processing. Since we use an equal segmented chopper-blade, the velocity distributions are found by differentiation of the detector response. The principle advantage of this method is that one obtains a high average flux, which enables easy alignment and continual monitoring of the beam intensity with a lock-in amplifier. This is particulary important with a species such as H in which rapid beam deterioration can result in signal averaging of a non-existent signal and much wasted effort. A box-car integrator was used for absolute intensity measurements. For these measurements the gas handling system included a calibrated volume of 1140 cc and an oil manometer.

The dissociator

Many publications concerning dissociation of hydrogen have appeared in the literature, discussing the specific problems associated with various techniques.[14] Thermal beams of hydrogen atoms are currently produced using electrodeless discharges employing r.f. or microwave power. We use a home-made reentrant cavity operated at 2450 MHz (λ=122 mm). The cavity, shown in Fig. 2, consists of a 28 mm ID outer conductor (OC) of length $5\lambda/4 \simeq 153$ mm and a (slightly shorter) inner conductor (IC) of 14.8 mm ID , A quartz

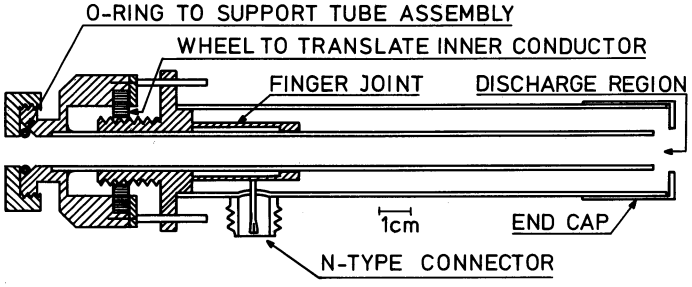

Fig. 2-Microwave cavity operating at 2450 MHz. The assembly of discharge tube and water cooling shown in Fig. 3 fits into the inner conductor. While the inner conductor remains fixed in position with respect to the discharge tube the outer conductor can be translated to tune the cavity for optimum coupling.

discharge tube is inserted coaxially through the IC and the discharge occurs in the gap of approximately 3.5 mm between the end of the IC and a cap tightly fitting over the end of the OC. The cavity is tuned capacitively by varying the gap-spacing. For this purpose the IC can be moved relative to the OC using a fine adjustment screw. A simple $\lambda/4$ finger joint[15] was used to minimize electrical losses in the sliding contact. The power is coupled in inductively via an N-type connector making contact with the IC via the finger joint. The discharge is started using a spark from a tesla coil.

A variety of discharge tubes were tried. The discharge was most easily operated using a 12 mm OD quartz tube which completely filled the bore of the inner conductor, however poor cooling inherent to this geometry caused a high operating temperature and resulted in irreversable deterioration of the tube after a few hours. Deteriorated tubes invariably showed a dark deposit, sometimes exhibiting a metallic appearance. The surfaces usually could be cleaned somewhat using a strong oxidizing acid mixture (HNO_3 + H_2SO_4). However, the only way to completely remove the dark film was to wash the tube in concentrated HF or NaOH for many hours after which the film "peeled off" but did not dissolve. Our chemical experiences are consistent with the Auger analysis of darkened surfaces of pyrex dissociator envelopes obtained by Ritz et al.[16], who attributed the films to deposits of carbon in its amorphous and carbide forms and to a lesser extent to Si_3N_4. Many procedures were tried to clean the tubes but in our experience the best way to improve the discharge in case of deterioration was to replace the tube.

In our present system the discharge region is cooled from two sides. as shown in Fig. 3, using water as a coolant, carefully shielded from the microwave by a metal envelope. Additional cooling is obtained by blowing air in the cap region. Incorporation of the cooling facilities limited the size of the discharge tube to approximately 6 mm o.d. and was found to make the tuning procedure a bit more subtile. Typically the dissociator is operated at a pressure of 0.5 torr using 25 W of microwave power; the system reliably yields a degree of dissociation of order 90% up to a few torr. We use standard 6 x 4 mm quartz tubing in which a flow impedance is fused in to separate the discharge region from the transport tube which serves to guide the atoms to the accommodator. The impedance is a 0.35 mm orifice in a disk of 1 mm thickness sliced off from thick walled quartz cappillary

tubing. Connections to the discharge tube are made using standard teflon swagelock vacuum connectors.

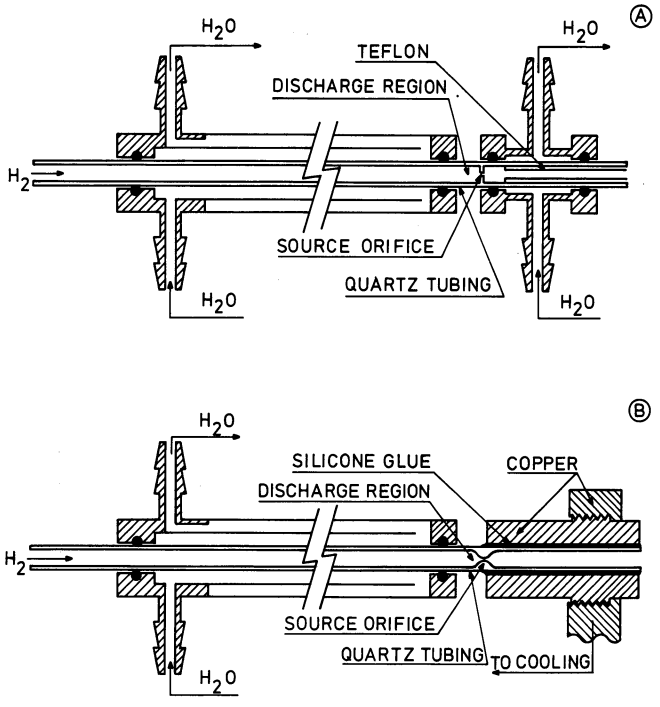

Fig. 3-Two examples of discharge tube assemblies.

A- Water-cooled system used for room temperature dissociation.

B- Assembly where the temperature of the outstreaming gas can be varied from 77 K to 600 K by varying the temperature of a copper cold plate.

Transport of the Gas

A flexible teflon tube connects the dissociator with the accommodator. We shall present a simple phenomenological model describing Knudsen flow of atoms through the tube in the presence of surface recombination. The model enables an estimate of the recombination losses. For convenience the last two centimeters of the tube are supposed to represent the accommodator and will be considered to be at the same temperature as the tube for our present purpose. The model is very useful for design purposes where often only an estimate of the effect of recombination is required. More accurate re-

sults can be obtained with an analysis in terms of exact integral equations.[17,18] The viscous flow regime is reviewed by Wise and Wood.[19] A useful formulation of the problem, in view of our needs, is obtained by considering a tube of length ℓ and radius r closed at the left and open at the right end and maintained at room temperature. The tube is assumed to be "long" ($\ell >> r$). At the left side we introduce H through a small orifice at the rate ϕ_{in}; the other side is assumed to end in an ideal vacuum. In the case of Knudsen flow we may estimate the density profile of H along the tube as well as the degree of dissociation of the gas leaving the tube using a diffusion model:

$$\phi(z) = -\pi r^2 D_{Kn} \frac{dn(z)}{dz} \qquad (1)$$

where $\phi(z)$ and $n(z)$ represent the atomic flux and density at distance z in the tube measured from the high pressure end, $D_{Kn} \equiv \frac{2}{3} r\bar{v}$ is the atomic diffusion constant for Knudsen flow, and $\bar{v}$ is the average atomic velocity. The variation of $\phi(z)$ along the tube due to recombination is written phenomenologically as a power series in $n(z)$:

$$\frac{d\phi}{dz} = -\pi r^2 K_v n^3 - 2\pi r K_{S2} n^2 - 2\pi r K_{S1} n \qquad (2)$$

The first term describes three-body volume recombination, with rate constant K_v, the other two terms arise from surface recombination which can be first or second order in nature, with rate constants K_{S1} and K_{S2}.[20] The surface density σ is built up of two components: $\sigma = \sigma_t + \sigma_m$. σ_t is the density of atoms trapped in catalytic sites. Below an activation temperature (which may be much higher than room temperature) these sites will be continuously saturated and σ_t will be a constant equal to the density of these sites. The second component, σ_m, represents weakly bound (physisorbed) mobile atoms. σ_m and σ_t are related to the bulk gas density through an adsorption isotherm. σ_m is proportional to n in the limit of low coverages. Recombination may proceed through interactions of trapped atoms with mobile surface atoms or with gas-phase atoms, giving rise to first order recombination or between two mobile adsorbate atoms resulting in second order recombination. On pyrex and quartz, recombination is known[19] to be first order over a wide range of temperatures, however for $T \lesssim 120$ K and $T \gtrsim 550$ K, recombination is a second order process. At room temperature recombination on teflon is thought to be first order[21] and we shall assume this to be the case.

Using equation (1) and (2) the diffusion problem is reformulated for Knudsen flow as

$$\frac{d^2n}{dz^2} = \frac{3}{r\bar{v}}\left(K_{S1}n + K_{S2}n^2 + \frac{1}{2}\,r\,K_v n^3\right) \tag{3a}$$

$$\frac{dn}{dz} = \frac{1}{2\pi}\,\frac{3}{r\bar{v}}\,\phi \tag{3b}$$

with boundery conditions $n(z=\ell)=0$ and $\phi(z=0)=\phi_{in}$.

For our present purpose volume recombination will be shown to be negligible so that we limit the analysis to surface recombination. In the absence of any recombination ($\phi_{out}=\phi_{in}$) we obtain the well known relations for Knudsen flow[22]:

$$n(z) = n_o\,(1 - z/\ell) \tag{4}$$

$$n_o = \frac{3}{2\pi}\,\frac{\ell}{r\bar{v}}\,\phi_{in} \tag{5}$$

Equation (5) is often written in the Clausing form[23]:

$$\phi_{out} = \frac{1}{4}K\,n_o\bar{v}\,A \tag{6}$$

where $A = \pi r^2$ is the cross-section of the tube and $K = \frac{8}{3}r/\ell$ is the Clausing factor in the Knudsen limit (long tubes). For short tubes values for K are tabulated[24]. The average number of wall collisions, $\bar{N}_c$, that a particle has ondergone after diffusing through the tube is given by

$$\bar{N}_c = \frac{\phi_{wall}}{\phi_{out}} = \frac{3}{8}\left(\frac{\ell}{r}\right)^2 \tag{7a}$$

where $\phi_{wall} = \int_0^{\ell} \frac{1}{4}\cdot n(z)\bar{v}2\pi r\,dz$ is the total number of wall collisions per unit time. The average time the particle has spent in the tube is given by

$$\bar{t} = \frac{N_{tot}}{\phi_{out}} = \frac{3}{4}\,\frac{\ell^2}{r\bar{v}} \tag{7b}$$

Here $N_{tot} = \int_0^{\ell} n(z)\pi r^2\,dz$ is the total number of atoms in the tube. We note that in general ϕ_{wall} and N_{tot} include a contribution due to particles which never reach the end of the tube. This is for instance the case in the classical geometry of Knudsen (a channel connecting two big vessels) where only a fraction z/ℓ of the particles colliding with the wall at a distance z in the tube will reach the end. The rest of the particles return to the prima-

ry vessel. As a result only a third of the particles in the channel will reach the secondary end, in which case

$$\bar{N}_c = \frac{1}{8}\left(\frac{\ell}{r}\right)^2 \text{ and } \bar{t} = \frac{1}{4}\frac{\ell^2}{r\bar{v}} \tag{8}$$

Our geometry is characterized by a negligible probability to return to the discharge region ($\phi_{in} = \phi_{out}$) and thus eqs. (7a,b) are applicable.

In the case of first order recombination the rate coefficient can be written as $K_{S1} \equiv \frac{1}{4}\gamma\bar{v}$, where γ is the recombination probability per wall collision. With this convention the solution of equations (3) is

$$n(z) = \frac{n_o}{\sqrt{2\gamma\bar{N}_c}} \frac{\sinh\left[\sqrt{2\gamma\bar{N}_c}(1-z/\ell)\right]}{\cosh\left[\sqrt{2\gamma\bar{N}_c}\right]} \tag{9a}$$

$\bar{N}_c$ is given by equation (7a). n_o is the atomic density, achieved immediately behind the source orifice and calculated using equation (5).

A plot of n(z) versus z is given in Fig. 4. The degree of dissociation α of the flux leaving the tube, defined as the fraction of all atoms in the dissociated state ($\alpha \equiv \frac{n_H}{n_H + 2n_{H_2}}$) may be expressed, using (3b), as

$$\alpha \equiv \frac{\phi(\ell)}{\phi_{in}} = \left[\cosh\sqrt{2\gamma\bar{N}_c}\right]^{-1} \tag{9b}$$

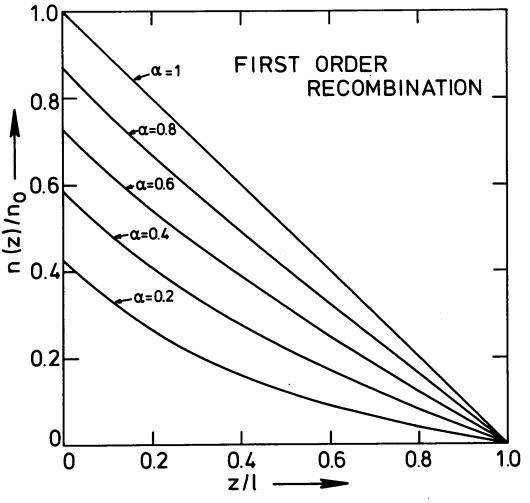

Fig. 4-Density profile of atomic hydrogen along a tube with length ℓ for the case of first order recombination. α is the degree of dissociation of the gas leaving the tube.

We note that the actual purity of the gas is higher (dissociation of one molecule yields two atoms), but in conforming with the literature on dissociation we shall use α. Furthermore $\alpha \simeq 0.46$ for $\gamma\bar{N}_c = 1$ so that, as a rule of thumb, for negligible recombination in the tube one should require

$$\gamma\bar{N}_c << 1 \tag{9c}$$

Our objective is to use these results for designing a source with an acceptable output flux. As an example we consider the teflon tube of typical length ℓ = 25 cm and radius r = 2.5 mm. We first estimate ϕ_{in}. In the discharge, operated at 0.5 torr, the atomic density is estimated to be $n_d \simeq 8 \times 10^{15}$/cc (for 600 K and full dissociation). This implies

$$\phi_{in} \simeq \frac{1}{4} K_o n_d \bar{v} A_o \simeq 1.8 \times 10^{17}/\text{sec}$$

for the flux entering the transport tube, where $K_o \simeq 0.25$ is the Clausing factor and $A_o \simeq 0.1$ mm^2 in the area of the source orifice. We calculate $n_o \simeq 6 \times 10^{14}/\text{cm}^3$ using (5), corresponding to a mean free path[25] of a few millimeters so that Knudsen flow may be assumed. Volume recombination can be neglected if $\frac{1}{2} r K_v n^3 << K_{S1} n$. This requirement leads to an upper limit for the density:

$$n << \left(\frac{\gamma\bar{v}}{2\, r\, K_v}\right)^{1/2} \tag{10}$$

Using the data of Mitchell and Le Roy[21] ($\gamma_{teflon} = 2.1 \times 10^{-5}$ and K_v 1.2×10^{-32} cm^6 atom^{-2} sec^{-1}) we conclude $n << 3 \times 10^{16}/\text{cm}^3$, a condition easily met without limiting n_o.

The degree of dissociation at the end of the tube can now be evaluated with the aid of equation (9b). We find $\alpha \simeq 93\%$. However, if we were dealing with an imperfect teflon *coating* on a pyrex tube and 5% of the pyrex was exposed to the atoms, we would have a larger effective recombination coefficient ($\gamma_{eff} \simeq 2.2 \times 10^{-4}$, with $\gamma_{pyrex} \simeq 4 \times 10^{-3}$, see ref. 19) yielding $\alpha \simeq 51\%$. This example shows that teflon tubing can be used to guide H-atoms over relatively large distances without excessive recombination and that pyrex is inadequate for this purpose, at least at room temperature. For a similar uncoated pyrex tube one finds $\alpha \simeq 8 \times 10^{-3}$. However, cooling this tube to $\sim$100 K, where the recombination coefficient for pyrex is minimal, one again finds $\alpha \simeq 93\%$, since for this temperature $\gamma_{pyrex} \simeq \gamma_{teflon} \simeq 2 \times 10^{-5}$. One should notice that recombination coefficient may vary from sample to sample as witnessed by the large scatter in γ_{pyrex} valu-

es[26,27,28,29] obtained by various authors in the literature. We have observed a teflon surface to deteriorate "overnight" in a vacuum chamber, probaly due to oil contamination.

In view of these uncertainties the calculated values for α agree fairly well with the experimental results where values of α up to $\simeq$ 60% were obtained using commercial teflon tubing for the transport tube and teflon coated quartz tube of 4 mm i.d. for the accommodator and for the first section of the tube , i.e. the section immediately behind the discharge region (see Fig. 1). A very pure atomic beam (α > 90%) was obtained using a 90 mm long 4 mm wide uncoated quartz tube operated at nitrogen temperature (see Fig. 3b).

For second order recombination the probability of recombination per wall collision becomes density dependent ($\gamma \equiv 4\, K_{S2} n/\bar{v}$). If we still use this concept to express our results the solution of the equations (3) is given by

$$n(z) = \frac{n_o}{\gamma_o \bar{N}_c (a+z/\ell)}\, x^2 P\,(x;0,1) \tag{11a}$$

$$\alpha \equiv \frac{\sqrt{-\xi}}{\gamma_o \bar{N}_c\, a^3} \tag{11b}$$

where P (x;0,1) is the equianharmonic case of the Weierstrass elliptic function[30] and $\gamma_o \equiv \gamma(z=0)$. Furthermore

$$x(z) \equiv \frac{2\omega_2}{\sqrt{3}} \cdot \frac{(z/\ell+a)}{(1+a)} e^{i\frac{\pi}{6}} \tag{11c}$$

$x_o \equiv x(z=0)$, $\xi = x_o^6$ and $\omega_2 \simeq 1.53$ (see ref. 30). The constant a has to be determined from the relation

$$\gamma_o \bar{N}_c = -\left(\frac{x_o}{a}\right)^3 P'(x_o;0,1) \tag{11d}$$

A plot of n(z) versus z according to equation (11a) is given in Fig. 5 for various values of α.

Equations (11a) and (11d) are most conveniently manipulated using economized polynomial expansions for $x^2P(x;0,1)$ and $x_o^3P'(x_o;0.1)$.[31] In terms of these polynomials n(z) is given by

$$n(z) = n_o \frac{a^3}{(z/\ell+a)} \cdot \frac{P_1(\eta)}{P_2(\xi)} \tag{12a}$$

The constant a (or ξ) has to be determined from

$$\gamma_o \bar{N}_c = - \frac{P_2(\xi)}{a^3} \qquad (12b)$$

To a good approximation (for $0 \leq \eta$(or ξ) ≤ 12.8

$$P_1(\eta) = 1 + 3.571 \times 10^{-2} \eta + 9.8 \times 10^{-5} \eta^2 \qquad (12c)$$

$$P_2(\xi) = -2 + 0.14286 \xi + 9.81 \times 10^{-4} \xi^2 \qquad (12d)$$

Here $\eta \equiv x^6$

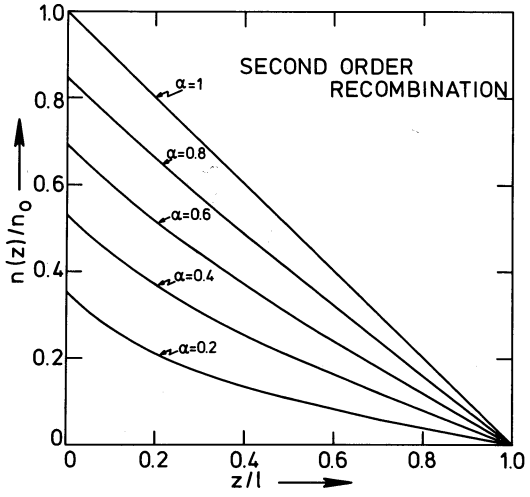

Fig.5-Density profile of atomic hydrogen along a tube with length ℓ for the case of second order recombination. α is the degree of dissociation of the gas leaving the tube.

The case of second order recombination is illustrated with the example of a tube with the same dimensions as the teflon tube discussed earlier (ℓ = 25 cm and r = 2.5 mm) but now maintained at T = 0.5 K and covered with a superfluid film of ^{4}He. Assuming a flux $\phi_{in} = 8 \times 10^{15}$/sec to enter the tube via a small orifice we again calculate $n_o \simeq 6 \times 10^{14}/cm^3$ using equation (5) so that the assumption of Knudsen flow is justified.[32] Volume recombination may be neglected if

$$n << \frac{2K_{S2}}{r K_v}$$

as seen from equation (3a). Using the data of Morrow et al. $K_{S2} = 8 \times 10^{-17}$ cm^4/sec, for T = 0.5 K and $K_v = 2.8 \times 10^{-33}$ cm^6/sec as measured by Hardy

et al.[33], we find $n << 2.3 \times 10^{17}/cm^3$. This condition is easily satisfied over the whole length of the tube. Using $\gamma \equiv 4K_{S2}n/\bar{v}$, (7a), (12b) and (11b), we may calculate $\gamma_o \bar{N}_c \simeq 0.14$, $a \simeq 2.65$, $\xi = -4.45$ and $\alpha = 0.81$. At this low temperature α does not represent the degree of dissociation (which is unity since H_2 will freeze out on the walls) but simply the reduction in flux due to recombination. We note that under these conditions transport of atoms at 0.5 K is comparable in efficiency with transport at room temperature with a teflon tube. However, in a high magnetic field recombination is known to be strongly suppressed at low temperatures. Matthey et al.[34] measured $K_{S2} \simeq 3.8 \times 10^{-21}$ cm^4/sec in 10 Tesla at T = 0.5 K. With this figure we calculate for a tube of $\ell = 2500$ cm and r = 2.5 mm $\gamma_o \bar{N}_c = 0.068$, again using $n_o = 6 \times 10^{14}/cm^3$ (or $\phi_{in} \simeq 8 \times 10^{13}$/sec). Thus a = 3.50, $\xi = -6.73$ and $\phi_{out} = 0.89\ \phi_{in}$. We note that the atoms have spent on the average a time of 1875 seconds in the tube , as determined by equation (7b), without significantly recombining. These results may be extended to other temperatures or other magnetic fields (B > 0.5 Tesla) using $K_{S2} = K_o B^{-2} T^{-1/2} \exp(2\varepsilon_a/kT)$,[34] where K_o is a scaling constant.

The accommodator

The considerations of the preceeding section can also be used for the design of an efficient accommodator. The aim is to cool the fluxing gas down to approximately the temperature of the surface without it recombining. At 4.2 K the best known accommodator surface, with a low vapor pressure, is H_2. However, we point out that H_2 has an adsorption energy $\varepsilon_a/k = 38 \pm 5$ K for H.[35] In thermodynamic equilibrium most of the H would rapidly condense and recombine. Thus the accommodator design must be such that the gas just approaches the wall temperature and then fluxes out into a subsequent stage. Accommodation can usually be achieved with just a few collision so that a choice of $\bar{N}_c \simeq 1/\gamma$, resulting in $\alpha \simeq 50\%$, (see relation (9c)) is satisfactory.

From these qualitative arguments one concludes that one should select wall materials with small adsorption energy, ε_a, for use at low temperatures. Then the surface coverage and thus γ will remain minimal. The best known surfaces to inhibit condensation of H are made of liquid ^4He, ^3He or ^3He-^4He mixtures with a measured $\varepsilon_a \simeq 0.9$ K and 0.34 K, respectively.[6,34,36,37] However, use of these surfaces require very low temperatures to maintain a low density of the saturated helium vapor which catalyzes volume re-

combination. Therefore, except for the lowest temperatures ($T \lesssim 0.6$ K) one must rely on other surfaces with a weak physisorption potential for H, such as H_2 or Ne. From the work of Crampton[35] we calculate $K_{S2} \simeq 3 \times 10^{-12} cm^4/sec$ at T = 4.2 K. With the aid of $\gamma \equiv \frac{4}{\bar{v}} K_{S2} n$ and using $n = 10^{13}/cm^3$ one finds $\frac{1}{\gamma} \simeq 250$ showing that only very short H_2 plated tubes can be used to accommodate H to 4.2 Kelvin.

In practice it is difficult to select a well characterized geometry to cool H. Surface composition is often poorly known and temperature gradients complicate the picture; therefore we have tested several accommodator designs. Initially we followed the concept utilised by Toennies, Welz and Wolf (TWW)[7], first described by Wilsch.[38] In this design H, produced by RF discharge, is cooled to ~90 K by passing the gas through a narrow metal channel cooled with liquid nitrogen. Various wall metals were tested by TWW (pyrex, boron nitride, copper), but best results were obtained using an aluminum channel. Since aluminum surfaces efficiently catalyze surface recombination,[19] the result was attributed to the formation of a thin oxide layer efficiently cooled by the metallic substrate. It is interesting to note that we have observed the *copper*-oxide surface to be unstable in direct contact with H. A black, heavily oxidized, copper sample regained its metallic appearance in a few minutes under bombardment with H at a rate of $10^{17}/cm^2$ sec. TWW also tried cooling their beams to hydrogen temperature (20.4 K). However, under these conditions considerable recombination took place while the remaining atoms were not effectively accommodated.

Following the concept of TWW an aluminum cap, containing a 0.5 mm diameter channel, was attached to the (uncooled) end of our discharge tube. We found a good thermal contact between the aluminum and quartz to be of vital importance to prevent the discharge tube from overheating. This requirement caused a considerable heat load on the cooling system. Although the degree of dissociation was high (> 90%) down to nitrogen temperature, cooling to helium temperatures was unsuccessful, while the system was susceptible to breakage due to differential thermal contraction.

Good dissociation was also obtained using a discharge tube as drawn in Fig. 3b. This tube was partially water cooled and partially cooled with liquid nitrogen. For this purpose the quartz tube was glued into a copper cylinder using silicone cement, an adhesive remaining reasonably flexible at low temperature and consequently capable of compensating for the rather large differences in thermal contraction between copper and quartz. The

copper cylinder was screwed into an aluminum cold plate, cooled by circulation of cryogenic liquids. Although this geometry worked very reliably down to liquid nitrogen temperature, it had the disadvantage that a considerable fraction of the microwave power dissipated in the discharge still had to be carried away through the low temperature cooling system, limiting the lowest achievable temperatures to about 20 K.

The most detailed study was made using a design where the accommodator is completely thermally decoupled from the discharge region (see Fig. 1). The atoms are guided to the accommodator using teflon tubing. In this way an extremely flexible geometry is obtained. For an accommodator we used a cylindrical pyrex tube (6 x 4 mm; 20 mm long) coated with teflon, using FEP teflon dispersion[39] fused at 350 K in a flowing oxygen atmosphere. Using (7a) we calculate $\bar{N}_c \simeq 38$. The accommodator was glued into a copper block, again employing silicone glue. The block is screwed to the bottom of a small can which holds approximately 1 liter of liquid helium. The arrangement is shown in Fig. 6. The main disadvantage of this design was that for

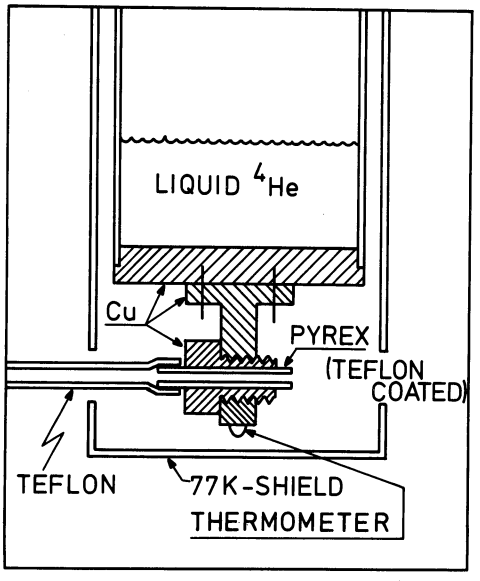

Fig.6-Schematic diagram of the low temperature section of a helium cryostat used to cool a teflon coated pyrex tube to helium temperatures.

high flows a background gas built up interfering with the beam and thus limiting the fluxes that could be studied. The properties of the accommodator were studied as a function of temperature. At high temperature the teflon

surface is exposed to the H gas, whereas at helium temperature the teflon is coated by H_2. The lowest achievable temperatures were limited to 7.7. K due to conduction and radiative heat leaks. For an accommodator used in studying H as a stable low temperature gas[4], we simply used a copper or german silver wall which is coated with H_2 at T ≃ 5 K.

Beam formation

The atomic beam that results when the gas leaving the accommodator expands into vacuum can be described by a model of Giordmaine and Wang (GW)[40], who successfully applied kinetic theory to the problem of molecular beam formation by long cylindrical channels connecting a source volume to an ideal vacuum. A similar study was made by Troitskii.[41] GW assumed the density n(z) to fall linearly with the distance (z) along the channel as in the case of Knudsen flow

$$n(z) = n_s \frac{z}{\ell} \tag{13}$$

where n_s is the density in the source, z is measured from the low pressure end and ℓ is the total length of the channel. Better approximations accounting for the non-zero density at the end of a real channel have also been studied[42] but lead to corrections which hardly affect our results.

GW considered two contributions to the center-line intensity, I, of the beam:

a) A contribution due to atoms passing through the channel without collisions

$$I_1 = \frac{1}{4\pi} n_s \bar{v}_s A \exp\{-\ell/2\lambda_s\} \tag{14}$$

where λ_s is the molecular mean free path at density n_s and the exponent accounts for beam attenuation due to scattering by the stagnant gas in the channel.

b) A contribution due to particles scattered into the axial direction by interatomic collisions in the channel

$$I_2 = \int_0^{\ell} dz \frac{1}{4\pi} n(z) \bar{v} A \frac{1}{\lambda(z)} \exp\{-z/2\lambda(z)\} \tag{15}$$

Adding (14) and (15) one attains the total center-line intensity which may be conveniently written as

$$I = \frac{F(n)}{\pi} \frac{1}{4} n_s \bar{v} A \tag{16a}$$

$$F(\eta) \equiv \frac{\sqrt{\pi}}{2} \frac{\mathrm{erf}(\sqrt{\pi})}{\sqrt{\eta}} \tag{16b}$$

$$\eta \equiv \frac{\ell}{2\lambda_s} \tag{16c}$$

Peaking of the beam

It will turn out to be useful to characterize a beam source with a parameter χ, called the peaking factor of the source, which relates the total intensity with the center-line intensity:

$$I = \chi\Phi/\pi \tag{17}$$

For a cosine emitting source $\chi = 1$ so that the peaking factor is a measure for the directivity of a beam source, normalized to that of an ideal effusive source. Comparing (16) with (17) and recalling the well known Clausing formula (6) for the total flow through a channel ($\Phi = \frac{1}{4} K_o n_s \bar{v} A$; where K_o is the Clausing factor) χ may be written as

$$\chi = \frac{F(\eta)}{K_o} \tag{18}$$

The opaque mode

A specific mode of operation, of particular importance for our analysis, is the opaque mode, where particles have a negligible probability to pass through the channel without a collision. In this mode we are still dealing with Knudsen flow, but only process "b" will contribute to the beam. The condition for opacity in the channel is $\eta \gtrsim 6$ where the error function approaches unity to within 1% and can be approximated by

$$F(\eta) = \frac{1}{2}\left(\frac{\pi}{\eta}\right)^{1/2} \tag{19}$$

Expressing λ in terms of the density, $\lambda = (\sqrt{2}\sigma n)^{-1}$, where σ is a collision cross-section, and using the "long channel approximation" for the Clausing factor ($K_o = \frac{8}{3} \frac{r}{\ell}$) leads, after a few manipulations, to a compact formula for χ:

$$\chi = \frac{1}{8}\left(\frac{3}{2}\pi\sqrt{2} \frac{\bar{v}A}{r} \frac{1}{\phi}\right)^{1/2} \tag{20}$$

Equation (20) expresses a characteristic property of the opaque mode: for a given total flow the peaking factor is independent of the length of the channel.

Velocity distribution

Another property of importance for this study is the velocity distribution characterizing the channel sources. We assume thermal equilibrium in the source. Hence the velocity distribution of the stagnant gas is given by the Maxwell-Boltzmann (MB) expression:

$$f_s(x)dx = 4\pi^{-1/2}x^2e^{-x^2}dx \qquad (21a)$$

with normalization $\int_0^\infty f_s(x)dx = 1$ and

$$x \equiv \frac{v}{v_\alpha} \quad ; \quad v_\alpha \equiv (2kT/m)^{1/2} \qquad (21b)$$

where T is the source temperature, m the molecular mass and k the Boltzmann constant. At pressures low enough that only process "a" will contribute to the beam, (this is called the transparant mode of the channel source) one is clearly sampling the source volume in a "effusive" way, and the beam resulting from the channel possesses a velocity-weighted Maxwellian distribution[43]:

$$f_b(x)dx = 2x^3e^{-x^2}dx \qquad (22)$$

again normalized to unity. If the source pressure is increased, the beam will be attenuated in the channel. In the GW-model this is accounted for by the exponentials in equations (14) and (15).

In order to obtain a first order correction to the velocity distribution Olander, Jones and Siekhaus (OJS)[44] extended the GW analysis, which is essentially a one-speed model, to allow for velocity dependence of the mean free path, utilising the classical expression for the velocity averaged mean-free-path of a Maxwellian gas.[45] This model leads to a shift of the most probable velocity to a slightly higher value and predicts this effect to "saturate" with increasing opacity. In the opaque mode the velocity distribution is found to be independent of the total flow. OJS also reconsidered the peaking effect employing a velocity dependent mean free path, but the differences with the GW-model were found to be insignificant for practical use and hence eq. (20) remains adequate to estimate the peaking in channel sources.

Velocity distributions of channel sources have been reported at various places in the literature.[46,47,48] However, none of these experiments showed the saturation effect in the opaque mode. To our knowledge no adequate theo-

ry is available describing this aspect of the velocity distribution of channel sources.

3. Measurement procedures

Mass flow

The gas supply to the dissociator is controlled with a needle valve which determines the total flow through the system. The primary side of the valve is connected to a gas handling manifold, including branches to a simple oil manometer and a pyrex bulb with a calibrated volume of 1140 cc. The bulb serves as an H_2 reservoir of known volume. Monitoring the pressure decay in the bulb as a function of time by means of the oil manometer enables an accurate determination of the mass flow (ϕ_m) through the system, defined as the flow of pairs of atoms (either in the atomic or molecular form). The data were corrected for dead volume in the gas handling system and for changes in the dead volume arising from varying levels in the oil manometer. During the measurements the temperature of the bulb was observed to be stable within 0.1 K. The reference arm of the manometer was continiously diffusion pumped to avoid errors caused by degassing of the oil. Typically our beams were operated at $\phi_m = 10^{17}$ pairs/sec.

Calibration of the quadrupole for H_2

The quadrupole mass-spectrometer is used to provide a convenient secondary standard for the mass-flow through the system. Calibration, however, is not straight forward since the experimental arrangement, shown in Fig. 1, provides information only about the center-line intensity of the beam (I; units of the flux/sterradian) and not about the total flux (ϕ). As a result the peaking effects, discussed earlier, will complicate the analysis. Furthermore the quadrupole measures the effective beam density in the ionizer, i.e. a velocity weighted intensity S instead of I directly:

$$S = \Gamma_o \frac{I}{\bar{v}_s} \Omega L \qquad (23)$$

where Γ_o is the ionisation and extraction rate per particle, Ω is the solid angle of detection, L the length of the ionizer and $\bar{v}_s = (8\ kT/\pi m)^{1/2}$, the average velocity in the source.

In the case of non-Maxwellian velocity distributions, not $\bar{v}_s$, but (in general) a different weighting factor is obtained. Γ_o is in general a function

of velocity as discussed by Siekhaus, Jones and Olander.[46] This effect is strongly dependent on the type of ionizer and assumed to be negligible in our case since Maxwellian distributions were obtained for low source pressures. Combining (17) and (23) yields

$$\phi = \frac{\pi}{\Omega L \Gamma_o} \frac{\bar{v}_s}{\chi} S \tag{24}$$

With these considerations in mind an H_2-calibration of the quadrupole is obtained by chopping the beam with an equal segmented chopper and measuring the peak to peak value (S_{pp}) of the observed waveform with the quadrupole tuned to mass 2. S_{pp} is proportional to the total H_2-flux as long as the period of the chopper-function is much longer than the average time of flight through the system. A simultaneous measurement of ϕ_m, using the mass-flow technique discussed in the preceeding section, provides the corresponding total flow ϕ_{H_2} since for a purely molecular beam $\phi_{H_2} \equiv \phi_m$.

Once ϕ_m and S_{pp} are determined for one specific combination of temperature and mass-flow, scaling of χ and $\bar{v}_s$ may be used to obtain a calibration of the quadrupole reading for different temperature and flow conditions. Special care is required if the velocity distributions show deviations from Maxwellian behavior as a consequence of different velocity weighting in relation (24). Scaling of $\bar{v}_s$ is straightforward; scaling of χ is discussed later in this section.

Calibration of the quadrupole for H

The calibration procedure used for H_2 could also be applied to H if striking of the discharge in the dissociator would result in a 100% pure atomic beam, for then every molecule contributing to the mass flow (ϕ_m) through the flow impedance would simply result in a pair of atoms, or $\phi_H = 2\phi_m$. However, under typical experimental conditions the dissociation is not complete. The correction is straightforward once the degree of dissociation (α), i.e. the dissociated fraction of ϕ_m is known:

$$\phi_H = 2\alpha\phi_m \tag{25}$$

The degree of dissociation

The experimental arrangement also enables a particularly simple determination of the dissociated fraction (α) of the beam by observation of the relative change in mass 2 intensity upon striking the discharge. First the

H_2 signal (S_{pp}^{off}) is measured with discharge off. This provides us with a measure for the total H_2 flux, using (24), which equals the mass flux in this case. Then the discharge is started and the H_2 signal drops until (after some transient effects) a new steady value is achieved (S_{pp}^{on}). Since the total mass flow is not affected by the status of the dissociator the H_2 flux now represents a direct measure of the non-dissociated fraction (1-α) of the mass flow:

$$(1-\alpha) = \phi_{H_2}^{on}/\phi_{H_2}^{off} = \frac{\chi_{off}\bar{v}_{on}S_{on}}{\chi_{on}\bar{v}_{off}S_{off}} \qquad (26)$$

By stabilizing the accommodator temperature one achieves $\bar{v}_{on} = \bar{v}_{off}$. This was checked experimentally by measuring the TOF distribution of H_2 with discharge on and discharge off. In practice determinations of α were made using

$$\alpha \simeq 1 - \frac{S_{pp}^{on}}{S_{on}^{off}} \qquad (27)$$

This implies that errors due to possible changes of χ were neglected.

The density in the accommodator

An estimate for the (average) density in the accommodator is obtained in a simple way using equation (3b):

$$\bar{n} = \frac{3}{4\pi}\frac{\ell}{r^3}\frac{}{\bar{v}}\phi \qquad (28)$$

Here ℓ is the length of the accommodator and $\bar{v}$ is the average velocity of the stagnant gas. We note that this expression is only valid when the accommodator is operated in the opaque mode.

The peaking correction

The geometry of our system, as described in Section 2, deviates in various ways from the geometry studied by Giordmaine and Wang (GW). Nevertheless we shall assume the GW results to be transferable to our geometry as long as the source is operated in the opaque mode. This approximation can be considered to be a generalisation of the result (20) in the sense that it assumes the beam shape to be determined by the last section of the channel *only*. This section is defined by the condition $z \lesssim 2\lambda(z)$, where z is the distance in the accommodator, measured from the low pressure end. This is the distance up to the point where the source becomes opaque. Furthermore

we require a homogeneous temperature distribution over the accommodator.

The concept of beam peaking as discussed before implies a change in peaking when the temperature of the accommodator is changed. This aspect of the theory is of particular importance for the calibration of our measurements. In a hard sphere collision approximation $\chi(T) \sim T^{1/4}$ as results from (20). The main uncertainty in $\chi(T)$ is due to the temperature dependence of σ, which was neglected in our estimates for the total atomic flux.

Time of flight analysis

Information about the temperature at which H leaves the accommodator can be obtained by pulsing the beam and using the quadrupole to observe the temporal dispersion of the pulses. We first present a somewhat general approach to be used in our subsequent analysis. If the shape of the pulse in time is represented by e(t) the response of the detection system can be written as

$$S(t) = \underline{\underline{T}}\, e(t) \tag{29}$$

where $\underline{\underline{T}}$ is a linear operator. Let $h(t-t_o)$ be the linear response of the system to a δ-function pulse at $t = t_o$

$$h(t-t_o) = \underline{\underline{T}}\delta(t-t_o) \tag{30}$$

with

$$\int_{-\infty}^{+\infty} h(t-t_o)dt = 1; \quad h(t-t_o) \equiv 0 \text{ for } t < t_o \text{ (causality)} \tag{31}$$

The relation between the number of particles in the velocity interval (v, v + dv) and the corresponding time interval (t, t + dt) is

$$h_o(t-t_o) = -f_b(v)dv/dt \tag{32}$$

where $t-t_o \equiv L/v$, L being the distance between chopper and detector and h_o is the real (i.e. uncorrected for detector properties) time of flight (TOF) distribution.

For a Maxwellian velocity distribution $f_b(v)dv$ is given by equation (22). Setting $t_o = 0$ and using (32) we find

$$h_o(t) = f_b(L/t)L/t^2 \tag{33}$$

For analysis of our measurements this result has to be corrected for the v^{-1} dependence in the sensitivity of the quadrupole (see the section on calibration), yielding the effective TOF distribution $h(t) \sim f_b(L/t)/t$ written in a normalized form as

$$h(t) = f_s\ (L/t)L/t^2 \tag{34}$$

For our Maxwellian distribution $f_s(x)$ is defined by (21) and we can write

$$h(t) = \frac{4}{\sqrt{\pi}} \frac{1}{\theta} \left(\frac{\theta}{t} \right)^4 e^{-\left(\frac{\theta}{t} \right)^2} \tag{35}$$

where $\theta = L/\alpha$ is the TOF of the atoms with velocity α (see Fig. 7, curve 1). Thus a very simple relation exists between the velocity distribution in the accommodator and the effective TOF distribution h(t) as measured using a mass-spectrometer.

The linearity of $\underline{\underline{T}}$ may be used to show that S(t) can be written as a convolution integral:

$$S(t) = \int_{-\infty}^{t} e(\tau)h(t-\tau)d\tau \equiv e(t) * h(t) \tag{36}$$

A useful property of this integral involves the time derivative:

$$\dot{S}(t) = \dot{e}(t) * h(t) \tag{37}$$

Narrow slit chopper

A common procedure to pulse atomic beams is to use fast rotating chopper-blades containing one or more narrow slits. The finite width of any real beam or chopper can be accounted for using equation (36). Assuming a rectangular gate function (Fig. 7, curve 2') the response of the detector is given by Fig. 7, curve 2:

$$S(t) = S_o \int_{t_o}^{t_1} h(t-\tau)d\tau \tag{38}$$

where S_o is the signal in absence of the chopper and the gate is assumed to be open between t_o and t_1. High resolution requires the use of narrow slits. However, (38) shows that in the limit of a vanishing slit width $(t_1 - t_o \to 0)$, the signal also vanishes.

Equal segmented chopper

In our apparatus we employ an equal segmented chopper to obtain the TOF. Here the stimulus e(t) is ideally represented by a step function $\theta(t-t_o)$ changing value at $t = t_o$

$$S(t) = S_o \int_{-\infty}^{t} \theta(\tau-t_o)h(t-\tau)d\tau \tag{39}$$

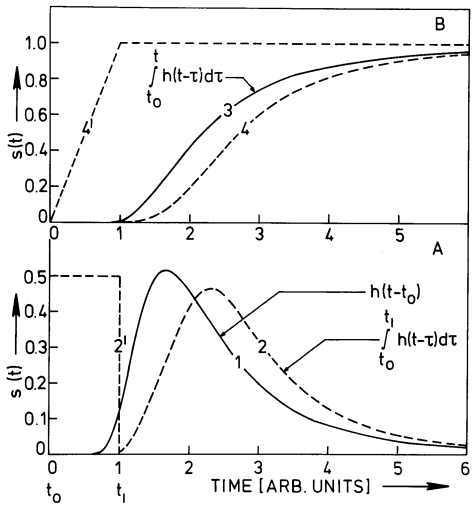

Fig. 7-TOF distribution for a Maxwellian beam and various choices of e(t).

A- Case of narrow slit chopper. Curve 1: response to delta function stimulus. Curve 2: response to block pulse shown as curve 2'.

B- Case of equal segmented chopper. Curve 3: response to step function. Curve 4: response to step function, taking into account the finite cut-off time of the beam as shown with curve 4'. The areas under curves 1 and 2 are normalized to 1. Note that curves 1 and 2 are the derivatives of curve 3 and 4 respectively.

Knowing the response to the step function (Fig. 7, curve 3), the (effective) TOF distribution is obtained by differentiating S(t) with respect to time

$$\dot{S}(t) = S_o h(t-t_o) \tag{40}$$

As in the case of the narrow slit chopper, one has to account for the finite width of any real beam. This results in a distortion of the step function, which however remains simple if slit shaped diaphragms are used to define the beam (Fig. 7, curve 4'):

$$e(t) \equiv \begin{cases} 0 & \text{for } t < t_o \\ \dfrac{t-t_o}{t_1-t_o} & \text{for } t_o < t < t_1 \\ 1 & \text{for } t < t_1 \end{cases} \tag{41}$$

The response to this e(t) is calculated by substituting equation (41) into equation (36) and is plotted in Fig. 7, curve 4. The response is related to the TOF by applying equation (37):

$$\tilde{h}(t) \equiv \dot{S}(t) \frac{S_o}{t_1 - t_o} \int_{t_o}^{t_1} h(t-\tau)d\tau \qquad (42)$$

$\tilde{h}(t)$ is called the convoluted (effective) TOF distribution and is recognized as closely equivalent to the convolution of h(t) with the rectangular gate function (i.e. equation (38)). However, in contrast to that case, in the limit $t_1 \to t_o$, $\tilde{h}(t)$ reduces to $S_o h(t-t_o)$ and high resolution may be obtained without any loss of signal. In comparing the merits of both techniques we must also include noise considerations. If one is completely limited by background noise the equal segmented chopper will be favorable, while in the limit of vanishing background noise the narrow slit chopper will yield better results, since it minimizes noise due to fluctuations in the signal itself, such as encountered for Poisson statistics. Except for the large background signal the possibility of simultaneously monitoring the total atomic flux by standard lock-in techniques was decisive for our choice. In the development of a cold H source, the beam flux is often unmeasurably small. Using a narrow slit chopper requires about 15 minutes of signal averaging to ascertain this, whereas about 1 sec is required with lock-in detection, using an equal segmented chopper.

Signal processing

The signal originating from the mass-spectrometer was averaged on a Fabri-Tek waveform analyser using 256 channels and a 20 μsec dwell time. Typically averaging was done over 10^5 spectra. The repetition rate is limited by the width of the TOF spectrum, too high a rate causing overlap of spectra and resulting in a distortion of the low velocity part of the distribution. No special arrangements, such as the use of a double bladed chopper[48,49], were undertaken to remove this low velocity tail. The data was transmitted to a PDP 11 mini-computer where further signal processing was done. $\tilde{h}(t)$ was obtained by numerical differentiation of S(t) with respect to time using the Lanczos method.[50] Then, applying equation (34) the data (transformed to the velocity domain) yielded the convoluted (effective) velocity distribution $\tilde{f}_s(v)$. Finally the data was smoothed using a Gaussian

smoothing procedure, where the width of the Gaussian ($2/\sqrt{\lambda}$) was 25 m/sec:

$$\langle \tilde{f}_s(v) \rangle = \int_{-\infty}^{+\infty} e^{-\lambda(v-\nu)^2} \tilde{f}_s(\nu) d\nu \qquad (43)$$

For high velocities ($v \gtrsim 2$ km/sec) the width was taken slightly larger in order to prevent the corresponding width in the time domain from becoming less than the experimental resolution (.13 msec).

Any smoothing results in deformation of the signal, most apparent in regions of large curvature. This effect is minimized by first subtracting a theoretical curve $\tilde{f}_s^{th}(v)$ selected by trial and error to approximately fit the data and then to do the smoothing on the noisy difference signal, where significant deviations from the trial distribution must have a small second derivative.Then, after smoothing, the difference signal is added again to $\tilde{f}_s^{th}(v)$ to produce the (smoothed) total signal:

$$\langle \tilde{f}_s(v) \rangle = \tilde{f}_s^{th}(v) + \int_{-\infty}^{+\infty} e^{-\lambda(v-\nu)^2} [\tilde{f}_s(v) - \tilde{f}_s^{th}(\nu)] d\nu \qquad (44)$$

The advantage of this method is that deformation due to smoothing can only occur in the relatively small difference signal, which in our case is the deviation from ideal Maxwell-Boltzmann behavior. The approach is especially useful in measurements where the exact shape of the distribution is not too critical, such as in the present experiment where the TOF is used to determine the (Maxwellian) temperature of an ensemble of H-atoms in a cryogenic environment.

Calibration of the time of flight scale

The signal averager was triggered using a pulse generated by an optical chopping indicator. There is however a phase difference between the real chopping function of the beam and the periodic trigger signal resulting from the electronics of the chopper indicator. Basically this phase difference originates from the difference in position between the beam and the chopper-indicator, but is also due to the ion extraction time, the finite width of the trigger pulse and the pulse handling electronics. Evidently the measurement time scale, i.e. the time initiated by the trigger pulse, has to be corrected in order to obtain the real experimental time scale. David et al.[51] determined this zero of flight time by variation of the flight path. Miller[52] used U.V. photons and an on axis ion detector. A mechanical velocity selec-

tor was used by Beijerinck et al.[49] to produce a known velocity beam, they also replaced the molecular beam by a light source using a photomultiplier for detection. Not all authors specify the estimated error in the zero of time determination, but it seems difficult to achieve a high absolute accuracy since uncertainties up to 50 μ sec are reported. Clearly this calibration requires great care because of the many aspects that come into play. We used two independent methods to calibrate the time-scale of our TOF-system. First an optical technique was used, replacing the beam by a small He-Ne-laser and detecting the light using a fast light power-meter. This measurement yielded a shift corresponding to 210 ± 20 μ sec. This figure has to be corrected for the time delay due to the finite ion-extraction time when using an atomic beam instead of light. Such a correction is mass dependent and for H and H_2 calculated to be of the order of 4.1 ± 1 and 5.8 ± 1 μ sec respectively. The second method used to calibrate the TOF-time scale is based on the assumption that our source, operated at low enough pressures, will yield a Maxwellian velocity distribution. Then a simple fitting procedure with a calculated distribution can be used to fix the time scale. This procedure was used with H, H_2 and ^4He at room temperature and leads to a phase correction of 240 ± 5 μ sec. We also measured the distributions of Ne, N_2 and Ar, but in these cases the pressures could not be reduced enough to observe Maxwell-Boltzmann behavior, due to noise limitations. In Fig. 8 the TOF distribution of N_2 at 295 K is plotted and compared with MB curves calculated for four different temperatures, taking into account convolution effects due to the slit function. The curves are normalized to the integrated intensity under the measured TOF distribution. The observed deviations from the 295 K MB curve cannot be eliminated by a shift in the time scale demonstrating that knowledge of the beam temperature is sufficient to distinguish a Maxwellian from a non-Maxwellian distribution and giving confidence that the observed (Maxwellian) TOF distributions of H, H_2 and ^4He can be used to obtain a reliable time scale calibration.

No satisfactory explanation was found for the 25 μ sec discrepancy between the two calibration techniques. A number of instrumental effects that can induce a systematic error consistent with the observed discrepancy will be briefly discussed here. The 0.13 m sec cut-off time of the beam gives rise to an important convolution correction expecially for low mass, high temperature beams (Fig. 9). A possible systematic error might be due to in-

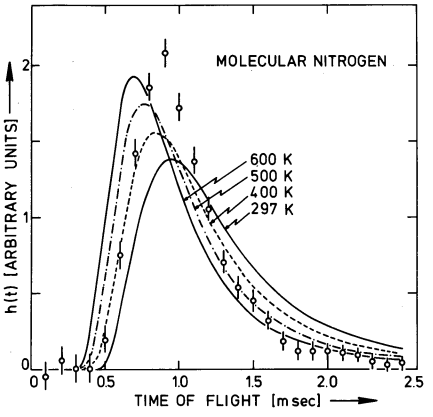

Fig. 8-Non-Maxwellian TOF distribution as measured in our system for molecular nitrogen at room temperature. For explanation see text.

Fig. 9-The importance of convolution for fast beams demonstrated for the TOF of atomic hydrogen at room temperature.

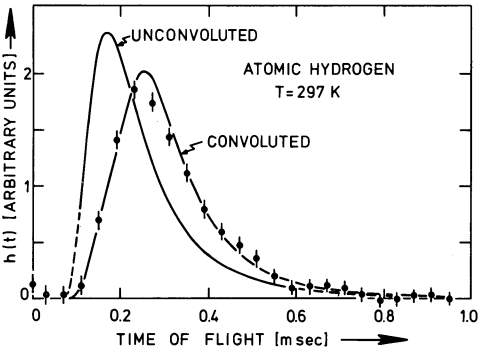

complete knowledge of the instrumental function used in the convolution. This function was calculated assuming an ideal rectangular cross-section of the beam and a position independent detection probability. The ionizer of a mass-quadrupole will induce a distortion of the TOF spectrum if it is operated above a critical emission current due to the build-up of space charge causing ion extraction problems. No changes in the TOF spectrum were observed by variation of the emission current up to 1.9 mA. Finally, memory effects may be present due to periodic fluctuations of the background pressure at the detection frequency caused by the beam randomized in the detection chamber. This effect is small in our system. The beam is passed through the open structured ionizer of the quadrupole and well collimated so that beam particles will not collide with the walls of the ionizer. Furthermore,

the final beam is randomized in a large volume (100 l) and pumped using a ion-getter:titanium sublimation pumping combination with an overall pumping speed of 6000 l/sec for hydrogen. For average beam velocities below 500 m/sec, of primary concern in studying low temperature beams, uncertainties of order 25 μsec in the TOF-timescale correspond to errors of less than 2.5% in the velocity or 5% in the Maxwellian temperature. The TOF system parameters are summarized in table 1.

TABLE 1

TOF system parameters

flight distance	: 525 ± 5 mm
beam diameter at chopper	: 1.5 ± 0.02 mm
angular velocity of chopper	: 177.5 ± 1 rad/sec
chopping period	: 8.85 ± 0.05 msec
resolution of signal averager	: 20 μsec
time resolution (cut-off time)	: 0.130 ± 0.002 msec

4. Results

As a typical example of the results that can be achieved with our dissociator design we first discuss a measurement of α that was done with the tube shown in Fig. 3b. Here, the H leaving the discharge enters into a L = 90 mm, r = 2 mm ($\bar{N}_c \simeq 759$, see eq. 7a) quartz tube cooled to liquid nitrogen temperature. We measured $\alpha \simeq 0.92 \pm 0.02$ for an estimated flux $\phi_{in} \simeq 2 \times 10^{18}$/sec. Analyzing this result on the basis of first order recombination kinetics ($\alpha \simeq 1 - \gamma\bar{N}_c$; for $\gamma\bar{N}_c \ll 1$, see (9c)). We calculate $\gamma \lesssim 10^{-4}$. This result represents an upper limit since we assumed implicitly that ϕ_{in} is fully dissociated. Moreover, experience with other tubes leads to the conclusion that the gas leaving the discharge region is never more than 94% dissociated.

The most complete set of results was obtained with the apparatus shown in Fig. 1, 2, 3a and 6.discussed in detail in Section 2. We stabilized the total mass-flow through the system using the precision needle-valve and selected a relatively low flow rate to ensure the absence of interference between beam and background gas. At room temperature we measured $\phi_H = 7.2 \times 10^{16}$/sec with $\alpha \simeq 0.31$. The teflon tube connecting dissociator with accommodator is characterized by $\bar{N}_c \simeq 3750$, using (7a). Equation (9b) now enables an estimate of γ_{teflon}, yielding $\gamma_{teflon} \simeq 4.5 \times 10^{-4}$. Under best conditi-

ons we observed $\gamma_{teflon} \simeq 10^{-4}$ for commercial teflon tubing. No attempts were made to study the recombination kinetics. Reducing the accommodator temperature to 78 K the H flux decreased to 65% of the room temperature value. Further cooling to 7.7 K (the lowest achievable temperature for the accommodator) resulted in a flux decrease to 32% or $\phi_H \simeq 2.4 \times 10^{16}$ H_1/sec. On the basis of these results we calculate average densities of $3.4 \times 10^{13}/cm^3$ at T = 7.7 K in the accommodator, using (28). Once the temperature of the accommodator is reduced a detailed comparison between experiment and the model presented in Section 2 is no longer justified due to the presence of temperature gradients. Especially at the lowest temperatures, care is required in interpreting our results in view of uncertainties in the peaking correction for the beam, which is hard to estimate but could be of order of a factor 1.5. However, it is most likely that the reduction in atomic flux -with lowering of the accommodator temperature- is due to an increase in the recombination probability γ. If we assume this point of view we must conclude that the surface of the accommodator is not covered with a saturated layer of solid molecular hydrogen. Using the results of Crampton[35] we calculate $\gamma = 5 \times 10^{-6}$ at 8 K and $n = 10^{14}/cm^3$. For our accommodator $\bar{N} \simeq 38$, implying that recombination would be negligible. A thick film of H_2 is also inconsistent with our H_2 intensity measurements. A saturated vapor pressure would result in an H_2 beam three orders of magnitude more intense than was observed experimentally. The exact composition of the accommodator surface is unknown, although it seems reasonable to assume a surface coverage of at most a few monolayers of solid H_2.

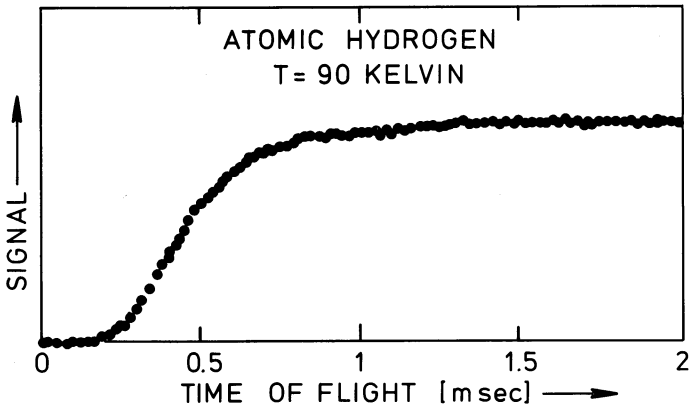

Fig. 10-An example of raw data as obtained for atomic hydrogen at T = 90 Kelvin.

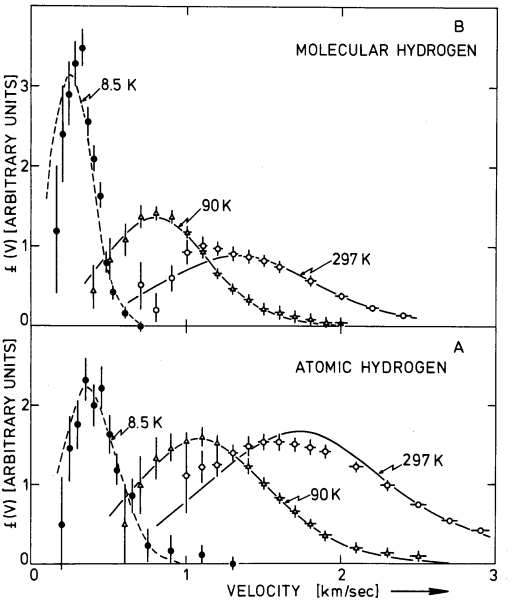

Fig. 11-The velocity distribution of atomic and molecular hydrogen as measured for three different temperatures.

Evidence that the gas was well accommodated to low temperature was obtained by measuring the TOF distribution at the various accommodator temperatures. The raw data, an example of which is shown in Fig. 10, was reduced to velocity distributions using the formalism of Section 3. Results are shown in Fig. 11a for the three different measured temperatures: 297 ± 3 K, 78 ± 2 K and 7.7 ± 1 K. The difference in error bar for different velocities results from the transformation from time to velocity space: the TOF can be measured very accurately for a low velocity beam due to a large dispersion in time. However, this dispersion also leads to low intensities and thus relatively large vertical error bars. The data can be fit to Maxwellian distributions (convoluted with the slit function) corresponding to temperatures 297 ± 5 K, 90 ± 5 K and 8.5 ± 1 K. These temperatures were found to be consistent with the distributions measured for H_2 (see Fig. 11b) with discharge on. On the basis of the 8.5 K TOF we calculate an increase in the flux of low velocity atoms ($v < 2v_\beta$ = 918 m/sec; where v_β is the most probable velocity in the beam) by a factor ≃ 20 with respect to the room temperature beam. (The reduction from the theoretical maximum value of 71 is due to increased recombination losses.) This result shows that our source, in combination with a velocity selector, could be a valuable tool for low

energy atomic beam scattering experiments with hydrogen atoms.

It is useful to raise the question what is to be expected if the accommodator is operated at still lower temperatures, say below 4 K. We expect a steadily growing layer of solid molecular hydrogen to form; the calculated output flux of H_2 -based on the known vapor pressure of the solid[53]- is much smaller than typical input fluxes. We thus may base our analysis on the work of Crampton[35], using an exponential scaling of the recombination rate with temperature $K_{S2} = K^o_{S2} T^{-1/2} \exp(2\varepsilon_a/kT)$.[34] Recombination rapidly becomes limiting once $\bar{N}_c \gtrsim \frac{1}{\gamma} = \bar{v}/(4K_{S2}n)$. Replacing n by the average density in the accommodator and using expressions (7a) and (28) we obtain a simple criterion to decide whether the flux is recombination limited or not

$$\phi_H \gtrsim \frac{64}{9} \cdot \frac{r^5}{\ell^3} \cdot \frac{kT^{3/2}}{m_H} \cdot \frac{1}{K^o_{S2}} \cdot \exp(-2\varepsilon_a/kT) \qquad (45)$$

where r, ℓ and T are the radius, length and temperature of the accommodator respectively, ε_a = 38 K and $K^o_{S2} = 8.4 \times 10^{-20} cm^4 K^{1/2} sec^{-1}$.[54] With this expression recombination is found to become limiting for our accommodator at 4 K if $\phi_H \gtrsim 10^{16}$/sec. However, the effect has a strong temperature dependence. At 2.5 K we expect to be recombination limited already for $\phi_H \gtrsim 10^{11}$/sec. Of course one may try a brute force approach of using high input fluxes and accept considerable recombination losses to obtain some increase in output flux. We note that this approach is very inefficient since recombination on H_2 is second order and therefore scales with $\bar{n}^2$. To double ϕ_H (roughly proportional to $\bar{n}$) we thus have to quadruple the input flux into the accommodator so that, even with $\phi_{in} = 10^{17}$/sec one only obtains $\phi_H \simeq 10^{14}$/sec at 2.5 K. Additional disadvantages of the brute force approach are the considerable heat load and the rapid build-up of bulk solid which may give rise to plugging up of the accommodator. A recombining flux $\phi_H = 10^{17}$/sec corresponds to 7 mm^3 bulk solid per hour and a recombination heat load of 36 mW.

A simple method to increase the recombination limited flux by approximately one order of magnitude would be to reduce the length of the accommodator by a factor 2. This would of course reduce the number of wall collision to below 10 but the masses of H and H_2 are well enough matched to enable efficient energy accommodation in a few collisions so that the beam temperature would remain unchanged.

A serious problem which can exist is a vacuum leak of air into the teflon tube. In one such case after cooling we observed the flux of H to dete-

riorate from a high value to zero within some tens of minutes. Presumably the air condenses on the cold teflon surface before the accommodator and these air surfaces, which are not covered with H_2, are efficient for recombination. We believe that the most important process is first order recombination of H with oxygen. Precautions should always be taken to use pure H_2 gas and to protect the teflon from condensable gases or oils.

Subsequent to the measurements reported here, sources based on these designs, operated at an accommodator temperature of T = 4 - 6 K were used to load H into cells with liquid helium covered walls at temperatures below $\sim$ 0.5 K (see Fig. 12 and Ref. 4).

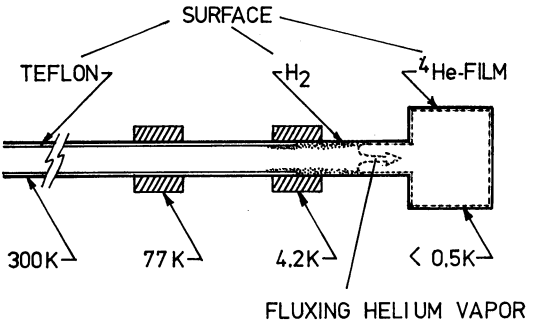

Fig. 12-Schematic diagram of the experimental arrangement of Ref. 4 to load H into a cell with helium covered walls at temperatures below 0.5 K.

An important design consideration of these sources has been to avoid collisions of H with non-helium covered surfaces below 4.2 K. This was realized by using a very short tube between accomodator and helium covered region, thus tolerating imcomplete accommodation on the H_2 surface to avoid total recombination. A non-quantitative confirmation of the importance of the accommodator wall temperature was found when deuterium was loaded into a similar helium covered cell.[55] In this case the flux was orders of magnitude lower than when loading with H under similar conditions, due to the larger adsorption energy of D on D_2 (this is unmeasured but much larger due to the lower zero-point energy). Moderate heating of the accommodator yielded substancial gains in flux.

An additional complication of configurations employing superfluid helium covered surfaces at low temperature may be the presence of stagnant helium

gas in accommodator and transport tube. If the mean free path λ of the H-atoms in the stagnant gas is smaller than the diameter of the tube, the transport of the H gas is no longer Knudsen-limited but may be described by ordinary diffusion (with $D = \frac{1}{3}\lambda\bar{v}$). This leaves the analysis of Section 2 unchanged if we correct for an enhanced number of wall collisions in accommodator and transport tube: $\bar{N}_c^{diff} = \bar{N}_c \cdot 2r/\lambda$. For a pressure $p = 10^{-2}$ torr (corresponding to the saturated vapor pressure of ^{4}He at 0.8 K), the density of the stagnant gas in the accommodator (assumed to be at 4 K) is $n \simeq 3 \times 10^{16}/cm^3$, corresponding to $2r/\lambda \simeq 50$ or equivalently a reduction of ϕ_H by the same amount if the flux is recombination limited.

Further we note that the most perilous region for the H-atoms is that between the 4 K accommodator and the $\sim$ 0.5 K cell. Between these two regions of the tube the helium film is driven towards the accommodator and vaporizes at a point where $T \lesssim 1$ K, fluxing back to the cold region.

In the region 1 - 4 K the H_2 wall may be covered by but a monolayer or so of helium and we expect most H-atoms that strike those walls to recombine. Obviously this region should be made as short as possible so that atoms can make the transition without wall collisions. A stagnant He gas can possibly frustrate this. Alternatively much "hotter" atoms can be fluxed through this region.

5. Acknowledgements

The authors thank E. Hartman for assistance with the data handling, O.H. Höpfner for his technical support and A. Zwart for making the dissociator tubes. We gratefully acknowledge the financial support of the Stchting FOM.

References

1. S.B. Crampton, T.J. Greytak, D. Kleppner, W.D. Phillips, D.A. Smith and A. Weinrib, Phys. Rev. Lett. 42, 1039 (1979)
2. W.N. Hardy, M. Morrow, R. Jochemsen, B.W. Statt, P.R. Kubik. R.M. Marsolais, A.J. Berlinsky and A. Landesman, Phys. Rev. Lett. 45. 453 (1979)
3. I.F. Silvera and J.T.M. Walraven, Phys. Rev. Lett. 74A, 193 (1979)
4. I.F. Silvera and J.T.M. Walraven, Phys. Rev. Lett. 44, 164 (1980)
5. S.B. Crampton, W.D. Phillips, D. Kleppner, Bull. Am. Phys. Soc. 23, 86 (1978)
6. M. Morrow, R. Jochemsen, A.J. Berlinsky and W.N. Hardy, Phys. Rev. Lett. 46, 195 (1981); 47, 455 (1981)
7. W. Welz, Thesis, Bonn 1976, Max Planck-Institut für Strömungsforschung, Göttingen, Bericht 20/1976, see also J.P. Toennies, W. Welz and G. Wolf, J. Chem. Phys. 71, 614 (1979)
8. M. Perrenoud, W. Grüebler and V. König, Helv. Phys. Acta 44, 594 (1971)
9. A.A. Belushkina, V.P. Vadeev, A.I. Valevich, G.I. Goi, E.D. Donets, V.P. Ershov, L.S. Kotova, Y.A. Plis, Y.K. Pilipenko and V.V. Smelyanskii, Instrum. & Exp. Tech. (U.S.A.) 19, 1618 (1976)
10. Y. Wakuta, Y. Koga, H. Hasuyama and H. Yamamoto, Nucl. Instr. Meth.147, 461 (1977)
11. L. Dick and T. Niinikoski; G. Clausnitzer, private communications
12. A.M. Bass and H.P. Broida (ed.) Formation and trapping of free radicals (Acad. Press 1960)
13. R. Hess, Thesis, Stuttgart (1971)
14. Our system is similar to the dissociator described by G.O. Brink, R.O. Fluge and R.J. Hull, Rev. Sci. Instr. 39, 1171 (1968)
    Other designs are discussed in F.C. Fehsenfeld, K.M. Evenson and H.P Broida, Rev. Sci. Instr. 36, 294 (1965)
    B. McCarroll, Rev. Sci. Instr. 41, 279 (1970)
    A. Ding, J. Karlau and J. Weise, Rev. Sci. Instr. 48, 1002 (1977)
    D. Walker, R.M. St.John, J. Chem. Phys. 61, 2394 (1974)
    K.R. Way, Sze-Cheng Yang and W.C. Stwalley, Rev. Sci. Instr. 47, 1049 (1976); see also Ref. (7)
15. Very High Frequency Techniques, vol. II, H.J. Reich ed., McGraw-Hill, New York 1947

16. V.H. Ritz, V.M. Bermudez and V.J. Folen, J. Appl. Phys. 48, 2096 (1977)
17. P.L. Chambré, J. Chem. 32, 24 (1960)
18. A.T. Lifshits, I.M. Metter and L.E. Rikenglaz, Sov. Phys. Tech. Phys. 16, 276 (1971)
19. H. Wise and B.J. Wood, Adv. in At. and Mol. Phys. vol. 3 ed., D.R. Bates and I. Estermann (Academic Press, New York 1967) pag. 291-353
20. We note that except for the factor $\frac{A}{V}$, K_{S2} equals K_S^{eff} used in Ref. (34)
21. D.N. Mitchell and D.J. Le Roy, J. Chem. Phys. 67. 1042 (1977)
22. M. Knudsen, Ann. Phys. 28, 999 (1909)
23. P. Clausing, Zeitschrift für Phys. 66, 593 (1930)
P. Clausing, Thesis, Leiden 1928
24. S. Dushman, in Scientific Foundations of Vacuum Technique, J.M. Lafferty, ed. (Wiley, New York 1962), 2nd ed., pag. 93
25. As the cross-sections are different for singlet and triplet collisions we used here an average, the viscosity cross-section, $\sigma = 55$ Å^2 at T = 300 K as calculated by R.A. Buckingham and E. Gal, Adv. At. Mol. Phys. 4, 37 (1968)
26. J.E. Bennet and D.R. Blackmore, Proc. R. Soc. A. 305, 553 (1968)
27. A. Salop and A. Mandl, J. Phys. E 4, 645 (1971)
28. A. Mandl and A. Salop, J. Appl. Phys. 44, 4776 (1973)
29. M. Coulon, J.C. Fanton and L. Bonnetain, J. Chim. Phys. 70, 1493 (1975)
30. N. Abramowitz and I.A. Stegun eds., Handbook of Mathematical Functions, National Bureau of Standards, Applied Mathematics Series no.55
31. See Ref. (30) relations 18.13.67 and 18.13.68
32. We use $\sigma = 1.6 \times 10^{-16}/cm^2$, where $\sigma = 4\pi a^2$ and a = 0.72 Å is the s-wave scattering length as calculated for the triplet potential by D.G. Friend and R.D. Etters, J. Low Temp. Phys. 39, 409 (1980)
33. W.N. Hardy, M. Morrow, R. Jochemsen, B.W. Statt, P.R. Kubik, R.M. Marsolais, A.J. Berlinsky and A. Landesman, Phys. Rev. Lett. 45, 453 (1980)
34. A.P.M. Matthey, J.T.M. Walraven and I.F. Silvera. Phys. Rev. Lett. 46, 668 (1981)
35. S.B. Crampton, J. de Phys. 41. C7-249 (1980); see also S.B. Crampton, T.J. Greytak, D. Kleppner, W.D. Phillips, D.A. Smith and A. Weinrib, Phys. Rev. Lett. 42, 1039 (1979)

36. G.H. van Yperen, A.P.M. Matthey, J.T.M. Walraven and I.F. Silvera, Phys. Rev. Lett. 47, 800 (1981)
37. R. Jochemsen, M. Morrow, A.J. Berlinsky and W.N. Hardy, Phys. Rev. Lett. 47, 852 (1981)
38. H. Wilsch, J. Chem. Phys. 56, 1412 (1971)
39. Du Pont de Nemours
The use of this dispersion was pointed out to us by W.D. Phillips
40. J.A. Giordmaine and T.C. Wang, J. Appl. Phys. 31, 463 (1960)
41. V.S. Troitskii, Sov. Phys. Techn. Phys. 7, 353 (1962)
42. D.R. Olander and V. Kruger, J. Appl. Phys. 41, 2769 (1970)
43. N.F. Ramsey, Molecular beams (Clarendon Press, Oxford 1956)
44. D.R. Olander, R.H. Jones and W.J. Siekhaus, J. Appl. Phys. 41, 4388 (1970)
45. E.H. Kennard, Kinetic Theory of Gases (McGraw-Hill, New York 1938)
46. W.W.J. Siekhaus, R.H. Jones and D.R. Olander, J. Appl. Phys. 41, 4392 (1970)
47. R.G. Wilmoth, J. Vac. Sci. Techn. 9, 1121 (1972)
48. H.C.W. Beijerinck and N.F. Verster, J. Appl. Phys. 46, 2083 (1975)
H.C.W. Beijerinck, Thesis, 1975, Eindhoven, The Netherlands
49. H.C.W. Beijerinck, R.J.G. M. Moonen and N.F. Verster, J. Phys. E Sci. Instr. 7, 31 (1974)
50. C. Lanczos, Applied Analysis, Pitman and Sons Ltd, London 1957
51. R. David, M. Faubel and J.P. Toennies, Chem. Phys. Lett. 18, 87 (1973)
52. T.M. Miller, J. Appl. Phys. 45, 1713 (1974)
53. B.N. Esel'son, Y.P. Blagoi, V.N. Grigor'ev, V.G. Manzhelli, S.A. Mikhailenco and N.P. Neklyndov, Properties of Liquid and Solid Hydrogen, Keter Press, Jerusalem 1971
54. This value was derived from the results of Crampton, see Ref. (35)
55. I.F. Silvera and J.T.M. Walraven, Phys. Rev. Lett. 45, 1268 (1980)

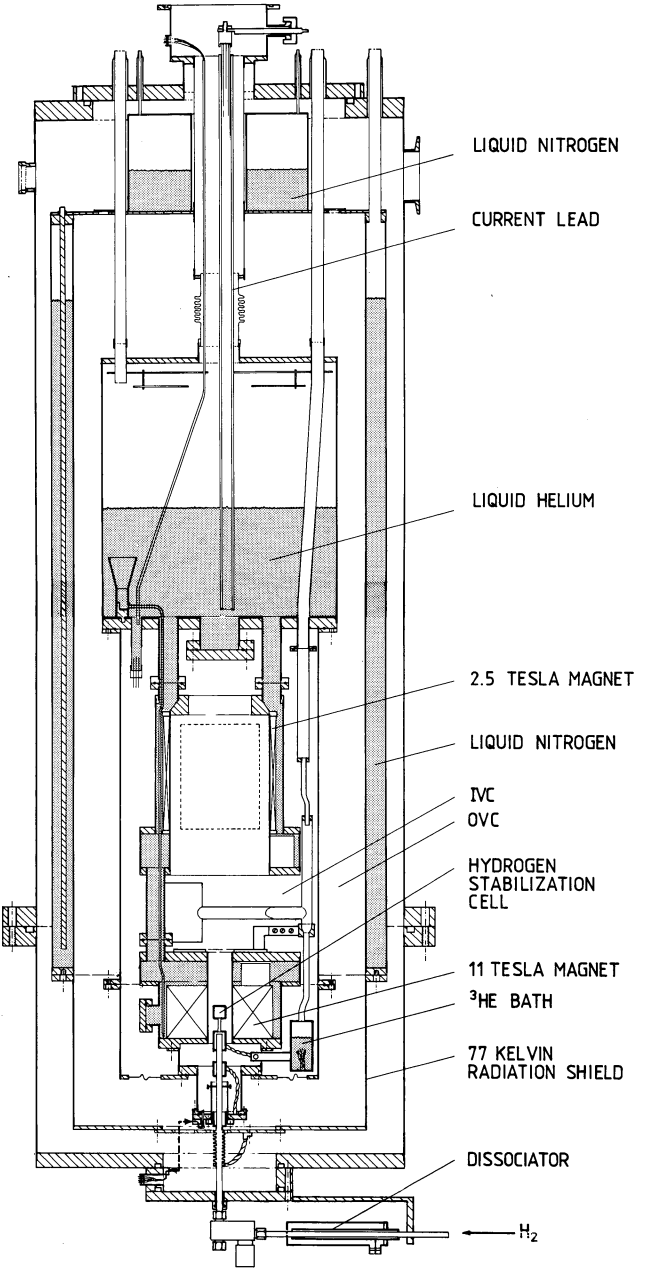

Fig.1-Schematic diagram of the cryogenic system.

2.2. THE CRYOGENIC SYSTEM

The cryostat used to stabilize atomic hydrogen and deuterium is schematically shown in Fig. 1. H is produced in a coaxial dissociator of the type discussed in chapter 2.1, mounted at the bottom-side of an all-metal cryostat with bottom access. By opening a teflon valve (shown in Fig. 2.) the gas runs up a tube towards the stabilization cell positioned in the bore of a superconducting magnet.

The helium reservoir is a 15 liter cylindrical tank connected to the top-flange by four thin walled stainless steel tubes (317 mm long, 12 mm diameter. 0,2 mm wall thickness). A 50 mm diameter central tube is connected to the ^{4}He vessel via a thin walled bellows. The tube has no structural function but only serves to carry away the boil off of the main bath to a ^{4}He recovery system. Two Nb-Ti superconducting magnets contained in a stainless steel housing are connected to the bottom of the helium reservoir. The lower magnet, with a 25 mm bore and 100 mm long is used to produce the main field (up to 11 Tesla) needed for the experiments. The large bore magnet runs up to 2,5 Tesla and may hold a 0.5 l salt pill for adiabatic demagnetization. In our experiments this magnet was not used. The two magnets are surrounded by a 4.2 K shield which separates the inner vacuum can (IVC), including the experimental space, from the outer vacuum can (OVC), holding the liquid nitrogen radiation shield. The two magnets have one current lead in common so that three leads run up to room temperature current clamps via the central tube. The leads are designed to carry 100 A each and consist of a brass foil folded to fit into a pyrex tube extending to the bottom of the helium tank. The pyrex tubes serve to force-cool the leads employing the helium boil off from the main bath. The overall helium consumption of this geometry is approximately 150 cc/hr.

Temperatures below 1 K are achieved using two one-shot ^{3}He evaporation cryostats, included in the IVC. Before we enter in more detail we first briefly describe their operation. A one-shot ^{3}He evaporation cryostat, shown in Fig. 3, consists of four main components: a low temperature ($\sim$ 300 mK) liquid reservoir, a sorption pump, a condenser and a room temperature storage tank. In between measurements the ^{3}He is stored in a 7 l storage tank containing 8,5 liter NTP ^{3}He. This tank serves both low temperature ^{3}He systems. At the start of a low temperature run the ^{3}He is condensed into the liquid reservoir by slowly feeding the gas through the input line towards a small pumped ^{4}He bath, ope -

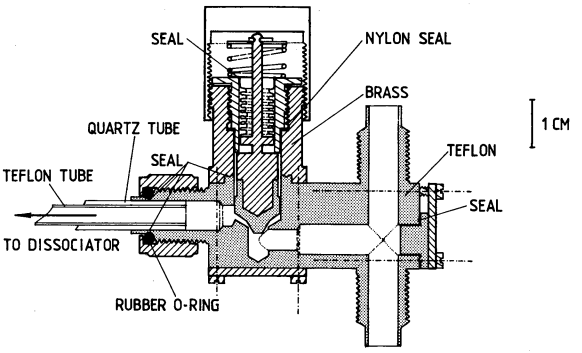

Fig.2-Valve assembly to isolate dissociator from the cryogenic stabilization cell. All surfaces that come into contact with the H atoms are made of teflon. To eliminate leaking, a commercial ("NUPRO-valves") bellows sealed construction is used. Vacuum tight connections are made by squeezing rubber "o" rings around thin walled teflon extension tubes on the main body of the valve, which in turn make the seal. Note that the construction enables a secondary access to the sample cell.

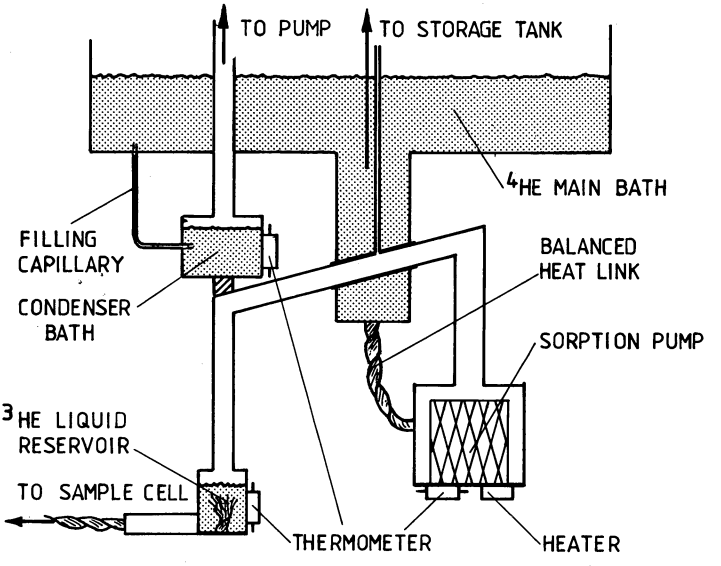

Fig.3-Schematic drawing of a one-shot ^{3}He evaporation cryostat. For explanation see the text.

rated at $\sim$ 1.4 K and acting as the condenser. The liquified ^{3}He runs down a tube to fill the liquid reservoir. Initially, when the reservoir is still warm, the liquid will rapidly evaporate and recondense. Once all liquid is collected we close the filling line. At this point we may start the pump-down of the liquid by allowing the sorption pump, kept warm (T $\approx$ 40 K) during the filling procedure, to cool down. For our system it takes approximately 30 minutes to reach the base temperature ($\sim$ 300 mK). In the initial cool down $\sim$10-15% of the liquid is lost. Obviously the running time depends on the heat load of the system. For our experiments rather high heat loads were required, $\sim$ 1-2 mW, limiting the useful running time to approximately 2.5 hours. Once the bath runs empty the sorption pump is heated to 40 K to desorp the ^{3}He and the procedure starts from the beginning.

The condenser bath shown in Fig. 4. is continuously filled from the main bath via a stainless steel capillary acting as a flow impedance. The pressure drop over the capillary determines the rate at which liquid ^{4}He enters the condensor bath. The liquid level raises until the evaporation rate matches the input rate. This implies that the steady state refrigeration power is a fixed value determined by the size of the capillary. Without an external heat load the level raises into the pump line. Once we apply a thermal load, for instance by condensing ^{3}He , the level falls, thereby reducing the heat input from the main bath by an amount equal to the thermal load. Thus with varying input power only the liquid level varies while the steady state temperature remains constant. To minimize the heat load due to film flow and the associated fluxing vapors (which may be considerable even if the liquid level is low) a 1 mm diaphragm is placed in the pump line. The condenser bath, used in our system, is designed to provide a steady state cooling power of 35 mW corresponding to a helium consumption of 85 cc/hr. The properties of such a configuration are discussed by De Long et al.[1] in relation to the application in a ^{3}He-^{4}He dilution refrigerator (1 K-"pot"). An Allan-Bradley carbon resistance thermometer[2] (47 Ω nominal resistance) is used to monitor the temperature of the condenser bath. We note that the second one-shot ^{3}He -system was added to the system in a later stage which made it impossible to implement a second condenser bath. Therefore both systems were connected to the same bath, which could not be realized in an optimum way, reducing the useful amount of liquid ^{3}He.

The liquid reservoir is a small $\sim$ 8 cc copper cylinder connected by a thinwal-

led stainless steel "pumping line" (8 mm in diameter, 2oo mm long and with a wall-thickness of 0.2 mm) via the condenser bath to the sorption pump. In order to guarantee a good thermal contact between the liquid ^{3}He and the copper wall a copper braid is silver soldered into the bottom of the reservoir to minimize the thermal boundary resistance. The connection between sample cell and the reservoir is also made by means of a copper braid. The temperature of the reservoir is measured using a Speer carbon resistance thermometer[2] of 470 Ω nominal resistance. The sorption pump consists of a cylindrical copper housing, containing a brass basket to hold approximately 25 cc of zeolite 5A.[3] The pump is heated to ∿ 40 K to desorp[4] the ^{3}He using a button shaped heater glued to the bottom of the copper housing. The heater is made of 37 Ω/m manganin wire bifilary wound on a copper former and impregnated with 1266 Stycast epoxy.[5] Once the heater is switched-off the sorption pump cools down via a heat link to the main bath. The choice of the heat link results from a trade-off process. One has to optimize the cooling rate while keeping the heat input into the main bath acceptable during the desorption. In our case approximately 5.6 W is reuired during 2.5 minutes to desorp the ^{3}He. The system cools down again in about half an hour. The temperature of the sorption pump is monitored using a button shaped copper wire resistance thermometer[6] of a similar construction as the button heaters. The thermometer is made to have a 100 Ω resistance at 0 °C.

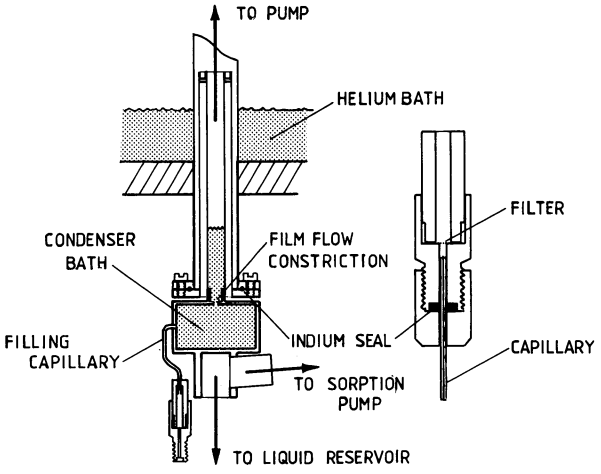

Fig.4-Drawing of the condenser, continuously filled from the main bath via a stainless steel capillary. The thin walled tubing is folded to keep the design compact. The indium sealed capillary joint, including a fine mesh metal filter is shown in detail at the right.

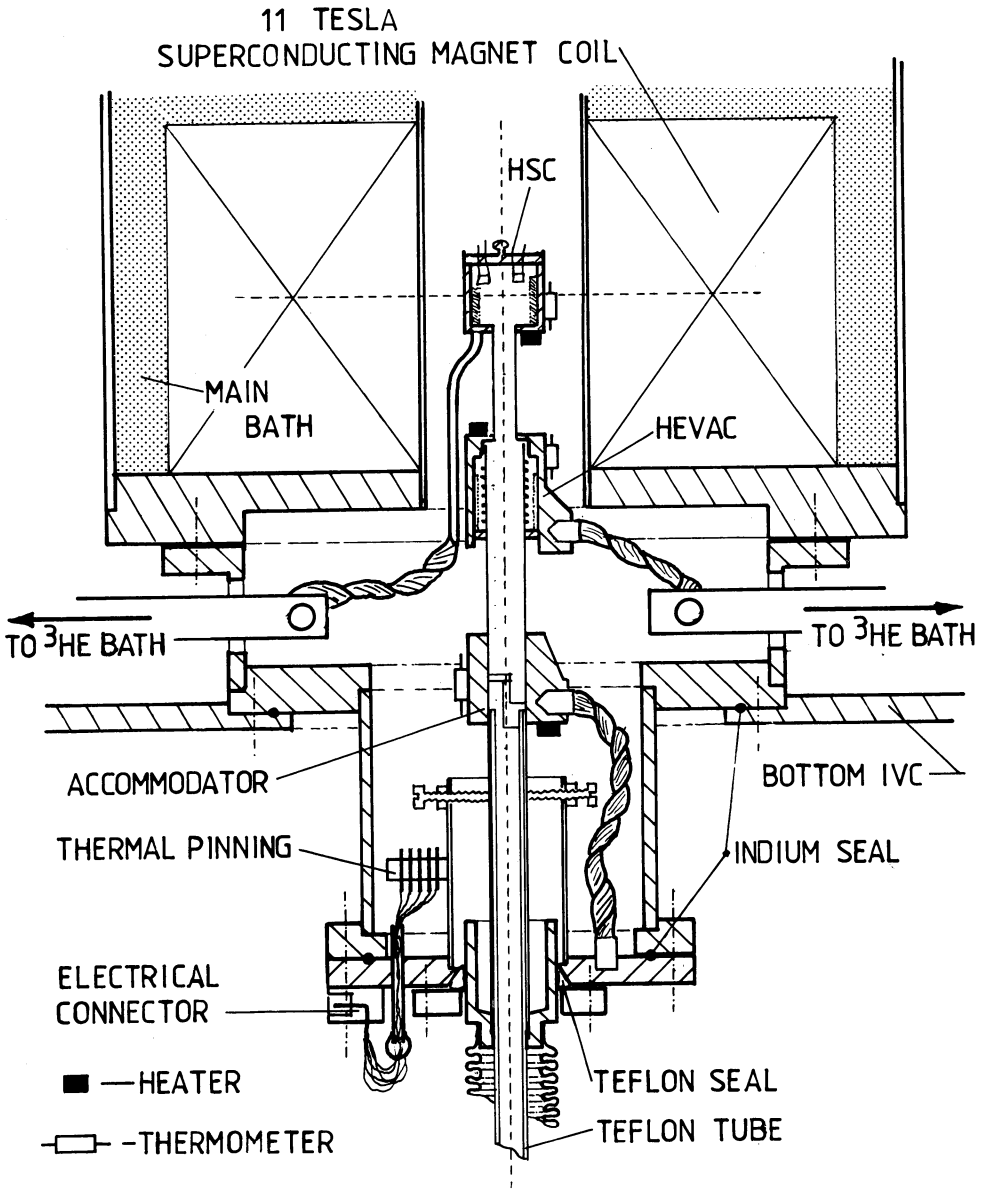

Fig.5-Drawing of the experimental cell on a 80% reduced scale.

We discuss the cryogenic aspects of the experimental cell. The aspects associated with the physics of stabilizing H and the detection principle are discussed in chapter 3. The cell assembly is very compact and shown on a 80% reduced scale in Fig. 5. It may be considered as a modular unit inserted into the bore of the 11 T superconducting magnet. The various components are mounted along a thin walled stainless steel tube providing thermal isolation between the sections. The tube is fed through a support flange, using a teflon seal, the flange sealing the bottom of the IVC.

During operating conditions ^{4}He is present in the cell and a film of the superfluid covers all surfaces which are below $\sim$ 1 K. Once the teflon valve (see Fig. 1 and 2.) is opened the H atoms run up the tube, are thermally accommodated at $\sim$ 5 K and then enter the low temperature region where the walls are covered by the superfluid. The gas is collected in the HSC (Hydrogen Stabilization Cell) which is thermally connected to one of the ^{3}He reservoirs, using a copper braid. A single ^{3}He system turned out to be inadequate to achieve temperatures below $\sim$ 0.6 K due to back fluxing helium vapor. The fluxing vapor originates from the evaporating superfluid film which is driven to the lower sections of the cell (the accommodator region) both by gravity and the thermomechanical effect. To reduce the heat load on the HSC a second cooling stage, the HEVAC (Helium Vapor Compressor) was added. With this two-stage design base temperatures of $\sim$ 270 mK were achieved at the HSC with ^{4}He in the cell. Although the fluxing vapors are detremental from a cryogenic point of view they are put to advantage in this design since they give rise to some additional compression of the gas. This explains the name. The HEVAC also contains a small reservoir in which some bulk liquid may be collected. In this way the heat load on the HEVAC does not depend critically on the amount of ^{4}He introduced in the cell. More details are given in chapter 3. The various components of the cell are equipped with thermometers and heaters to register and regulate the temperature. For the HSC and the HEVAC Speer carbon resistors[2] (470 Ω nominal resistance) are used for thermometry. On the accommodator we use an Allan-Bradley resistor (47 Ω nominal resistance).[2] The HSC thermometer is calibrated against a germanium thermometer in turn calibrated in Leiden against CMN and checked in our laboratory against an NBS 768 superconducting fixed point device.[7] The field dependence of the thermometer was established by running the field up and down under stable temperature conditions. The thermometry is believed to have an accuracy of approximately 3% in the experiments described in chapter 3, 4, 5 and 6.

REFERENCES

1. L.E. De Long, O.G. Symko and J.C. Wheatley, Rev. Sci. Instr. 42, 147 (1971).
2. G.K. White, *Experimental Techniques in Low Temperature Physics*, Clarendon Press, Oxford 1979.
3. Supplied by BDH Chemicals Ltd, Poole, England.
4. R.R. Conte, *Elements de cryogenie*, Masson & Cie, Paris 1970
5. Supplied by Emerson and Cumming Inc., Oevel, Belgium.
6. T.M. Dauphinee and H. Preston-Thomas, Rev. Scientific Instr. 25, 884, 1954.
7. Supplied by U.S. Department of Commerce, National Bureau of Standards, Washington DC, USA.

CHAPTER 3

STABILIZATION OF ATOMIC HYDROGEN AT LOW TEMPERATURE

Isaac F. Silvera and J. T. M. Walraven

Natuurkundig Laboratorium der Universiteit van Amsterdam
1018 XE Amsterdam, The Netherlands

Atomic hydrogen has been stabilized at temperatures of 270 ± 20 mK and in magnetic fields up to 7 T. It is believed to be gaseous. A sample displayed no measurable decrease in density after 532 sec. Covering of exposed surfaces with a film of ^{4}He is essential.

[Phys. Rev. Lett. 44, 164 (1980)]

Stabilization of Atomic Hydrogen at Low Temperature

Isaac F. Silvera and J. T. M. Walraven
Natuurkundig Laboratorium der Universiteit van Amsterdam, 1018 XE Amsterdam, The Netherlands
(Received 19 November 1979)

Atomic hydrogen has been stabilized at temperatures of 270 ± 20 mK and in magnetic fields up to 7 T. It is believed to be gaseous. A sample displayed no measurable decrease in density after 532 sec. Covering of exposed surfaces with a film of ^{4}He is essential.

Atomic hydrogen (H) with one proton and one electron is the simplest atomic system provided by nature. Just as helium and its isotopes display fascinating properties at low temperature and high density, atomic hydrogen and its isotopes are expected to exhibit spectacular phenomena. Until now it has not been possible to study condensed atomic hydrogen experimentally, as under normal circumstances it is highly unstable with respect to recombination to H_2 which has a binding energy $\epsilon_b/k_B = 52\,000$ K in the singlet spin state, $^1\Sigma_g^+$. However, in the spin-polarized state, $^3\Sigma_g^+$, a pair of atoms have no bound state. We refer to a dense gas of atoms with electron spins polarized, so that all pairs interact within the $^3\Sigma_u^+$ potential, as polarized hydrogen ($H\uparrow$). We have created a gas of H in a cell at $T = 270 \pm 20$ mK and in magnetic fields up to 7 T. Using specially developed detectors we have established that after loading the cell, the density did not change to within experimental error for periods up to 532 sec, the longest period investigated. Without our special conditions, we calculate that the sample would have a decay-time constant of ~ 80 μsec, due to surface recombination if kinetic effusion of the gas to the surface is rate limiting. The lifetime of this sample was increased by at least a factor 7×10^7 in this sense. We shall refer to samples with increased lifetimes of $> 10^6$ as stabilized. In most cases we observed stabilized

samples for times of order 10–60 sec before destroying them. The highest density of a stabilized sample was $n > 1.8 \times 10^{14}$ atoms/cm^3.

The first published discussion of some of the exciting phenomena expected for stable H↓ is due to Hecht,[1] who, in 1959, suggested that superfluidity should exist in this boson gas. His article was evidently overlooked by researchers who became actively interested in H↓ in the 1970's, including ourselves. Etters and colleagues[2] and Stwalley and Nosanow[3] reconsidered the properties of the hydrogen isotopes. The stability of H↓ was first considered by Jones *et al.*,[4] who found that it would be unstable at very high densities. Stwalley[5] suggested that H↓ would be stable in a magnetic field B for ratios $B/T > 10^2$ T/K. However, Berlinsky *et al.*[6] showed that his reasoning was incomplete and that even at $T = 0$, for a given magnetic field there is a critical density above which the H↓ gas will become spontaneously unstable.

Our research program to create and stabilize H began in 1972 and was directed at stabilizing H by polarizing an atomic beam and depositing it on a cold inert surface in a weak magnetic field, with the eventual objective of studying Bose-Einstein condensation in a quasi-two-dimensional system. The results were discouraging as the atoms rapidly depolarized on the surface and recombined.[7] On the basis of the stability conditions found in Ref. 6 we decided to redirect our efforts to stabilization of H↓ as a three-dimensional gas in high magnetic fields at low temperatures.

Our design aims were based on an applied magnetic field $B = 10$ T and a temperature $T \simeq 300$ mK. We recently developed a high-flux source of He-temperature atomic hydrogen[8] required for the ultimate goal of loading a cold cell to densities of 10^{18}–10^{19} atoms/cm^3. Our earlier experience with rapid recombination of H on surfaces suggested that any stabilization attempt using currently available fields would be doomed because of condensation of the H on the surface followed by recombination. We conceived of the idea of coating all surfaces with a (superfluid) helium film,[9] believing that of all known materials this would have the weakest adsorption potential for H. This turns out to be vital for stabilization.

There are three important considerations for the selection of the operating temperature. First of all, as discussed in the accompanying Letter,[10] compression of a gas of H from a field-free region to a region of magnetic field B is proportional to $\exp(\mu B/kT)$ (μ is the magnetic moment of the H atom), which favors lowest possible temperatures. The region $T \to 0$ is also favored to minimize recombination due to spin-flip mechanisms[11,4] and to minimize the density of thermally populated spin-flipped states, which depends on $\exp(-2\mu B/kT)$. However, as a third point, the low operating temperatures may be limited by condensation of H↓ on the liquid-helium–covered surfaces, where critical densities may be exceeded. Recent calculations[12,13] suggest that a surface state exists with a binding energy possibly greater than 0.6 K.

The heart of our low-temperature apparatus is shown in Fig. 1. The copper hydrogen stabilization cell (HSC) is in the center of a superconducting solenoid (maximum field, $B = 11$ T). This is connected by thin-walled German silver (GS) tubing to a helium vapor compressor (HEVAC). This is actually a miniature vapor diffusion pump which uses a reservoir of superfluid helium as its pumping fluid. Both the HSC and the HEVAC are cooled by sorption-pumped ^{3}He refrigerators. During operation the HSC runs at $T = 270$ mK and has an estimated residual background helium vapor density of $\sim 5 \times 10^8$ atom/cm^3. The HEVAC which operates at $T = 480$ mK is connected by GS tubing to a copper H accomodator pinned to ^{4}He temperatures. A Teflon-lined GS tubing continues out of the vacuum to a room-temperature hydrogen discharge. The hydrogen atoms are fed in

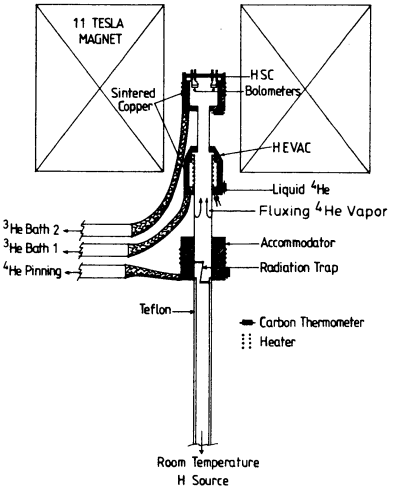

FIG. 1. Low-temperature part of stabilization apparatus. See text for an explanation.

from the bottom of the cryostat to minimize the distance and thus the recombination of H during transportation to the HSC; the atoms are cooled to liquid-helium temperature by the accomodator as described elsewhere[8] and are still unpolarized at this point. The electron spin-down atoms are drawn into the HSC by the field gradient, whereas the spin-up states are retarded and either relax to spin down or recombine. The system is prepared as follows. All surfaces above the Teflon lining are coated with molecular H_2. The ^{3}He refrigerators are activated and ^{4}He gas is condensed in the HEVAC and HSC.

We shall briefly describe the operation of the HEVAC. A superfluid helium film is driven from the reservoir of the HEVAC, up, then down the GS tube towards the accommodator. As the film flows down it comes into increasingly warmer regions, vaporizes and fluxes back to recondense at the HEVAC. Without this fluxing gas the density of ^{4}He gas in the region of the HEVAC would be $\sim 10^{14}/\text{cm}^3$ and the collisional mean free path (λ) for H-He would be about 2 cm.[14] The backfluxing gas is much denser (we estimate $\lambda \sim 0.36$ mm for H-He collisions) so that hydrogen atoms will be directed into the HSC by momentum transfer from the four times more massive helium atoms. The HEVAC not only guides the atoms into the HSC, but also retards their leakage out when the discharge is turned off. As discussed in the accompanying Letter, the cell should empty when the density of H in zero field is zero. We estimate that the emptying time constant is increased by a factor 79 by the HEVAC.

The presence of H in the HSC is detected with special bolometers. The principle is to build up a density of H in the cell and then trigger its recombination by selectively making the bolometers active recombination surfaces. The concomitant heating due to the recombination energy is easily

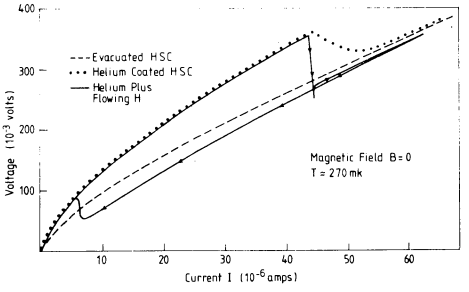

FIG. 2. Current-voltage characteristics of a hydrogen bolometer detector.

detected and provides a measurement of the H density. The bolometers were made by cutting $2\times1\times0.2$-mm^3 chips from Speer resistors. They are connected to the top plate of the HSC by fine copper wires which serve not only as current-voltage (I-V) leads but also as the path which allows the ^{4}He film to cover their surfaces. In Fig. 2 we show the I-V curves. When ^{4}He is introduced into the HSC the I-V curves develop a peak. The ^{4}He on the bolometer surface is evaporated as a result of Ohmic heating. Fresh ^{4}He will flow along the wire leads to replenish the film; however, this flow is limited by the wire circumference.[15] The peak in the I-V curve represents the point where the H_2-covered surface is first exposed. This surface is an active source for recombining H.[16] When H is present while tracing an I-V curve, arrival at the desorption peak will trigger recombination. This destroys the H gas with a time constant $\tau \simeq 4V/\bar{v}A$, where V is the volume of the HSC, $\bar{v}$ is the average velocity, and A is the total area of the bolometer; we assume a probability of 1 for recombination when a particle strikes the surface. For our system at $T = 270$ mK, $\tau = 8$ msec. Thus we see a sharp downward-going spike on the I-V curve and a return to a level determined by the steady-state recombination on the bolometer of H flowing into the HSC. The I-V curve has hysteresis because of the extra heating after desorption. From earlier work[16] it is known that the recombining atoms deposit only a small portion of the recombination energy on the bolometer surface, since the H_2 molecules are desorbed upon recombination. The second bolometer, operated below its desorption peak, will absorb part of this energy from the "hot" molecules. The rest will be absorbed in the copper walls of the HSC (or blown out of the filling tube) and is detected with a thermometer. By calibrating the heating of the HSC with an electrical heater, a lower bound for the number of recombinations, or the H density, can be determined.

Proof of stabilization was obtained as follows. With the magnetic field and discharge on, we measured the recombination spike height as a function of cell loading time. As the loading period was increased the size of the spike increased, indicating that larger densities of H were being built up. We then loaded the cell for a period of time t_L ($\sim$30 sec), turned off the discharge, and waited a time, t_s, before triggering. Starting with $t_s \simeq 1$ sec we continually doubled the wait time, finding no measurable attenuation in

the size of the spikes. Periods longer than 532 sec were not measured as we chose to use our limited experimental measuring time to investigate other aspects of the system. This provides proof of long-term stability of H. This was performed with a field of 7 T at $T = 270 \pm 20$ mK. Although no detailed systematic studies have been performed we found that the recombination spike height decreased with both decreasing fields and increasing temperature for a constant filling rate, as is to be expected. The largest density we observed was at 6 T (270 mK) with a *very conservative* lower bound of 1.8×10^{14} atom/cm^3. No effort has been made as yet to determine a maximum achievable density.

We have also measured the time dependence of the density in zero field, where the gas is certainly H (not H$\uparrow$) and should not be stable. The results are shown in Fig. 3. The decay does not appear to be controlled by volume recombination, probably because the density is low. If we roughly fit by an exponential decay, as would be expected for thermal effusion, we find a time constant of 1.5 sec, as compared to a calculated 19 ms without the HEVAC. This implies a compression factor of 79 for the HEVAC.

Indications that H exists in the gas phase are the following. On the basis of the theoretical estimate for the binding energy of H on a He surface, at the employed temperatures we expect that in thermodynamic equilibrium a considerable fraction will be gaseous. Second, the H totally recombines in about 80 msec as measured by the full width at the base of the bolometer spike. Since this can be several time constants long, the recombination rate is of the expected order as determined by gaseous effusion to the bolometer surface. Third, if the bolometer signals were due only to H on its surface, then, assuming a coverage of maximal 10^{14}/cm^2, the signal would correspond to 2×10^{12} recombinations, inconsistent with observations; a second triggering without reloading the cell did not result in a recombination spike as would be expected as a result of surface diffusion which would recover the bolometers. Finally, we performed experiments in which we sequentially triggered the two bolometers within 100 msec. Only the first triggered bolometer displayed a recombination spike, which would not be the case if the H resided mainly on the surface. Although no one argument here provides a hard proof of the state of H, altogether the evidence points to gaseous H. We hope to be able to increase the density by some orders of magnitude to study the interesting properties of this almost ideal Bose gas. Already at present densities there are important implications for increased stability of the hydrogen maser.[17]

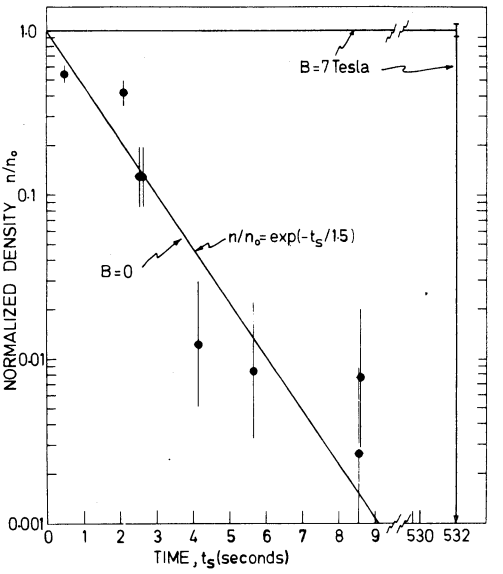

FIG. 3. Decay rate of H for $T = 270$ mK at $B = 0$ and 7 T. t_s is the elapsed time after loading the cell and n_0 is the density for $t_s = 0$. The error bars are due to calibration uncertainties only.

We thank A. P. M. Mattheij, R. Sprik, and M. B. J. Diemeer for their help with the apparatus and measurements. We warmly acknowledge discussions with A. J. Berlinsky and E. R. Eliel at the beginning states of these experiments. The rapid and expert constructional work by O. H. Höpfner has been of inestimable value. We thank the Stichting voor Fundamental Onderzoek der Materie for their great flexibility and understanding in supporting this research of a more speculative nature.

[1]C. E. Hecht, Physica 25, 1159 (1959).

[2]J. V. Dugan and R. D. Etters, J. Chem. Phys. 59, 6171 (1973); R. D. Etters, J. V. Dugan, and R. W. Palmer, J. Chem. Phys. 62, 313 (1975); R. D. Etters, R. L. Danilowitz, and R. W. Palmer, J. Low Temp. Phys. 33, 305 (1978).

[3]W. C. Stwalley and L. H. Nosanow, Phys. Rev. Lett. 36, 910 (1976).

[4]J. T. Jones Jr., M. H. Johnson, H. L. Mayer, S. Katz,

and R. S. Wright, Aeronutronic Systems Inc. Publication No. 6-216, 1958 (unpublished).

[5]W. C. Stwalley, Phys. Rev. Lett. 37, 1628 (1976).

[6]A. J. Berlinsky, R. D. Etters, V. V. Goldman, and I. F. Silvera, Phys. Rev. Lett. 38, 356 (1977).

[7]J. T. M. Walraven, E. R. Eliel, and I. F. Silvera, Phys. Lett. 66A, 247 (1978).

[8]I. F. Silvera and J. T. M. Walraven, Phys. Lett. 74A, 193 (1979).

[9]Others have evidently also had this idea. W. C. Stwalley, in *Quantum Fluids and Solids*, edited by S. B. Trickey, E. D. Adams, and J. W. Dufty (Plenum, New York, 1977, p. 293.

[10]J. T. M. Walraven and I. F. Silvera, following Letter [Phys. Rev. Lett. 44, 168 (1980)].

[11]The necessary field for stability considered in Ref. 6 will increase for $T \neq 0$ as the pair distribution function will allow for more penetrating pair collisions as T increases.

[12]R. A. Guyer and M. D. Miller, Phys. Rev. Lett. 42, 1754 (1979).

[13]I. B. Mantz and D. O. Edwards, to be published.

[14]J. P. Toennies, W. Welz, and G. Wolf, Chem. Phys. Lett. 44, 5 (1976).

[15]For properties of these films, see, for example, J. Wilks, *The Properties of Liquid and Solid Helium* (Clarendon, Oxford 1967), Chap. 14.

[16]See Ref. 7 and references therein.

[17]S. B. Crampton, W. D. Phillips, and D. Kleppner, Bull. Am. Phys. Soc. 23, 86 (1978).

CHAPTER 4

DENSITY, MAGNETIZATION, COMPRESSION, AND THERMAL LEAKAGE OF LOW-TEMPERATURE ATOMIC HYDROGEN

J. T. M. Walraven and Isaac F. Silvera

Natuurkundig Laboratorium der Universiteit van Amsterdam
1018 XE Amsterdam, The Netherlands

The density distribution of low-temperature spin-polarized atomic hydrogen in a realistic magnetic field profile is calculated for densities below and above the critical value for Bose-Einstein condensation. The distribution is an identifying characteristic. Magnetic compression and instability due to thermal leakage of the atoms is treated.

[Phys. Rev. Lett. 44, 168 (1980)]

Density, Magnetization, Compression, and Thermal Leakage of Low-Temperature Atomic Hydrogen

J. T. M. Walraven and Isaac F. Silvera
Natuurkundig Laboratorium der Universiteit van Amsterdam, 1018 XE Amsterdam, The Netherlands
(Received 19 November 1979)

The density distribution of low-temperature spin-polarized atomic hydrogen in a realistic magnetic field profile is calculated for densities below and above the critical value for Bose-Einstein condensation. The distribution is an identifying characteristic. Magnetic compression and instability due to thermal leakage of the atoms is treated.

Atomic hydrogen (H) which has been shown in the accompanying Letter[1] to exist in a long-time stable state provides us with a new Bose fluid. Since in general it is necessary to prepare this gas by injecting atoms into a magnetic field, a treatment of the effect of magnetic field gradients is required. In this Letter we calculate the density distribution for spin-polarized H ($H\uparrow$) in a realistic magnetic field profile. Results are obtained below and above n_c, the critical density for Bose-Einstein (BE) condensation; the effects of interactions in the high-density BE condensed state are shown to be non-negligible. The density profile is a characteristic identifying feature of the gas. This calculation immediately provides the local static magnetization, which is related to the density by a proportionality constant: the Bohr magneton. The important concept of a magnetic compression is introduced. Finally, we consider the instability of a magnetically confined gas in an open-ended container, due to thermal leakage. Comparisons are made with experiment where possible.

At low temperatures $H\uparrow$ is considered to be an extremely weakly interacting Bose gas.[2] To illustrate this point we have plotted in Fig. 1 the p-V curves for $H\uparrow$ at $T = 0$ K as calculated by Etters, Danilowicz, and Palmer[3] and for an ideal Bose gas at $T = 0.1$ and 0.3 K. As the 0-K curve can be looked upon as a measure of the interactions

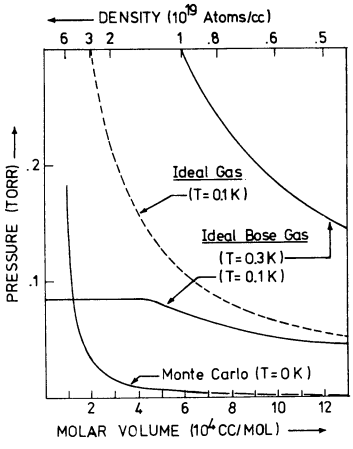

FIG. 1. p-V relation for $H\uparrow$ in various approximations and at various temperatures.

within the system, no significant deviations from ideal-Bose-gas behavior are to be expected for many properties down to molar volumes and temperatures of order 10^5 cm^3/mol and 100 mK. This feature makes H↑ an ideal test probe to compare theory and experiment for a weakly interacting Bose fluid.

H↑ can only be maintained as a stable gas in a magnetic field. The confinement space (cell) must be open ended to allow loading from a source of cold atoms which can extend to zero-field regions. As a consequence the density distribution will be inhomogeneous since the field gradients exert a force on the magnetic moments of the atoms. This leads to compression of atoms in the lower two hyperfine states[4] into the high-field region, whereas the other states are repelled. We first focus our attention on the steady-state properties of H↑ in the field of a small superconducting magnet as used in the experiment described in the preceding Letter.[1] The field profile along the symmetry (z) axis is shown in Fig. 2 and is approximately quadratic over a range of 60 mm around the field maximum. Any field gradients in the xy plane are neglected since the atoms are confined to the vicinity of the z axis by means of a cylindrical tube. If we neglect

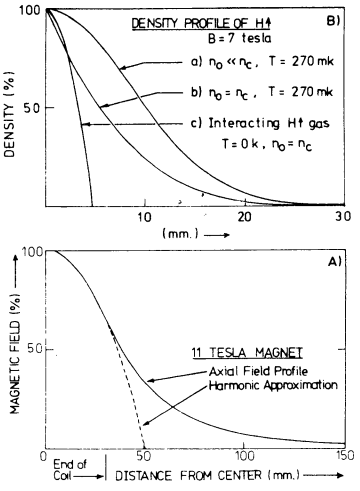

Fig. 2. (a) Magnetic field profile as a function of the distance from the center of the magnet. The end of the magnetic coil and a quadratic fit to the field are indicated. (b) Density profiles on an expanded scale. See text for explanation.

wall effects as well as all terms in the Hamiltonian beyond the electronic Zeeman term (i.e., we assume a high-field approximation), and replace the real field profile by its quadratic approximation, $B(z) = B_0[1 - (z/z_m)^2]$, the Schrödinger equation for atoms in the $m_s = -\frac{1}{2}$ electronic spin state reduces to a harmonic-oscillator (HC) problem:

$$\left[-\frac{\hbar}{2m}\nabla^2 + \mu_B B_0\left(\frac{z}{z_m}\right)^2\right]\psi = \epsilon\psi, \tag{1}$$

where m is the mass of the H atom, $2\pi\hbar$ is Planck's constant, $g = 2$ is the Landé g factor, μ_B is the Bohr magneton, B_0 is the field at the center of the magnet, and $z_m = 51$ mm in our system [see Fig. 2(a)].

The solutions of (1) are

$$\psi_{n_z \vec{k}_\perp} \sim \varphi_{n_z}(z)\exp(i\vec{k}_\perp \cdot \vec{r}_\perp), \tag{2}$$

where $\varphi_{n_z}(z)$ is a HO state and $\exp(i\vec{k}_\perp \cdot \vec{r}_\perp)$ a plane-wave state with propagation perpendicular to the symmetry axis. The energy spectrum consists of a series of bands, labeled by the HO quantum number and spaced at approximately 4×10^{-8} K. The corresponding oscillator frequency ω_0 is given by

$$\omega_0 = (2\mu_B B_0/m z_m^2)^{1/2}, \tag{3}$$

where $\omega_0 \simeq 5.5\times10^3$ rad/sec for a field of 7 T.

If one considers a *collection* of H atoms in the magnetic field, the occupation of the various states is governed by Bose statistics. As a consequence the density distribution of H↑ depends dramatically on the total number of atoms in the field as shown in Fig. 2(b). At low density (curve a) the system behaves like an ideal gas. If the density is increased the statistics lead to a compression of the gas, causing a peaking of the distribution as shown in curve b. Beyond a critical density (n_c) a "divergence" in the density occurs at the maximum field position because of the Bose condensation into the HO ground state. The classical turning points for this state are separated by 6.8 μm. However, at these densities it is no longer realistic to treat the system as an ideal Bose gas and interactions will cause the divergence to broaden as shown in curve c for $T = 0$ K.

The density distribution $n(z)$ of the gas is calculated with use of

$$n(\vec{r}) = \sum_i W_i |\psi_i(\vec{r})|^2, \tag{4}$$

where W_i is the Bose probability for the occupation of a given state. Even at the lowest achieva-

ble temperatures many states will be occupied and as a consequence (for $n \leq n_c$) Eq. (4) can be calculated very accurately using the classical approximation for the expectation values $|\psi_i(\vec{r})|^2$ of the HO states.[5] This leads to

$$n(z) \simeq \lambda_{th}^{-3}\, \zeta_{3/2}(F), \tag{5}$$

where $\lambda_{th} = (2\pi\hbar^2/mkT)^{1/2}$ is the thermal wavelength,

$$\zeta_{3/2}(F) = \sum_{l=1}^{\infty} F^l/l^{3/2},$$

$$F = \exp[(\mu - \tfrac{1}{2} m\omega_0^2 z^2)/kT],$$

μ is the thermodynamic potential, and k is Boltzmann's constant. $n \leq n_c$ corresponds to the condition $F \leq 1$.

The effect of the broadening of the condensate peak is estimated using the theoretical results for the ground-state energy per atom $E_1(n)$ as a function of density.[3,6] The energy to add a particle to the system is then given by

$$\mu = (\partial/\partial n)[nE_1(n)] \simeq 2an - \mu_B B \tag{6}$$

for relatively low densities, where one may write $E_1(n) = an - \mu_B B$ with $a/k = 306$ K Å.[3] Setting $n = n_c = 1.4\times 10^{20}$ atoms/cm^3 at 7 T and 0.27 K one easily finds the density distribution (for the field profile under study) to depend quadratically on the distance from the center [curve c, Fig. 2(b), for $T = 0$].

In order to study the consequences of these concepts for somewhat realistic experimental conditions, consider a tube extending from zero to maximum field along the axis of a magnet. The tube is assumed to be at constant temperature and does not catalyze recombination. The zero-field density of H is maintained constant. This sets a value for the thermodynamic potential and the density can be calculated at any point using Eq. (5). It is elucidating to express this relation in terms of a compression factor, $c(z)$, and the density at maximum field: $n_0 = c(z)n(z)$. In the low-density limit

$$c(z) = \exp\{\mu_B[B_0 - B(z)]/kT\}. \tag{7}$$

The strong dependence on B and T is seen in the following examples. For the profile of Fig. 2(a) with a 7-T field at $T = 0.27$ K and $z = 40$ mm, we have $c = 8.6\times 10^3$, whereas at 0.5 K, $c = 133$. For 10 T and $T = 0.1$ K, $c = 1.5\times 10^{15}$.

From expression (7) we see that if, in an equilibrium condition, the density in zero field is suddenly reduced to zero (experimentally this corresponds to turning off the H discharge source), then the density n_0 in the high field must go to zero. This presents an instability for an open-ended system. The time constant for this thermal leakage in the low-density limit is found from

$$dN/dt = \int_0^{z_r} dz\, A P_1(z)\, n(z) \times \int_0^{\infty} dv_z\, P_2(v_z)\rho(v_z)\, v_z, \tag{8}$$

where N is the number of atoms in the field, A is the cross-sectional area of the tube, $P_1(x)$ is a geometric factor describing the probability to escape the system (pass beyond $z = z_r$) from the position z without a wall collision, $P_2(v_z) = \theta(v_z - w_z(z))$ is the probability that an atom moving in the proper direction with a velocity v_z can escape, θ is a unit step function, and

$$w_z(z) \equiv [2\mu_B(B(z) - B(z_r))/m]^{1/2}$$

is the escape velocity;

$$\rho(v_z) \equiv \alpha^{-1}\pi^{-1/2}\exp[-(v_z/\alpha)^2]$$

is the normalized velocity distribution in the z direction and $\alpha \equiv (2kT/m)^{1/2}$. Evaluating the velocity integral yields a simple rate equation, $\dot{N} = N/\tau$, where $\tau = 4cV_{eff}/K\bar{v}A$, $\bar{v} \equiv (8kT/\pi m)^{1/2}$ is the average velocity of the atoms, $V_{eff} \equiv N/n_0$, and

$$K \equiv \tfrac{1}{8}\pi^{1/2}\int_0^{z_r} P_1(z)\, dz$$

is the effective Clausing factor[7] for the system. τ is the time constant of the system. For the experiment of Ref. 1 we have calculated a time constant $\tau = 19$ msec in zero field ($V_{eff} \simeq 1.2$ cm^3) and $\tau = 110$ sec at 7 T ($V_{eff} \simeq 0.8$ cm^3), using $K = 0.1$, $\bar{v} = 100$ m/sec, and $A = 12.5$ mm^2, for magnetic compression only. The experiment yielded $\tau \simeq 1.5$ and 532 sec, respectively. We attribute the difference to additional compression due to fluxing helium vapors (HEVAC), as discussed in Ref. 1. From the experimental zero-field time constant of 1.5 sec, a HEVAC compression of 79 is estimated. In the field of 7 T the time constant due to both compressions would then be 8.7×10^3 sec (2.4 h), consistent with observations.

In summary, we stress the important result that a realistic magnetic field profile leads to a density distribution that displays macroscopic features characteristic of the Bose nature of the particles: narrowing and peaking up at the field maximum as the gas approaches the critical density. Measurement of the density or magnetization should provide a method of detecting BE con-

densation. If this state can be created, from curve *c* Fig. 2(b) we see that a sharp interface or "surface" in coordinate space should be a characteristic of the condensate at low temperature. At low density the gas behaves classically. The maximum density that can be loaded into a magnetic field for a gas stabilized against recombination is limited by $\exp(B/T)$ and the zero-field density.

The authors acknowledge a number of stimulating discussions on these subjects with A. J. Berlinsky, H. P. Godfried, V. V. Goldman, and A. P. M. Mattheij, as well as the financial support of the Stichting voor Fundamental Onderzoek der Materie.

[1]I. F. Silvera and J. T. M. Walraven, preceding Letter [Phys. Rev. Lett. 44, 164 (1980)].

[2]C. E. Hecht, Physica (Utrecht) 25, 1159 (1959); R. D. Etters, J. V. Dugan, and R. W. Plamer, J. Chem. Phys. 62, 313 (1975); W. C. Stwalley and L. H. Nosanow, Phys. Rev. Lett. 36, 910 (1976).

[3]R. D. Etters, R. L. Danilowicz, and R. W. Palmer, J. Low. Temp. Phys. 33, 305 (1978).

[4]N. F. Ramsey, *Molecular Beams* (Clarendon, Oxford, 1956), p. 263.

[5]L. I. Schiff, *Quantum Mechanics* (McGraw-Hill, New York, 1955), 2nd ed., p. 65.

[6]M. D. Miller and L. H. Nosanow, Phys. Rev. B 15, 4376 (1977).

[7]S. Dushman, in *Scientific Foundation of Vacuum Technique*, edited by J. M. Lafferty (Wiley, New York, 1962), 2nd ed., p. 93.

CHAPTER 5

MAGNETIC EQUATION OF STATE OF A GAS OF SPIN-POLARIZED ATOMIC HYDROGEN

J. T. M. Walraven, Isaac F. Silvera, and A. P. M. Matthey

Natuurkundig Laboratorium der Universiteit van Amsterdam
1018 XE Amsterdam, The Netherlands

The magnetic equation of state of spin-polarized atomic hydrogen is reported, relating density to magnetic field ($B \lesssim 10.5$ T), temperature ($T \lesssim 300$ mK), and atomic flux used to fill the sample cell. Densities greater than 10^{16} atoms/cm^3, more than two orders of magnitude greater than initial observations, have been achieved. Results are also presented on the buildup and decay of the density as a function of external conditions. Preliminary observations on the Fermi fluid, atomic deuterium, are reported.

[Phys. Rev. Lett. 45, 449 (1980)]

Magnetic Equation of State of a Gas of Spin-Polarized Atomic Hydrogen

J. T. M. Walraven, Isaac F. Silvera, and A. P. M. Matthey
Natuurkundig Laboratorium der Universiteit van Amsterdam, 1018-XE Amsterdam, The Netherlands
(Received 8 April 1980)

The magnetic equation of state of spin-polarized atomic hydrogen is reported, relating density to magnetic field ($B \lesssim 10.5$ T), temperature ($T \gtrsim 300$ mK), and atomic flux used to fill the sample cell. Densities greater than 10^{16} atoms/cm^3, more than two orders of magnitude greater than initial observations, have been achieved. Results are also presented on the buildup and decay of the density as a function of external conditions. Preliminary observations on the Fermi fluid, atomic deuterium, are reported.

PACS numbers: 67.40.Db, 75.10.-b

Spin-polarized atomic hydrogen ($H\downarrow$) has recently[1,2] been stabilized over periods of minutes at 270 mK and densities of order 10^{14} atoms/cm^3. In order to observe many of the fascinating predicted properties such as Bose-Einstein condensation and the gaseous nature of this many-body system at $T = 0$ K, it is necessary to achieve substantially higher densities. In this Letter we report density increases of more than two orders of magnitude over previous values; no fundamental limitations have yet been encountered. Experimental results are presented on the temporal behavior of $H\downarrow$ during filling of a hydrogen stabilization cell (HSC) and the subsequent decay after filling. We have also studied the magnetic equation of state of $H\downarrow$ which provides an important guide for efforts to increase the density. Finally we report some preliminary measurements on the stabilization of the Fermi fluid, spin-polarized atomic deuterium.

One of our principle objectives in this article is to thermodynamically demonstrate that, although exotic, $H\downarrow$ behaves as a gas of magnetic moment bearing atoms that exists at very low temperatures. An ideal geometry for studying the thermodynamic properties would be an infinite space with no surfaces having a uniform temperature and including a region with a nonzero static magnetic field. The requirement that the chemical potential be uniform in such a system yields a relationship between the equilibrium local magnetization $\vec{M}$, the magnetic field $\vec{B}$, and the temperature T. This is the magnetic equation of state. Since $|\vec{M}| = \mu_B n$ (n is the local gas density and μ_B the Bohr magneton), establishment of the relationship between n, B, and T provides thermodynamic evidence of the gaseous nature of $H\downarrow$.

In our actual system,[1] the gas is fed into the HSC from a room-temperature source with intermediate cooling states; it can exist in a nonequilibrium steady-state condition with a temperature extending from ~0.3 to 300 K. However, the gas is confined in the HSC by magnetic compression and a miniature low-temperature helium vapor compressor (HEVAC) and the density only suffers slow decay due to leakage or recombination. As a consequence we treat the gas as a quasiequilibrium system. For the density distribution we have[2]

$$n(B) = n(B_0)\exp[-\mu_B(B_0 - B)/kT], \quad (1)$$

where B_0 is the maximum field. The ratio of the density at field B_0 to that at field B is called the magnetic compression factor, $c_M \equiv \exp[\mu_B(B_0 - B)/kT]$. The time constant τ is determined by the experimental design. In our system (described in Ref. 1)

$$\tau = 4c_H c_M V_{eff}/K\bar{v}A, \quad (2)$$

where c_H is the HEVAC compression, $V_{eff} \equiv N/n(B_0)$ is the effective volume[2] of the HSC (with total number of particles N), A is the cross-sectional area of the fill tube with Clausing factor K, and $\bar{v}$ is the average atomic velocity of the gas. The expression for τ is again only valid in the low-density limit; it neglects any recombination in the cell and thus the decay is fully ascribed to free atomic flow of $H\downarrow$ towards the HEVAC where an atom has a probability of $1/c_H$ to escape. This model predicts the density to change exponentially towards a new steady-state value when the conditions are changed.

In our present geometry the HSC and the HEVAC are in fields B_0 and $0.56B_0$, respectively. The HSC can be varied in temperature from ~0.27 to 0.8 K; the HEVAC operates at ~0.5 K. Below the HEVAC the temperature rises rapidly to 4.2 K at an accommodator[3] used to cool the H gas generated in a room-temperature discharge. It is quite clear that the configuration differs from the ideal uniform temperature system, yet we believe that our system can be approximated by Eqs. (1) and

(2) with c_M evaluated with respect to the field at the HEVAC. When the discharge is turned on a steady-state density (n_{eff}) of cold H is maintained in front of the HEVAC in spite of surface recombination processes. If we assume these processes to be first order in the density we expect n_{eff} to scale linearly with the incoming flux, φ; we conclude[4] that $n(B_0) \sim c_H c_M \varphi$.

Measurements were made by filling the cell at a constant flux for specified periods. The density was determined by triggering the stable $H\downarrow$ gas to recombine by means of a bolometer.[1] The recombination energy was mainly dissipated in the cell and caused an easily measured temperature rise of the HSC with a characteristic wave form. The cell was calibrated for density by electronically generating heat pulses in the bolometer to reproduce this wave form. Since after triggering, atoms and recombined molecules could also be blown out of the HSC, our measured densities represent lower bounds.

We shall first discuss our low-density ($n \lesssim 3 \times 10^{14}$ atoms/cm^3) results. In Fig. 1(a) we show a typical curve for the time dependence of filling the HSC. When the discharge is turned off, the density in the cell decays exponentially with a time constant τ as shown in Fig. 1(b). In zero field at $T = 0.27$ K we measured[1] $\tau \equiv \tau_0 = 1.5 \pm 1$ sec. For 4 T, 0.39 K and 8 T, 0.37 K we find 38.6 ± 1 and 1998 ± 37 sec, respectively. The longest period of stabilization was 47 min before triggering.

Writing $\tau = \tau_0 (V_{eff}/V_0) \exp[\gamma \cdot \mu_B B_0/kT]$, where V_0 is the geometric volume of the cell and $\gamma \equiv (B_0 - B)/B_0$, enables us to solve for τ_0 and γ using the measured time constants for 4 and 8 T. This yields $\tau_0 = 1.7$ sec and $\gamma = 0.53 \pm 0.05$, where we give the error in γ due to uncertainties in temperature. The value of τ_0 agrees well with our direct measurement at $B_0 = 0$; $\gamma = 0.53$ corresponds to a point within 2 mm of our estimate of the location of the compression side of the HEVAC,[5] suggesting that c_M should be calculated with respect to the field in the HEVAC.[6] In some circumstances we observed almost steplike changes of the time constant by factors of 2 or 3. We believe this may be due to different modes of operation of the HEVAC. During the measurements of τ at 4 and 8 T used to calculate γ, changes of this nature were not observed. At higher densities, $n \gtrsim 10^{16}$ atoms/cm^3, we observed initial decay rates of order five times faster so that simple exponential decay no longer applies. This may imply that recombination is becoming a problem.

One of our objectives has been to determine the magnetic equation of state. In steady-state equilibrium we can write $n_{sat}(B_0) = \varphi \tau_0 c_M / V_0$. Flux was easily measured by filling the HSC for a time $t \ll \tau$ and triggering to determine the number of atoms N or $\varphi = N/t$. In Fig. 2 we plot the satura-

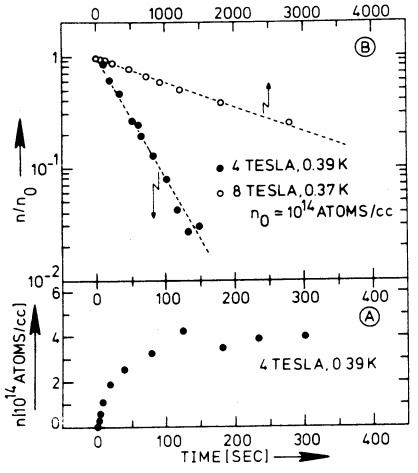

FIG. 1. (a) Density as a function of time during filling of the cell at constant φ, B_0, and T. (b) Decay of $n(B_0)$ in time at constant B and T. The upper scale is for the 8-T data.

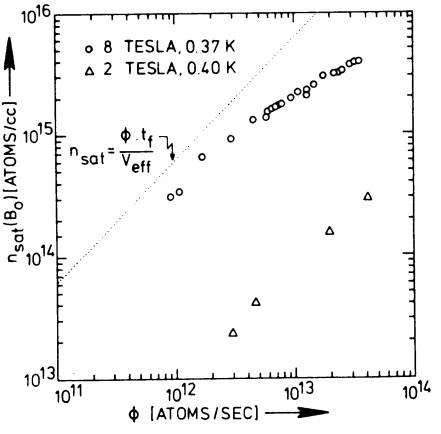

FIG. 2. Saturation density as function of the incoming flux at constant B_0 and T. The dotted line represents the maximum possible density in case of systematic error.

tion density as a function of flux, with B_0 and T held constant. The simple theory suggests a linear relationship which is found for low density (triangles). However, for higher density (circles), we see a deviation. Our detection method only determines a lower bound of $n(B_0)$. We can also set an upper bound by noting that the measured density must be less than $\varphi t_f/V_{\rm eff}$, where t_f is the fill time used to ensure that $n(B_0)=n_{\rm sat}$. This upper bound is given by the dotted line. In Fig. 3 we plot the saturation density versus B_0/T for a constant flux, $\varphi \simeq 1.3\times10^{13}$ atoms/sec. The open circles represent data obtained from variation of the magnetic field at constant temperature while the solid circles are obtained by varying the temperature, keeping the field constant. The dashed line represents the predicted behavior where $n_{\rm sat}=\varphi\tau_0 c_M/V_0$ and $\gamma=0.53$; the dotted line again represents an upper bound as determined by the integrated flux of atoms. The data are corrected for changes in the mode of operation of the HEVAC which were detected by measuring the saturation density at regular time intervals for a reference value of B, T, and φ. The instability of operation was mainly responsible for the scatter in the data. The statistical error in measurement of field, temperature, time, and the wave forms used to determine the density was at most a few percent. However, we estimate that the density calibration, which covered more than three orders of magnitude could have a systematic error, in particular at high density, of order 2. At a density of 10^{15} atoms/cm^3 the measured density could be as much as a factor of 5 lower than the actual density due to leakage of recombination energy (or atoms) out of the HSC.

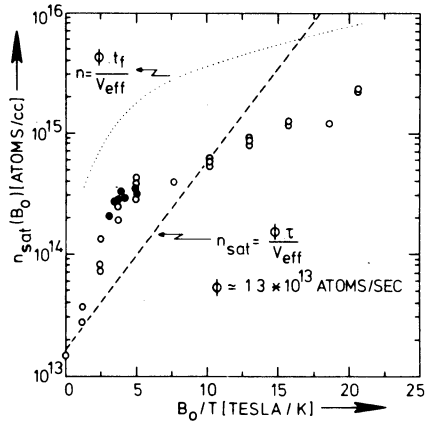

FIG. 3. Saturation density as a function of B_0/T for constant incoming flux. For densities above $\sim3\times10^{14}$, the data are thought to represent a lower limit. The dotted line represents an upper limit. For the dashed line, see text.

The highest $H_\downarrow$ density achieved to now is $n(B_0)\geq 1\times10^{16}$ atoms/cm^3 in 10.5 T at 0.4 K. As the flux is increased the HSC warms up, probably due to recombination that occurs during loading and sorting out of spin-up and spin-down atoms. Thus our maximum density is limited by our current refrigeration power. The flux itself was never a limit and usually was restricted to (1–10)% of its maximum value.

The presented data clearly show how higher densities can be achieved in the HSC. The simple theory of compression appears to have some validity but is not accurately applicable due to nonuniformities in the temperature. Moreover at higher densities we only observe a lower limit for the density, complicating interpretation. Deviations from the simple theory observed for higher densities may possibly be related to the location of the HEVAC and can be resolved by changing the geometry. If deviations are due to the onset of recombination in the HSC, then the problem is fundamental. However, density decay can also arise from recombination in the tail of the density distribution where a dense gas of helium can promote three-body recombination, or where the walls do not have a proper helium coverage.

We also report an interesting observation concerning the detection of $H_\downarrow$. With a sufficient number of atoms in the cell, after triggering, the cell temperature rises to a temperature T_f and then remains constant, for periods t_b up to 2.6 sec. Simultaneously triggering both bolometers in the HSC in order to double the active surface area did not affect T_f or t_b for a given density. However, simple kinetic considerations suggest that the rate of recombination is proportional to the bolometer area and that the process should be completed within tens of milliseconds.[1] This indicates that another (unidentified) process becomes important at higher densities. A possible explanation is that after triggering, the initial recombination heats the cell to temperatures greater than that of the HEVAC, also vaporizing some helium. At this point the helium vapors begin to flow towards the HEVAC, compressing the $H_\downarrow$ between the HSC and the HEVAC. This is a self-controlled feedback process that keeps the temperature of the HSC constant by recombining the H at a constant rate as long as a sufficient

number of atoms are available and for which t_b is independent of the bolometer area.

Two of us (I.F.S. and J.T.M.W.) have injected gas from a deuterium discharge into the HSC. The resultant trigger signals correspond to disappointingly low densities of stabilized gas. This result could be due to a higher surface adsorption energy[7] for D as compared to H. It is quite clear that D behaves differently than H, even at low density. A complete report will be made after further investigations are completed.

We thank R. Sprik for assistance with some of the measurements and gratefully acknowledge the financial support of the Stichting voor Fundamenteel Onderzoek der Materie.

---

[1]I. F. Silvera and J. T. M. Walraven, Phys. Rev. Lett. 44, 164 (1980); note that here we have changed the notation from $H^{\uparrow}$ to $H^{\downarrow}$ for spin polarized H, which is preferable since we stabilize the down ($m_s = -\frac{1}{2}$) spin state.

[2]J. T. M. Walraven and I. F. Silvera, Phys. Rev. Lett. 44, 168 (1980).

[3]I. F. Silvera and J. T. M. Walraven, Phys. Lett. 74A, 193 (1979).

[4]Measurements were mostly done at ~0.4 K, limiting gradients to 25% of the cell temperature so that thermomolecular effects are small.

[5]This enables an improved estimate of $c_H = \frac{1}{4}\tau_0 K\bar{v}A/V_0$. Use of $V_0 = 1.44$ cm^3, $\bar{v} = 93$ m/sec, $A = 0.125$ cm^2, and $K = 0.11$ with $\tau_0 = 1.7$ sec leads to $c_H = 38$. This value differs from that given in Ref. 2 as we have now determined the helium condensation point of the HEVAC (the compression side) to be further from the HSC, changing V_0 and K. In Ref. 2 due to a typographical error K was given as 0.1 instead of 0.18; the calculated estimate, $c_H = 79$, was correct as given.

[6]In Ref. 2 time constants were calculated taking $B = 0$ in the low-density tail.

[7]R. A. Guyer and M. D. Miller, Phys. Rev. Lett. 42, 1754 (1979).

CHAPTER 6

SPIN-POLARIZED ATOMIC DEUTERIUM: STABILIZATION, LIMITATIONS ON DENSITY, AND ADSORPTION ENERGY ON HELIUM

Isaac F. Silvera and J. T. M. Walraven

Natuurkundig Laboratorium der Universiteit van Amsterdam
1018 XE Amsterdam, The Netherlands

Current limitations on the density of stabilized spin-polarized deuterium($D\downarrow$) to $\sim 10^{14}$ atoms/cm^3 are shown to arise from condensation on the ^4He surface and subsequent recombination. A new technique for measuring the adsorption enery is employed to provide the first such measurement for $D\downarrow$ on helium, yielding $\varepsilon_a/k_2 = 2.5 \pm 0.4$ K.

[Phys. Rev. Lett. 45, 1268 (1980)]

Spin-Polarized Atomic Deuterium: Stabilization, Limitations on Density, and Adsorption Energy on Helium

Isaac F. Silvera and J. T. M. Walraven
Natuurkundig Laboratorium der Universiteit van Amsterdam, 1018-XE Amsterdam, The Netherlands
(Received 10 July 1980)

Current limitations on the density of stabilized spin-polarized deuterium ($D_\downarrow$) to $\sim 10^{14}$ atoms/cm^3 are shown to arise from condensation on the ^{4}He surface and subsequent recombination. A new technique for measuring the adsorption energy is employed to provide the first such measurement for $D_\downarrow$ on helium, yielding $\epsilon_a/k_B = 2.5 \pm 0.4$ K.

PACS numbers: 67.40.Db, 68.45.Da

We have recently reported the stabilization of a gas of spin-polarized atomic hydrogen, $H_\downarrow$, in a cell in which all surfaces were coated with superfluid ^{4}He.[1] Although densities greater than 10^{16} atoms/cm^3 have already been achieved for $H_\downarrow$,[2] attempts to achieve higher densities for spin-polarized atomic deuterium, $D_\downarrow$, have yielded densities $n \lesssim 10^{14}$ atoms/cm^3. In this Letter we show that the limitation is due to a fundamental problem: the adsorption of $D_\downarrow$ on the ^{4}He surface and subsequent recombination to D_2. The same process can ultimately prevent achievement of the higher densities necessary for Bose-Einstein condensation in $H_\downarrow$. We have developed a method for measuring the adsorption energy and find $\epsilon_a/k_B = 2.5 \pm 0.4$ K for $D_\downarrow$ on ^{4}He. We have also attempted to stabilize $H_\downarrow$ and $D_\downarrow$ using pure ^{3}He surfaces and detected no measurable density. However, a mixture of ^{3}He-^{4}He, which is known to phase separate and to provide a ^{3}He surface, is effective.

$D_\downarrow$ is a spin-$\frac{1}{2}$ or -$\frac{3}{2}$ particle and is expected to behave as a Fermi gas.[3] For temperatures lower than the Fermi temperature, $T_F = \hbar^2/2mk_B \times (6\pi^2 n/g)^{2/3}$ (g is the nuclear spin degeneracy) it becomes a degenerate quantum gas. At even lower temperatures it is conjectured to display superfluidity with several phases due to the various possible pairings of the fermion spin,[4] in some analogy with ^{3}He. Densities of order 10^{20} atoms/cm^3 are required to observe these properties with the existing low-temperature technology.

We briefly describe our experimental technique, which is similar to that of Ref. 1. Atomic D originating in a room-temperature microwave discharge enters our cryostat via a warm Teflon tube and is abruptly cooled by an accommodator. This is a short length of cylindrical tubing cooled to $T \simeq 5$ K by a weak thermal contact to a ^{4}He bath[5] and covered with solid D_2. The gas flows into a cold ($T \geq 270$ mK) stabilization cell, which we call the HSC (hydrogen stabilization cell), sitting in a solenoidal magnetic field which has a value of 8.0 T in the present experiments. This field polarizes and confines the atoms to the HSC.[2,6] Confinement is further aided by a mixture helium vapor compressor (HEVAC) located between the accommodator and the HSC. Before loading with $D_\downarrow$, the HSC and HEVAC walls are covered with a film of ^{4}He which extends almost to the accommodator. The density of $H_\downarrow$ confined in such a cell decays exponentially, as a result of thermal leakage,[2,6] with a time constant $\tau \sim 2 \times 10^3$ sec for the current conditions; we expect about the same value for $D_\downarrow$. The number of $D_\downarrow$ atoms in the cell are measured by precipitating rapid recombination on the surface of a bolometer and measuring the subsequent temperature rise of the HSC; calibration is done electronically.[1,2]

We have found the density of $D_\downarrow$ to be limited for two reasons. First, in the presence of a decay process, the maximum density in the HSC depends on the loading flux of atoms. The flux of $D_\downarrow$ was substantially lower than that of $H_\downarrow$. This was found to be due to condensation and recombination on the surfaces of the accommodator region. By heating the accommodator up by several degrees Kelvin, the $D_\downarrow$ flux could be increased by a factor 5–10. This implies a larger adsorption energy of D on D_2 than H on H_2.[7] A similar study for $H_\downarrow$ yielded an increased flux of 2–3. However, even with the increased flux of $D_\downarrow$ the maximum density was limited to $\sim 10^{14}$ atoms/cm cm^3, at least two orders of magnitude lower than what we have thus far achieved for $H_\downarrow$.

A second and more fundamental limitation was found by studying the temporal decay of $D_\downarrow$ samples. We have measured the decay rate of the number of atoms in the HSC, $N = N_g + N_s = Vn_g + An_s$, where N_g is the number in the gas phase and N_s in the surface phase, V is the volume, and A is the area available to the $D_\downarrow$. A theoretical

expression for the decay of atoms is found from the solution of the rate equation

$$-dN/dt = -V\,dn_g/dt - A\,dn_s/dt$$
$$= Vn_g/\tau + VK_v n_g^3 + AK_s n_s^2, \quad (1)$$

where K_v and K_s are the volume and surface recombination rate constants. For the measured decay times of ~ 10 sec the first term is negligible; we also expect the second term of (1) to be unimportant, although K_v has never been measured. Assuming that the surface coverage and gas density remain in thermodynamic equilibrium during decay, we can use the low-density–high-temperature form of the adsorption isotherm for a boson or fermion gas,[8] $n_s = n_g \lambda \exp(\epsilon_a/k_B T)$, where ϵ_a is the adsorption energy and $\lambda = (2\pi\hbar^2/mk_B T)^{1/2}$ is the thermal de Broglie wavelength. Substituting this in Eq. (1) and using the fact that $N = N_g + N_s \simeq N_g$, we find

$$-dN/dt$$
$$= [K_s A V^{-2} \lambda^2 \exp(2\epsilon_a/k_B T)]N^2 \equiv K_s^{\text{eff}} N^2, \quad (2)$$

which has the solution $N^{-1} - N_0^{-1} = K_s^{\text{eff}}(t - t_0)$. The decay of N was studied by filling the HSC to a known level, waiting for a time t, and then measuring the remaining number of atoms. The results for two different temperatures are shown in Fig. 1. The data have been corrected for a small hydrogen impurity that is present in our D_2 sample and arises from water that gets into the discharge and is dissociated, but could be minimized by judicious cold trapping. The $H_\downarrow$ impurity is long lived and thus the sample in the HSC decays rapidly to the $H_\downarrow$ level which ranged from ~ (0–20)%. The data could be fitted with a second-order process after correcting for the H impurity; a possible third-order term was zero to within experimental error. We conclude that the gas-phase density of $D_\downarrow$ is limited by adsorption and recombination on the ^{4}He surface. Uang and Stwalley[9] have recently suggested that a $D_\downarrow$ impurity in $H_\downarrow$ (the argument also applies for $H_\downarrow$ in $D_\downarrow$) has a giant spin-flip cross section relative to $H_\downarrow$-$H_\downarrow$ cross sections and would be destructive, leading to rapid recombination. Our measurements show that the two gases easily coexist at the densities studied here.

From these studies we have been able to make the first determination of the adsorption energy of a hydrogen isotope on ^{4}He. The slopes of the decay curves such as given in Fig. 1 yield K_s^{eff}, which we determined for several temperatures. The intrinsic rate constant K_s is expected to vary as $T^{1/2}$ at high temperature, coming to a nonzero value at $T = 0$. For our temperature regime we treat K_s to be independent of temperature. The slope of a plot of $\ln(TK_s^{\text{eff}})$ vs $1/T$, as shown in Fig. 2, yields $2\epsilon_a$ and we find $\epsilon_a/k_B = 2.5 \pm 0.4$ K. A $T^{1/2}$ dependence of K_s would increase the value by 4%. This value is substantially larger than the 1.11 K calculated by Guyer and Miller[10] or the 1.39 K due to Mantz and Edwards.[11]

The ^{4}He used for surface coverage was taken from an ultrahigh-purity lecture bottle. The ^{3}He impurity was unknown. We varied the quantity condensed in the cell by about a factor 4 so that the film was probably undersaturated. Since ^{3}He impurities would reside on the surface, this should vary a ^{3}He impurity effect. Any differences due to film thickness and impurity were within the noise level of our measurements.

Let us consider some of the implications of these results. First, using the adsorption isotherm and $n_g = 1 \times 10^{13}$ atoms/cm^3 sec at $T = 0.4$ K,

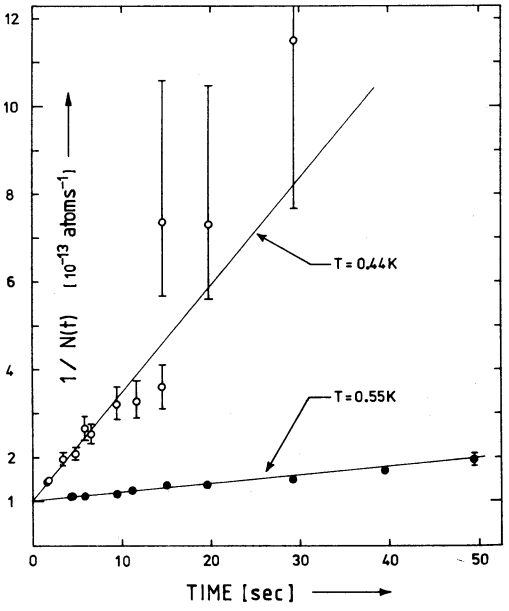

FIG. 1. Decay of the total $D_\downarrow$ particle number N in the HSC as a function of time (t) plotted as $1/N(t)$ vs t. All data are normalized to an initial value of $N = 1 \times 10^{13}$ atoms/cm^3. Open circles $T = 0.44$ K; closed circles $T = 0.55$ K. The lines represent a least-squares fit to the data for which a pure second-order decay process is assumed.

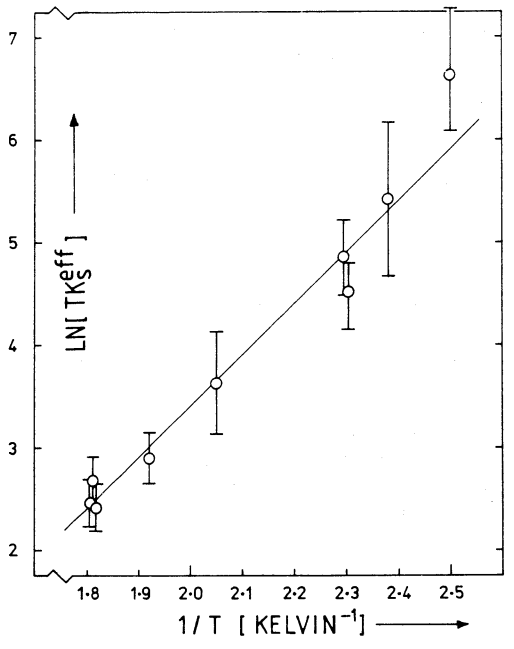

FIG. 2. Logarithmic plot of TK_s^{eff} vs $1/T$ allowing determination of the adsorption energy with application of a weighted–least-squares-fit procedure to a straight line. The value of the logarithm is given to within an additive constant.

we find $n_s = 1\times 10^9$ atoms/cm^2. This is a much lower limiting coverage than has been anticipated. Silvera and Goldman[8] have shown that at 8 T the critical coverage for static stability is 1.5×10^{14} atoms/cm^2 for $H_\downarrow$ and we expect about the same value for $D_\downarrow$. The present results show that this condition for metastability is of much less importance than the rates for dynamical three-body decay from the metastable spin-polarized state to the molecular state. Second, since at present there is no adequate theory for the dynamical decay processes, we cannot directly assess the implications for $H_\downarrow$. We would not expect K_s to be the same for $H_\downarrow$ and $D_\downarrow$, because the molecules have different energy levels.[12] We can make a rough check of this. Calculated values of ϵ_a/k_B for $H_\downarrow$ on ^{4}He are 0.1 K (Ref. 10) and 0.6 K.[11] If we take a value of 1 K and assume K_s to be the same for both $H_\downarrow$ and $D_\downarrow$, we estimate $K_s^{\text{eff}} \simeq 3.4\times 10^{-16}$/sec at $T = 0.37$ K and a half-life of 30 sec for an initial value $N_g \simeq 10^{14}$ atoms. However, under these conditions we did not observe experimentally[2] any significant deviation from an exponential decay with time constant $\tau \simeq 2000$ sec, indicating that for $H_\downarrow$ the values for K_s and/or ϵ_a should be considerably smaller. This result is only to be taken as an exercise to show that limitations on $H_\downarrow$ may be quite different. We note that to achieve Bose-Einstein condensation in $H_\downarrow$, a coverage $n_s \simeq 10^{13}$–10^{14} atoms/cm^2 must be contended with.[8] A *rough* estimate of the maximum coverage of $H_\downarrow$ on helium can be made as follows. The zero-field value of K_v for H-H-He collisions is 2.8×10^{-31} cm^6/sec.[13] We estimate (see last referral, Ref. 1) this to be reduced by a factor $\eta \simeq 8\times 10^{-6}$ in a field of 10 T. From the rate equation, $dn/dt = -(\eta K_v n_{\text{He}})n^2 + \varphi$ (which resembles a surface rate equation) for a flux $\varphi = 10^{16}$ cm^3/sec, we find a maximum density 1.7×10^{17} atoms/cm^3 (with $n_{\text{He}} = n$). Since final states in the recombination process on a surface are probably high energy and free particlelike, we treat the liquid helium as a dense gas of surface density $(10^{22})^{2/3}$ atoms/cm^2. Arguing that the dominant consideration of volume or surface recombination is the interparticle distance, we can scale the maximum volume density to find a maximum surface coverage of $H_\downarrow$ to be $\sim 5\times 10^9$ atoms/cm^2. We note that for densities of order 10^{16} atoms/cm^3 nonexponential-decay limitations were observed.[2] Assuming $\epsilon_a/k_B = 1$ K, we calculate $n_s = 3\times 10^{10}$ atoms/cm^2. As a third point, we note that we have a large amount of copper sinter in our HSC which provides a large value for $A \sim 400$ cm^2 in the expression for K_s^{eff}. This can be reduced by 50–100 cm^2 to enhance lifetimes and densities.

To relieve the surface problem it may be necessary to improve upon the use of ^{4}He as a surface. The adsorption energy is very sensitive to the surface density profile of the helium. ^{3}He is expected to have a more extended profile than ^{4}He and thus a lower $H_\downarrow$ or $D_\downarrow$ adsorption energy. We have lined our HSC with pure ^{3}He and found no measurable density of $H_\downarrow$ or $D_\downarrow$. We estimate our detection limit to be 10^8–10^9 atoms/cm^3. Evidently the problem is that the tubing between the accommodator and the HEVAC is not covered or protected and the H recombines in this region, never reaching the HSC. The superfluid properties of ^{4}He appear to be necessary. We have also used a ^{3}He-^{4}He mixture. This we found to be an effective coverage for stabilization. The components phase separate with the dilute-superfluid phase covering the vital surfaces. ^{3}He is expected to reside on top of the ^{4}He-rich phase to pres-

ent a ^{3}He surface to the $H_\downarrow$. At our current experimental temperature range the thermal response of the HSC is sluggish compared with pure ^{4}He because of the substantially higher vapor pressure. Lower temperatures will relieve this problem.

The authors thank O. H. Höpfner for his fine technical support, V. V. Goldman and E. J. M. Hartman for assistance with the data reduction, and gratefully acknowledge the financial support of the Stichting voor Fundamenteel Onderzoek der Materie.

[1]I. F. Silvera and J. T. M. Walraven, Phys. Rev. Lett. 44, 164 (1980), and J. Phys. (Paris), Colloq. 41, C7-137 (1980), and in Proceedings of the European Physical Society Conference on Condensed Matter, Antwerpen, 1980 (to be published).

[2]J. T. M. Walraven, I. F. Silvera, and A. P. M. Matthey, Phys. Rev. Lett. 45, 449 (1980); R. Cline, T. J. Greytak, D. Kleppner, and D. A. Smith, J. Phys. (Paris), Colloq. 41, C7-151 (1980).

[3]J. H. Freed, J. Chem. Phys. 72, 1414 (1980).

[4]A. J. Leggett, J. Phys. (Paris), Colloq. 41, C7-19 (1980).

[5]I. F. Silvera and J. T. M. Walraven, Phys. Lett. 74A, 193 (1979).

[6]J. T. M. Walraven and I. F. Silvera, Phys. Rev. Lett. 44, 168 (1980), and J. Phys. (Paris), Colloq. 41, C7-147 (1980).

[7]The measured adsorption energy of H on H_2 is 38 ± 8 K, S. B. Crampton, J. Phys. (Paris), Colloq. 41, C7-249 (1980).

[8]I. F. Silvera and V. V. Goldman, Phys. Rev. Lett. 45, 915 (1980).

[9]Y. H. Uang and W. C. Stwalley, Phys. Rev. Lett. 45, 627 (1980).

[10]R. A. Guyer and M. D. Miller, Phys. Rev. Lett. 42, 1754 (1979).

[11]I. B. Mantz and D. O. Edwards, Phys. Rev. B 20, 4518 (1979).

[12]W. C. Stwalley, Phys. Rev. Lett. 37, 1628 (1976).

[13]W. N. Hardy, M. Morrow, R. Jochemsen, B. W. Statt, P. R. Kubik, R. M. Marsolais, A. J. Berlinsky, and A. Landesman, Phys. Rev. Lett. 45, 453 (1980).

Summary

This thesis deals with the first of a series of experiments done at the University of Amsterdam to study the properties of spin polarized atomic hydrogen (H↓) and deuterium (D↓) at very low temperatures ($T \approx 0.3$ K) and in high magnetic fields ($B \approx 10$ T). The experiments show that H↓ and D↓ may be subjected to experimental investigation like any normal (i.e. stable) gas.

The thesis is divided in six chapters. Chapter 1 serves as an introduction and may be regarded as a motivation for our research. Partly this chapter deals with phenomena of direct relevance to our experiments such as the method of spin-polarization, the influence of the walls of the sample cell on the properties of the system and the magnetic field dependence of molecule formation. Other aspects are discussed to place the work into a broader perspective and are of importance for future research. This part includes a discussion of the Bose-nature of the gas and a treatment of Bose-Einstein condensation in an interacting Bose gas in the presence of surfaces and in an inhomogeneous magnetic field.

Chapter 2 deals with the experimental apparatus and resulted from a series of experiments done during the first part of my thesis work. In particular the development of a reliable method to cool atomic hydrogen to very low temperatures turned out to be decisive for our experiments. The two-stage ^{3}He refrigeration system discussed in the second part of this chapter, enabled an efficient cooling of the sample cell by dumping the heat of condensation of fluxing helium vapors (associated with the use of superfluid ^{4}He) into a first cooling stage in this way reducing the heat load on the low temperature stage. Moreover, the fluxing vapors were put to advantage and served to compress the H↓ into the cell.

An account of the first experiments with H↓ can be found in chapter 3. These experiments showed that H↓ can be stabilized for extended periods of time (at low temperature and in high magnetic fields) by covering all surfaces with a superfluid film of ^{4}He. The gas was detected by triggering recombination by locally breaking the helium film and measuring the heat of recombination. This method turned out to be very sensitive and easy to implement.

In chapter 4 the physical picture of the gas is discussed. This includes a discussion of the density profile and the phenomenon of thermal leakage from

the open structured sample cell. The density profile may be used to detect Bose-Einstein condensation.

A second series of experiments is discussed in chapter 5. These measurements were aimed at achieving high densities and to study the limiting processes. They demonstrate that H↓ behaves as a gas. Densities $n \gtrsim 10^{16}$ H↓/cm^3 could be achieved. At lower densities ($n \lesssim 10^{15}$ H↓/cm^3) thermal leakage turned out to be the dominant decay process while at higher densities also recombination turned out to be important. At this stage of the research it was unknown whether a bound state existed for the H-atom on the surface of the heliumfilm, although theoretical estimates pointed in this direction. To clearify this point and to obtain information concerning the nature of the recombination one can study the kinetics of the recombination process. Volume recombination appears at low temperatures as a third order decay process. The decay constant for the process only has a weak temperature dependence. In the presence of a bound surface state surface recombination may become important. This process leads to second order decay, decreasing exponentially with increasing temperature. This is caused by the exponential decrease of the surface density. Thermal leakage gives rise to first order decay exponentially increasing with the temperature. To study recombination one should thus aim for low temperatures. However, our cryostat did not enable measurements below $T \approx 270$ mK, not low enough to properly study recombination in H↓. Such a study could be done with D↓ where one expects a higher adsorption energy causing surface recombination to become dominant at higher temperatures. These measurements are discussed in chapter 6 and showed that recombination predominantly occurs on the surface of the helium film. From the temperature dependence of the recombination rate the adsorption energy of D↓ on ^{4}He surfaces could be determined. On the basis of these experiments one may also expect a bound state for H↓, which was confirmed experimentally in a later stage. However the higher binding energy causes D↓ to be much less stable than H↓.

Samenvatting

In dit proefschrift worden de eerste van een reeks experimenten besproken die in het Natuurkundig Laboratorium van de Universiteit van Amsterdam zijn uitgevoerd aan spingepolariseerde atomaire waterstof (H↓) en deuterium (D↓) bij zeer lage temperatuur ($T \approx 0.3$ K) en in hoge magneetvelden ($B \approx 10$ T). Deze experimenten tonen aan dat H↓ een gas is dat zich zoals ieder normaal (i.e. stabiel) gas leent voor natuurkundig onderzoek.

Het proefschrift bestaat uit zes hoofdstukken, waarvan hoofdstuk 1 dient ter inleiding en motivatie. Naast aspecten die van onmiddellijk belang zijn voor de hier beschreven experimenten zoals de methode van spin-polarisatie, het verschijnsel dat het gas zich niet in de vloeibare toestand laat brengen, het effect van wisselwerking met de wanden van de preparaat-ruimte en de (magnetische) veld afhankelijkheid van molecuul-formatie , worden hier aspecten beschreven die het onderzoek in een breder perspectief plaatsen en van belang zijn voor toekomstig onderzoek. Hieronder vallen de bespreking van het Bose-karakter van het gas en de condities waaronder Bose-Einstein condensatie waargenomen kan worden als men interacties tussen de atomen onderling en met de wanden in rekening brengt.

Hoofdstuk 2 bevat de beschrijving van de experimentele apparatuur en vormt de neerslag van een reeks experimenten uit de eerste fase van mijn promotie onderzoek. Met name de ontwikkeling van een betrouwbaar systeem om atomaire waterstof tot zeer lage temperaturen af te koelen, bleek van doorslaggevend belang voor onze experimenten. Bij de cryogene apparatuur verdient het tweetraps ^{3}He koelsysteem aandacht. Hiermede werd het mogelijk om de grote warmte belasting die samenhangt met het gebruik van ^{4}He in de experimenteercel, te onderdrukken. Bovendien blijkt de tweede koeltrap tevens te werken als miniatuur diffusie-pomp, waarmee H↓ naar de meetcel gepompt kan worden.

Een verslag van de eerste experimenten met H↓ vindt men in hoofdstuk 3. De metingen tonen aan dat H↓ voor langere perioden kan worden gestabiliseerd bij lage temperaturen en in hoge magneetvelden, indien de wanden van de meetcel worden bedekt met een laagje superfluide helium. De aanwezigheid van het gas wordt bij deze experimenten aangetoond door meting van de warmte die vrij komt bij recombinatie naar de moleculaire toestand (H_2). De recombinatie wordt op gang gebracht door locaal de heliumfilm te verbreken. Hierdoor treedt massale oppervlakte-adsorptie op met de gewenste recombinatie als gevolg. De

methode blijkt bijzonder gevoelig en vrij eenvoudig uitvoerbaar.

In hoofdstuk 4 wordt besproken hoe men zich het gas in de meetcel moet voorstellen. Hierbij komen de dichtheidsdistributie van het gas en het verschijnsel van thermische lek, samenhangend met de open structuur van de meetcel, aan de orde. Bovendien wordt opgemerkt, dat de dichtheidsdistributie kan worden gebruikt om het verschijnsel Bose-Einstein condensatie waar te nemen.

Een tweede serie experimenten is het onderwerp van hoofdstuk 5. Deze metingen tonen aan dat H↓ zich als een gas gedraagt. Zij hadden tot doel om een zo hoog mogelijke gasdichtheid op te bouwen en na te gaan welke processen hierbij beperkend zijn. Dichtheden $n \gtrsim 10^{16}$ H↓/cm^3 werden bereikt. Bij lagere dichtheden ($n \lesssim 10^{15}$ H↓/cm^3) bleek thermische lek het dominante vervalproces, terwijl bij hogere dichtheden ook recombinatie een rol bleek te spelen. In dit stadium van het onderzoek was het niet bekend of H↓ kon worden gebonden aan het oppervlak van de heliumfilm, alhoewel theoretische schattingen in deze richting wezen. Om dit punt op te helderen en informatie te verkrijgen over de aard van de recombinatie kan men de reactie kinetiek bestuderen. Volume recombinatie manifesteert zich bij lage temperatuur als een derde orde vervalproces, waarbij de vervalconstante slechts zwak van de temperatuur afhangt. Als er een gebonden oppervlaktetoestand bestaat kan oppervlakte recombinatie dominant worden. Dit proces geeft aanleiding tot tweede orde verval van de dichtheid, exponentieel afnemend met toenemende temperatuur tengevolge van een exponentiële afname van de oppervlakte dichtheid. Thermische lek geeft aanleiding tot een eerste orde vervalproces dat exponentieel toeneemt met de temperatuur. Om recombinatie te bestuderen moet men dus werken bij zo laag mogelijke temperaturen. Metingen beneden $T \approx 270$ mK waren echter met onze cryostaat niet mogelijk. Recombinatie kon daarentegen wel bestudeerd worden aan D↓ waarvoor op theoretische gronden een hogere adsorptieenergie wordt verwacht, zodat oppervlakte recombinatie reeds bij hogere temperaturen dominant wordt. De deuterium metingen komen aan de orde in hoofdstuk 6 en toonden aan, dat recombinatie voornamelijk aan het oppervlak plaats vindt. Uit de temperatuurafhankelijkheid van de recombinatiesnelheid kon bovendien de adsorptieenergie van D↓ aan het oppervlak van ^{4}He worden bepaald. Op grond van deze experimenten kon ook voor H↓ een gebonden toestand worden verwacht, hetgeen in later stadium is bevestigd. Ten gevolge van de grotere bindingsenergie is D↓ (bij gelijke temperatuur en veld) echter veel minder stabiel dan H↓.

Nawoord

Bij de voltooiing van dit proefschrift wil ik graag allen bedanken die, direkt of indirekt, hebben bijgedragen aan de tot stand koming ervan.

In de eerste plaats mijn promotor Prof.Dr.Isaac F. Silvera aan wie ik een groot deel van mijn wetenschappelijke vorming te danken heb. Hij heeft mij de kans gegeven te werken aan een probleem met uitzonderlijke mogelijkheden. In de eerste, moeilijke fase , waarbij het onderzoek de nodige scepcis ondervond is zijn inspirerende belangstelling en begeleiding bizonder waardevol geweest. Met het uitkristalliseren van onze ideeen omtrent de juiste benaderingswijze van het probleem, heeft zich onder zijn leiding een steeds intensievere en uiterst stimulerende samenwerking kunnen ontwikkelen, die van doorslaggevend belang is geweest voor het slagen van het onderzoek.

Daarnaast is ook de samenwerking op technisch gebied met Otto Hopfner van groot belang geweest. Ik wil hem bedanken voor zijn volle en vakkundige inzet die, met name in tijden van tegenspoed, altijd tot steun is geweest en die in niet geringe mate heeft bijgedragen tot het welslagen van het onderzoek.

Prof.Dr. N.J. Trappeniers wil ik bedanken voor zijn bereidheid om op te treden als coreferent. Dr.Victor V. Goldman ,Dr. Ad Lagendijk en Dr. A. John Berlinsky bedank ik voor de collegiale samenwerking en begeleiding op theoretisch gebied.

In de beginfase van het onderzoek hebben Herman Godfried en vooral Eric Eliel aan de experimenten meegewerkt,later hebben Mart Diemeer, Rudolf Sprik en Jeroen de Miranda een bijdrage geleverd. Hun enthousiasme is altijd een stimulans voor mij geweest. Stijn Mattheij en Gert van Yperen wil ik bedanken voor de plezierige samenwerking en het doorlezen van het manuscript.

Van de velen met wie ik op het lab heb samengewerkt wil ik nog een aantal met name noemen.
H.Witteveld hielp bij de het ontwerpen van de apparatuur. Martin Bekelaar en Jan hofman verzorgden een deel van de uitvoering. Ton Riemersma en Hugo Slatter losten een aantal lastige technologische problemen op. Bert Zwart en Frans Slagt verzorgden het glaswerk voor de dissociatorbuizen. Ad Veen, Rob Veen en Charly Alderhout hielpen bij electronische problemen. Eef Hartman gaf adviezen op softwaregebied. Mariet Bos zorgde er voor dat vele manuscripten snel de deur uit konden. Ben Leonards leverde de foto's en een aantal tekeningen.Herman Pothoven en Nico Jonker zorgden voor grote, grote hoeveelheden vloeibaar helium.

Daarnaast wil ik allen die hebben bijgedragen tot het tot stand komen van dit proefschrift, maar niet met name zijn genoemd, hartelijk bedanken.

Tenslotte, maar zeker niet in de laatste plaats wil ik mijn ouders bedanken, die mijn belangstelling voor de wetenschap hebben gewekt en die mij in de gelegenheid hebben gesteld om een academische opleiding te volgen. Ik wil hen ook danken voor de hulp bij het vervaardigen van het manuscript.

Mijn vrouw Marian wil ik bedanken voor de liefdevolle steun en rust, die altijd bij haar te vinden was.